NASA Contractor Report 4276

The Mechanisms of Dispersion Strengthening and Fracture in Al-Based XD™ Alloys

R. M. Aikin, Jr.

CONTRACT NAS1-18531
FEBRUARY 1990

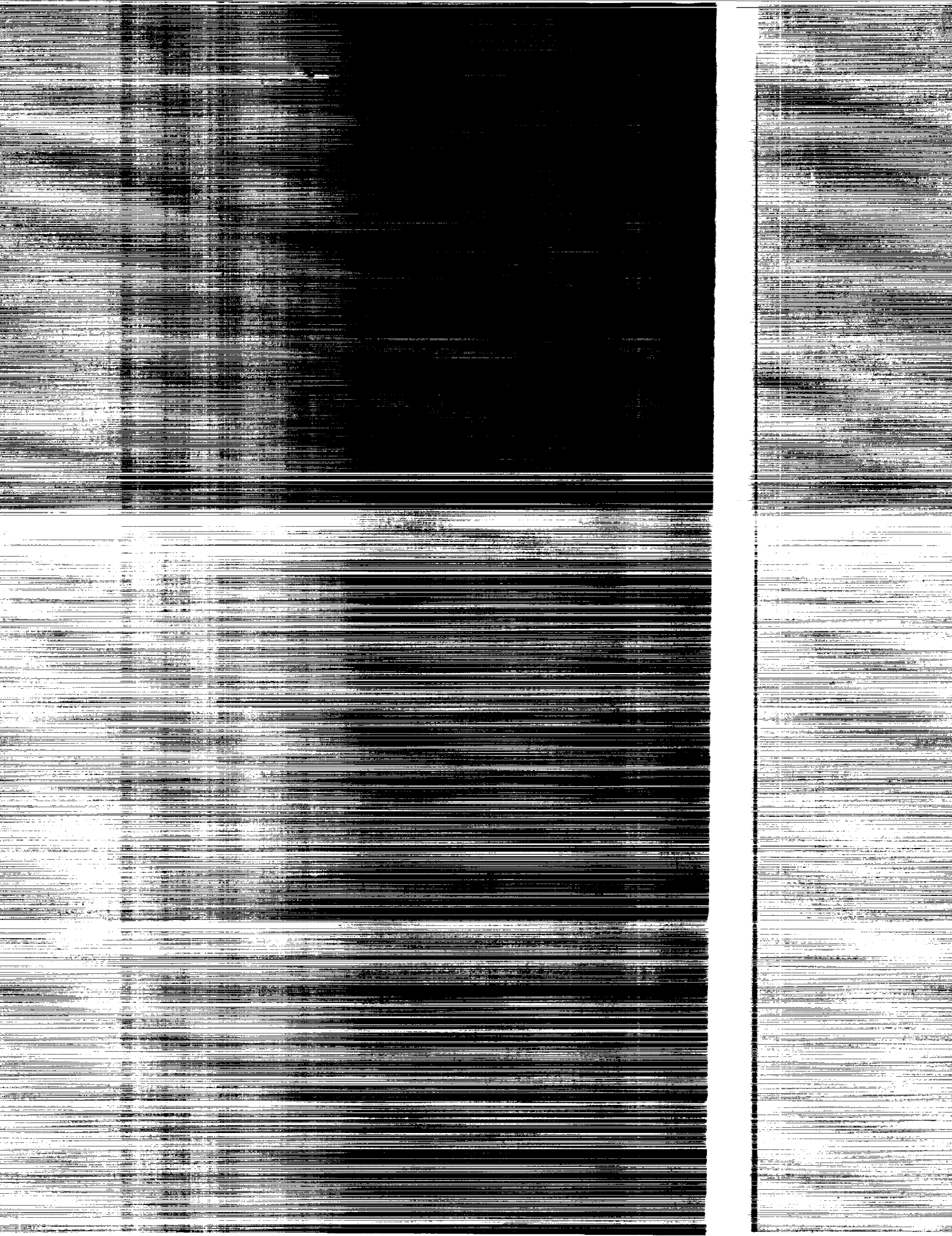

NASA Contractor Report 4276

The Mechanisms of Dispersion Strengthening and Fracture in Al-Based XD™ Alloys

R. M. Aikin, Jr.
Martin Marietta Corporation
Martin Marietta Laboratories
Baltimore, Maryland

Prepared for
Langley Research Center
under Contract NAS1-18531

National Aeronautics and
Space Administration
Office of Management
Scientific and Technical
Information Division

1990

ABSTRACT

The influence of reinforcement size, volume fraction, and matrix deformation behavior on room and elevated temperature strength, and the fracture toughness of metal matrix composites of both pure aluminum and Al-4%Cu-1.5%Mg with 0-15vol% TiB_2 have been examined. Higher TiB_2 volume fractions increased the tensile yield strength both at room and elevated temperatures, and reduced the elongation to fracture. Tensile tests also indicate that small particles provided a greater increase in strength for a given volume fraction than larger particles, whereas elongation to fracture appeared to be insensitive to reinforcement size. The fracture toughness of the Al-4%Cu-1.5%Mg alloys decreased rapidly with TiB_2 additions of 0 to 5vol% and more slowly with TiB_2 additions of 5 to 15vol%. Fracture toughness appears to be independent of TiB_2 particle size. The isothermal-aging response of the precipitation strengthened Al-4%Cu-1.5%Mg alloys was not altered by the presence of TiB_2.

TABLE OF CONTENTS

1. INTRODUCTION

The incorporation of stable particles that are unaffected by thermal exposure during both fabrication and operation offers a new set of possibilities for the alloy designer. Clearly, an alloy reinforced with non-deformable, non-shearable particles that are stable to the melting point of the alloy (and beyond) has a fundamental advantage over conventional alloys, which are reinforced with precipitates that can be sheared by dislocations and coarsen or go into solution if exposed to elevated temperature. Metals reinforced with nonshearable ceramic particles are referred to as metal matrix composites (MMC).

1.1 Program Goals

The mechanisms governing the properties of an alloy reinforced with equiaxed ceramic particles approximately 1 μm in diameter is not understood. Alloys reinforced with particles of this size occupy the middle ground between the true dispersion-strengthened metals, which have particles less than 0.1 μm, and conventional MMC's, which have reinforcements greater than 10 μm. The objective of this program is to determine the mechanism governing the mechanical behavior of alloys with particles in the 1 μm range. The specific goal of this program is to examine the influence of reinforcement size, volume fraction, and matrix deformation behavior on the strength, fracture toughness, and high-temperature strength of an aluminum MMC. Understanding how these parameters affect the properties of MMC's will allow us to engineer these

elements to produce composites with superior properties tailored to a specific application.

To meet these goals, two sets of MMC's were produced by the XD^{TM} process. The first of these sets contained from 0.5 to 15vol% 0.3 μm TiB_2 particles in pure aluminum. The second set consisted of 0 to 15vol% TiB_2 particles either 0.3 μm or 1.3 μm in diameter in a matrix of Al-4%Cu-1.5%Mg (a model ternary alloy similar to 2024 but without the grain refiner, Mn). In most of the heat treated conditions considered, the Al-4%Cu-1.5%Mg alloys has both the TiB_2 ceramic reinforcement and the G.P. zones or S' (Al_2CuMg) precipitates of the 2000-series aluminum matrix.

1.2 The XD^{TM} Process

The XD^{TM} process is a patented technique developed by Martin Marietta Corporation, in which ceramic particles are produced in-situ in a molten metal. The process enables the production of MMC's reinforced with a wide variety of transition metal carbide, boride, and nitride particles. The reinforcements are typically single crystals of high purity, which because they were formed in-situ, have clean unoxidized interfaces. By suitably altering the parameters of the in-situ formation step, the size of the reinforcements can be varied from approximately 0.2 μm to 10 μm.

Typically, a master alloy containing a large volume fraction of the desired reinforcement is produced by the XD^{TM} process in pure aluminum. In a subsequent casting process, this master alloy is diluted to the desired ceramic particle

loading and the matrix alloying additions are added. By using a master alloy, the amount of material produced by the XD™ process is kept to a minimum, thereby reducing production costs.

2. XD^{TM} ALUMINUM-TiB_2 SYSTEM

In this study XD^{TM} master alloys containing TiB_2 particles of two sizes were produced and examined. To determine the particle size the polished surfaces of alloys containing 5vol% TiB_2 was lightly etched and the major and minor diameters of individual particles was measured from micrographs taken on the scanning electron microscope (SEM).

Although the size distributions of major and minor diameters could be used directly as a measure of particle size, we use an alternative definition of particle size, the equivalent diameter. The equivalent diameter of the particle is defined as the diameter of a circular particle with the same area as the area of the elliptical particle. In determining the equivalent diameter, individual particles were assumed to be ellipsoidal. The effective area of each particle was calculated from the measured major and minor diameters.

For each alloy, the equivalent diameters of approximately 600 particles were determined, and from these measurements the mean diameter and frequency distributions were calculated. The equivalent diameter distributions of the two master alloys are shown in Fig. 2.1. The means of these distributions are 0.34 μm (0.34 $\pm$ 0.06 μm) and 1.29 μm (1.31 $\pm$ 0.10 μm), respectively. Although the shape of the major and minor diameter distributions are similar to that of the equivalent diameter distribution it is believed that the mean equivalent diameter better represents the particle size of different materials than the mean of either the minor or the major

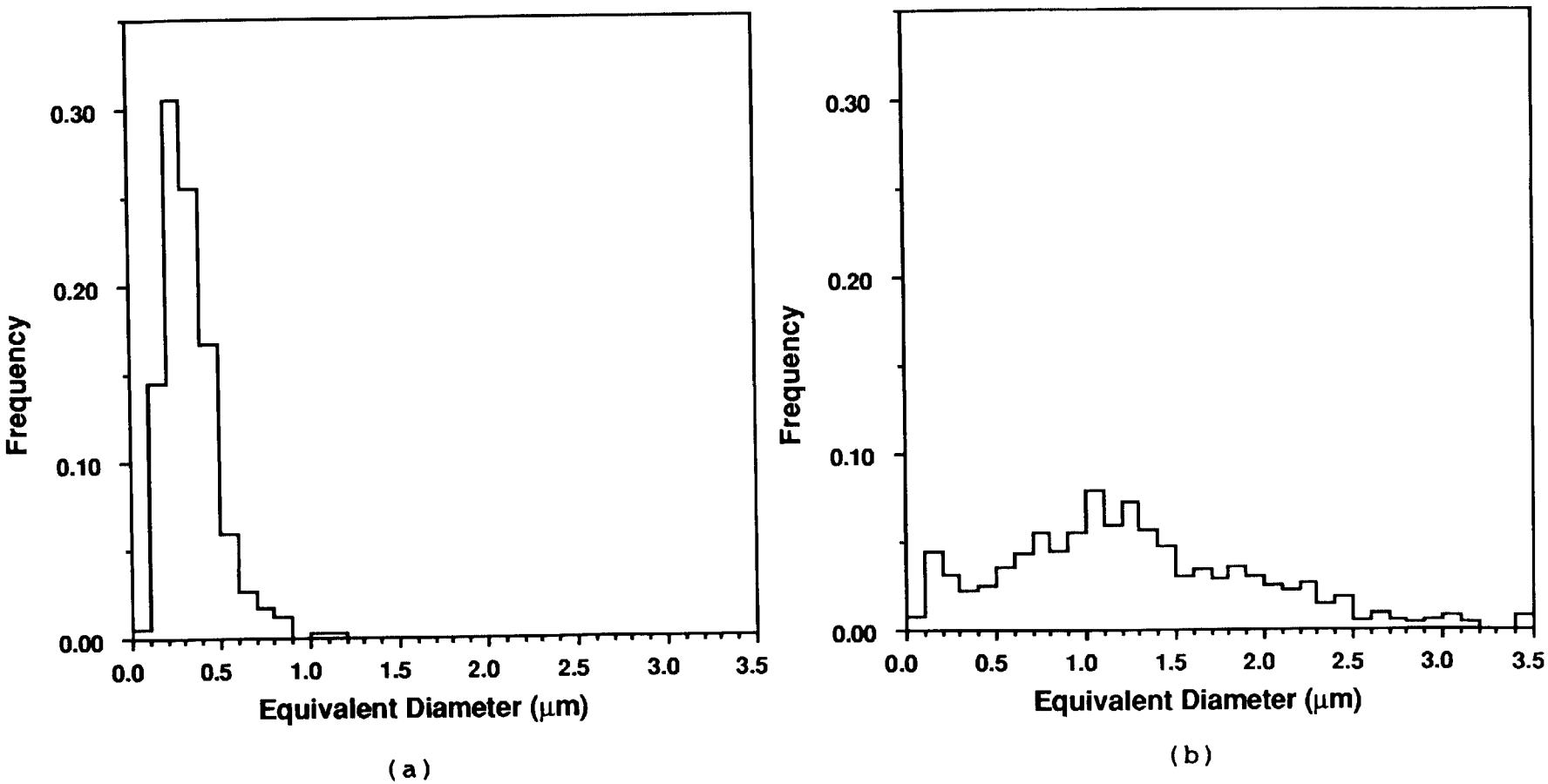

Figure 2.1 Particle size distributions of (a) small particles with a mean diameter of 0.34 μm and (b) large particles with a mean diameter of 1.31 μm.

diameter.

The TiB_2 particles present in both materials are roughly spherical; many are hexagonal cylinders with planar features along the (0001) and {1120} crystallographic planes. Measurements of major and minor diameters show the aspect ratio to be 1.29 ± 0.32 for the 0.3 μm particles and 1.29 ± 0.02 for the 1.3 μm particles. The typical shapes and size distributions of the lightly etched Al+10vol%TiB_2 samples are shown in the SEM micrographs in Fig. 2.2.

Comparing the breadth of the distributions of particle diameter shown in Fig. 2.1(a) with those in Fig. 2.1(b), it might appear that the size distribution is broader in the 1.3 μm TiB_2 material than in the 0.3 μm material. However, the normalized distributions in Fig. 2.3 (obtained by normalizing the abscissa by the mean diameter and normalizing the ordinate to unity) show that the breadth and roughly symmetric shapes of the two distributions are quite similar. Thus, the discrepancy between the distributions in Fig. 2.1 is due to the difference in scale (i.e., the difference in the size of the particles), not a difference in the shape and size of the distribution.

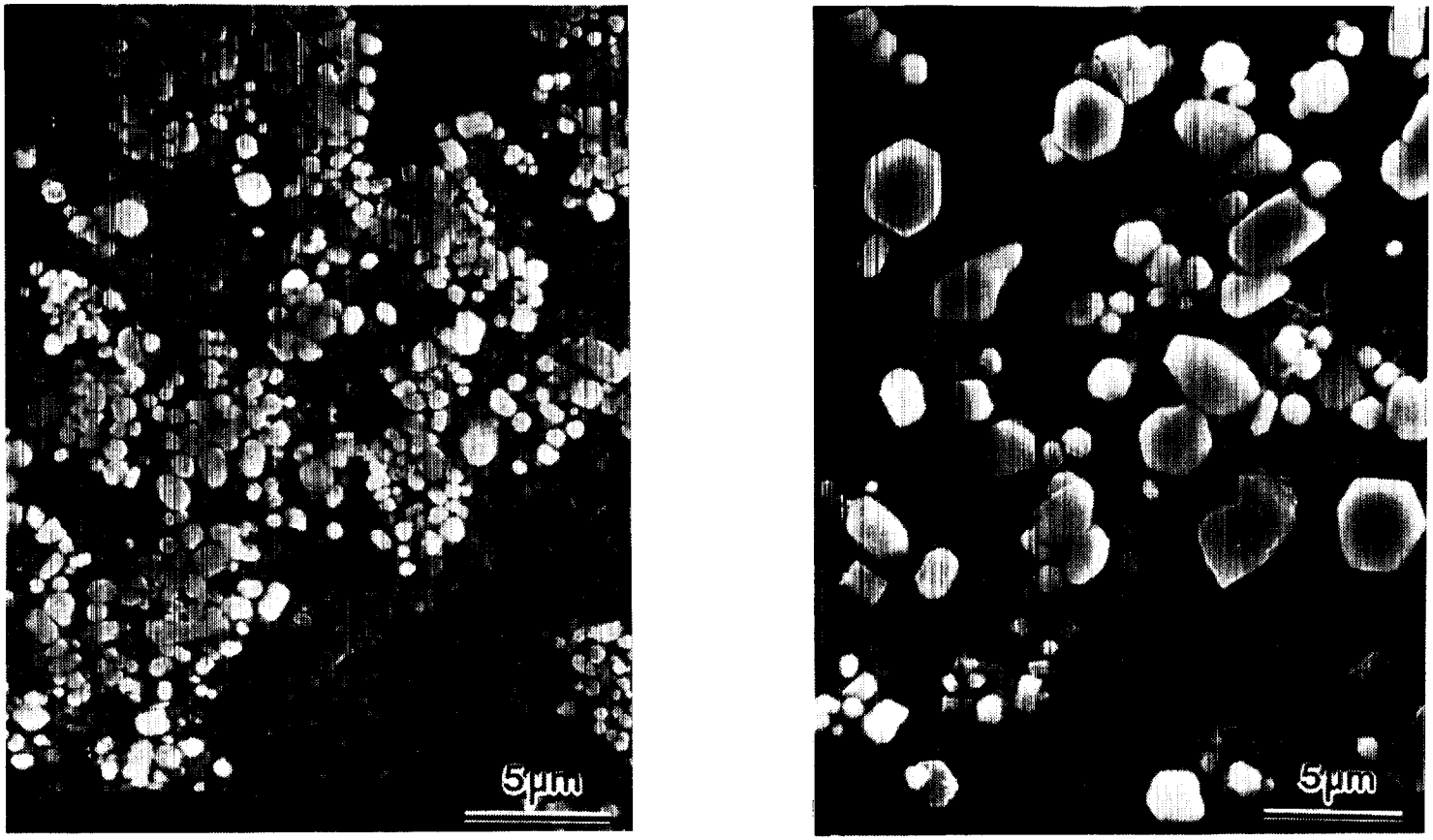

(a) (b)

Figure 2.2 Secondary electron micrographs of Al+10%TiB_2 made with two sizes of TiB_2; (a) small particles with a mean diameter of 0.34 μm and (b) large particles with a mean diameter of 1.31 μm.

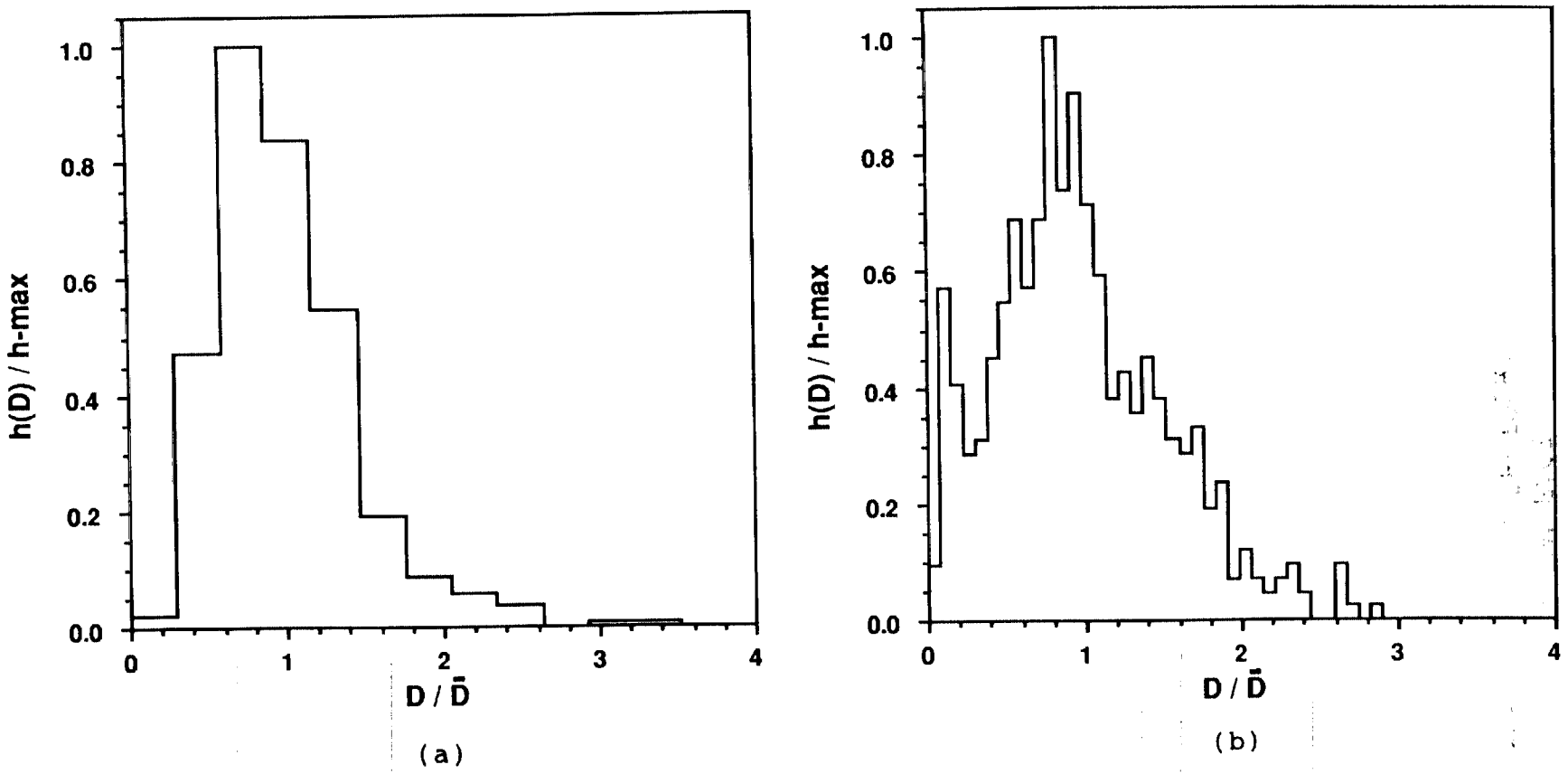

Figure 2.3 Normalized particle size distributions for (a) small particles with a mean diameter of 0.34 μm and (b) large particles with a mean diameter of 1.31 μm.

3. TiB_2 IN PURE ALUMINUM

To help understand the role of the TiB_2 on the mechanical behavior of aluminum alloys it is necessary to understand the impact of TiB_2 on the pure metal. Therefore, the behavior of TiB_2 in pure aluminum was examined.

3.1 Materials

3.1.1 Processing

Alloys with 0.5, 2, 5, 10, and 15 vol% TiB_2 were fabricated using the master alloy with 0.3 μm TiB_2. The alloys were induction melted using the XD^{TM} master alloy and 99.99% pure aluminum, and then casting it into a 3 in. diameter mold. These 5 lb ingots were then hot forged in three orthogonal directions. After forging, the alloys were heat treated at 932°F (500°C) for 2 hours. This high-temperature heat treatment allowed the alloys to recrystallize. Chemical analysis of these alloys show them to contain <0.08 wt% Si and <0.04 wt% Fe.

3.1.2 Microstructure

The particle distribution of the alloys is shown in the micrographs in Fig. 3.1. Some of the particles were pushed to the cell boundaries during solidification, producing regions with higher particle loadings. With increasing loading, the size of the solidification cell decreased and the particle distribution improved such that the 10 and 15% alloys have a uniform particle distribution.

The TiB_2 particles refined the as-cast grain size and

ORIGINAL PAGE
BLACK AND WHITE PHOTOGRAPH

(b)

(a)

Figure 3.1 Secondary electron micrographs of pure aluminum with (a) 0.5vol%, 0.3 μm TiB_2, and (b) 2vol%, 0.3 μm TiB_2.

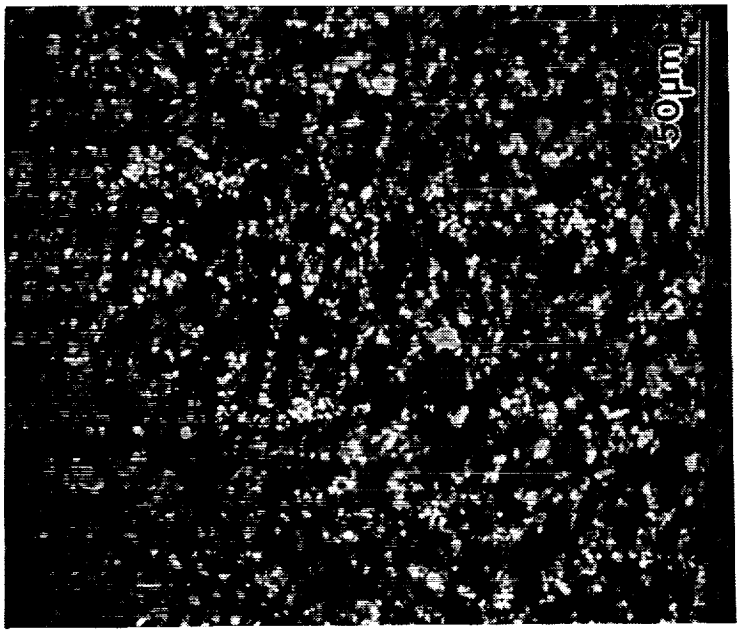

(d)

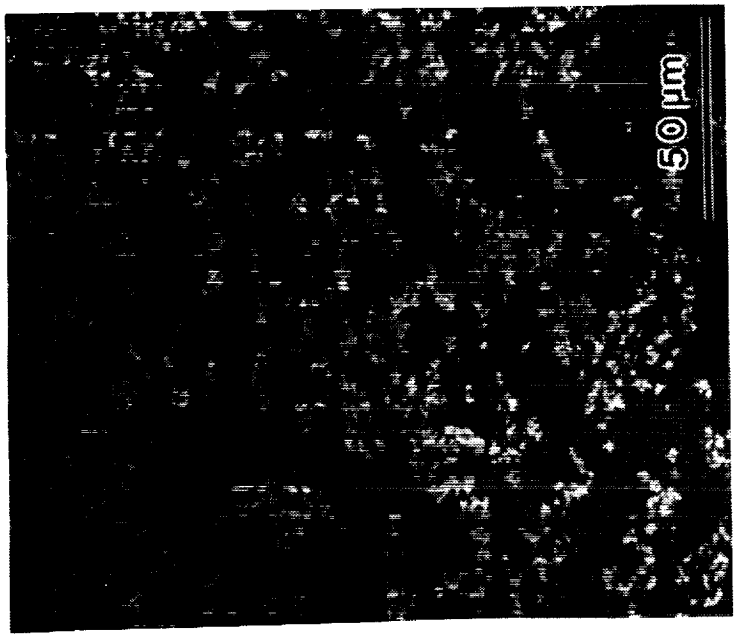

(c)

Figure 3.1 Secondary electron micrographs of pure aluminum with (c) 5vol%, 0.3 μm TiB_2, and (d) 10vol%, 0.3 μm TiB_2.

prevented grain growth during the long high-temperature anneal. The grain size of these alloys was found to depend greatly on particle loading. Figure 3.2 shows the grain size of these materials in micrographs of anodized samples taken in cross-polarized light. The materials with higher loadings of TiB_2 have a much smaller grain size; the grains are so small that grain size cannot be accurately measured using anodized samples.

3.2 Tensile Properties

The tensile tests were performed in a screw-driven mechanical test frame using a clip-on extensometer and threaded samples with a 0.25 in. diameter by 1 in. gauge section. In Fig. 3.3, the 0.2% offset yield stress is shown as a function of strain rate for the five particle loadings used. The yield stress was not dependent on strain rates ranging from 1.3×10^{-4} to 0.13 sec^{-1} at room temperature. This is not unexpected; typically strain-rate-dependent deformation is a thermally activated process. Because the mechanical properties do not depend on strain rate at room temperature, further discussion in this report is confined to tests performed at a strain rate of 1.3×10^{-3} sec^{-1}.

Figure 3.4 shows the dependence of the 0.2% offset yield stress and the ultimate tensile strength (UTS) for individual tensile tests of the pure aluminum with TiB_2. Both the yield stress and the UTS of these materials increased significantly with increasing particle loading. Although the exact contribution of various mechanisms to the increase in yield

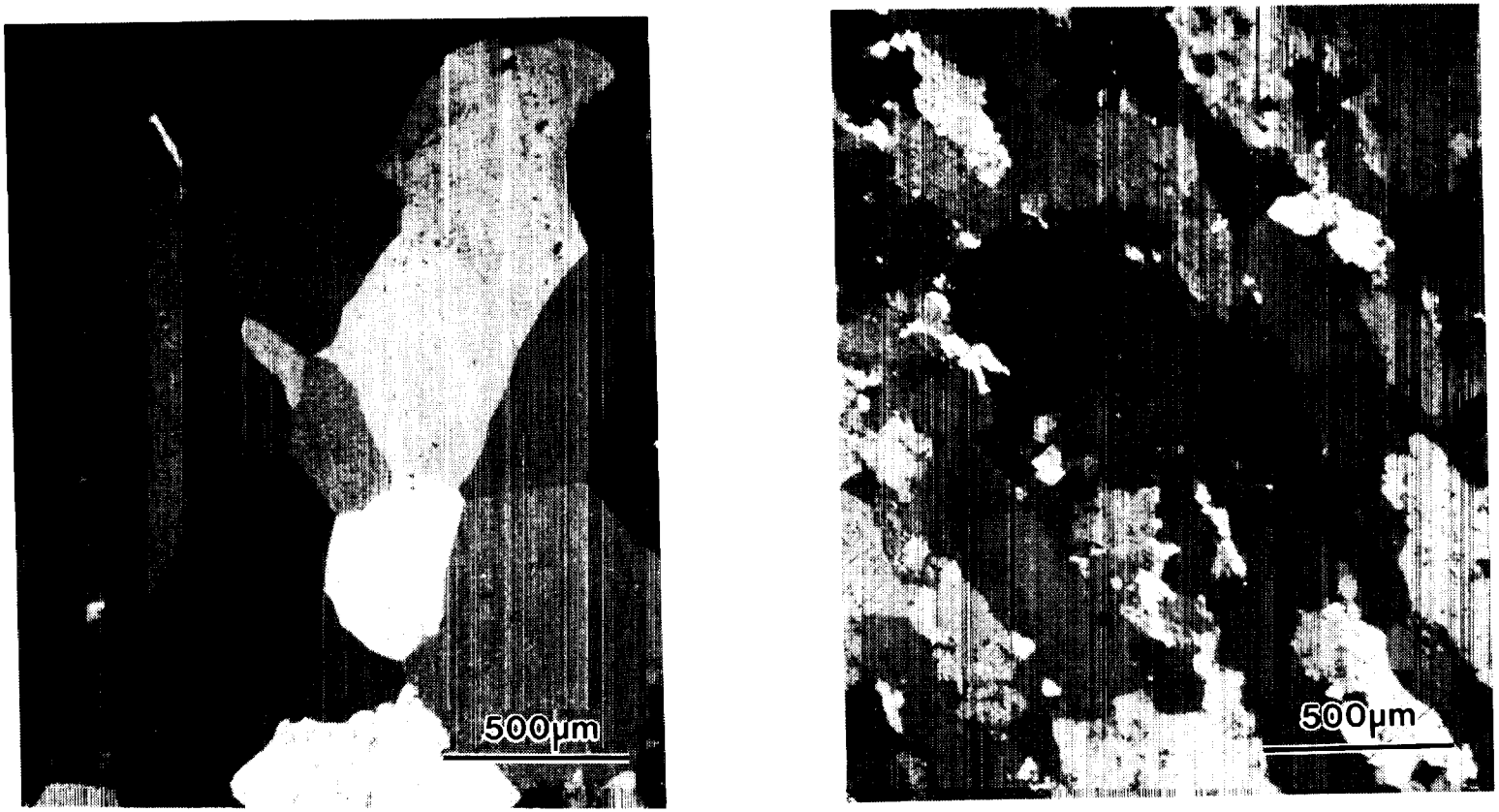

(a) (b)

Figure 3.2 Optical micrographs taken with cross-polarized light to show the grain size of forged and annealed pure aluminum alloys with (a) 0.5vol%, 0.3 μm TiB_2 and (b) 2vol%, 0.3 μm TiB_2.

(c) (d)

Figure 3.2 Optical micrographs taken with cross-polarized light to show the grain size of forged and annealed pure aluminum alloys with (c) 5vol%, 0.3 μm TiB_2, and (d) 10vol% 0.3 μm TiB_2.

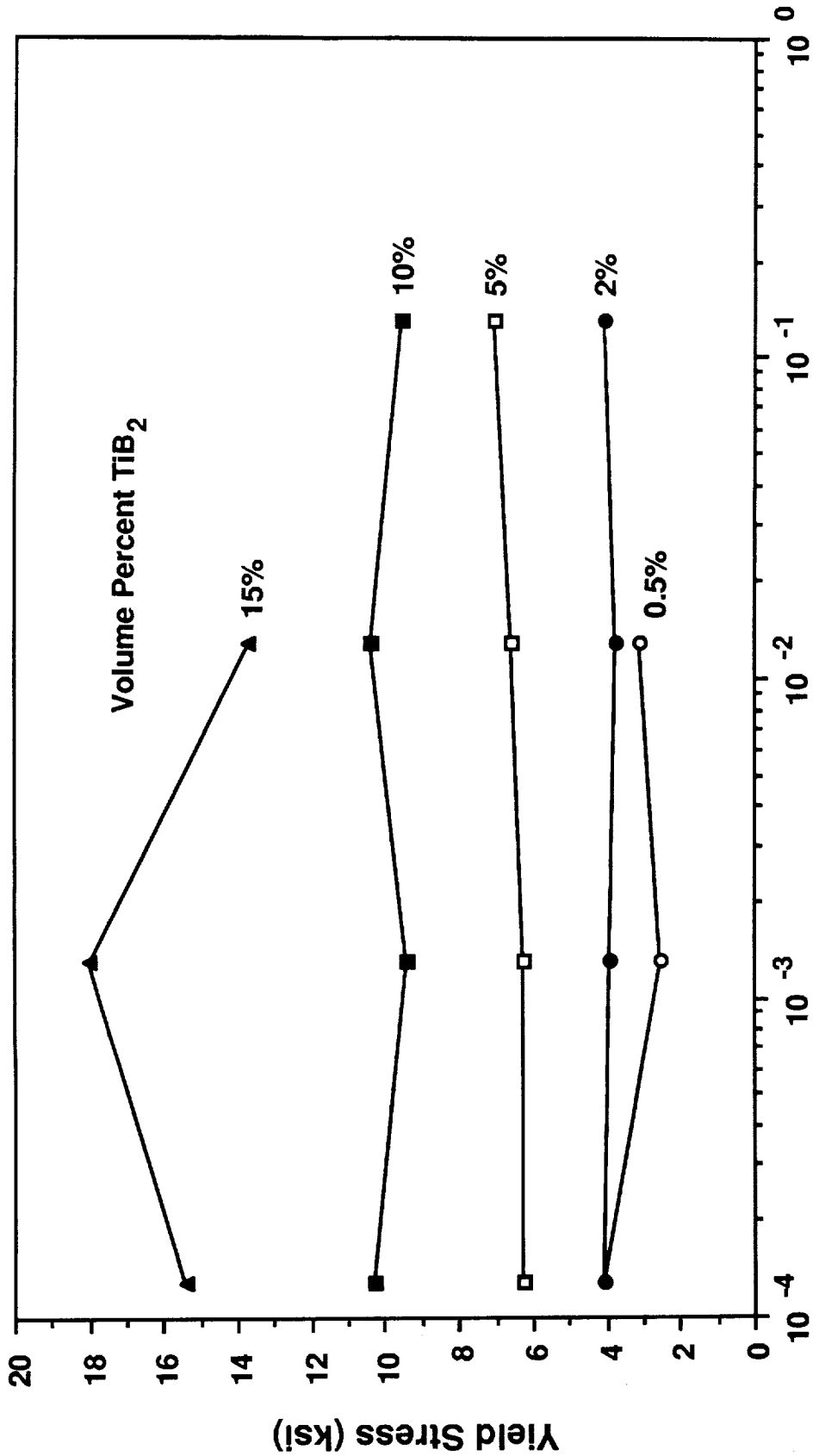

Figure 3.3 Dependence of yield stress on strain rate for forged and annealed pure aluminum with 0.5–10vol%, 0.3 μm TiB_2.

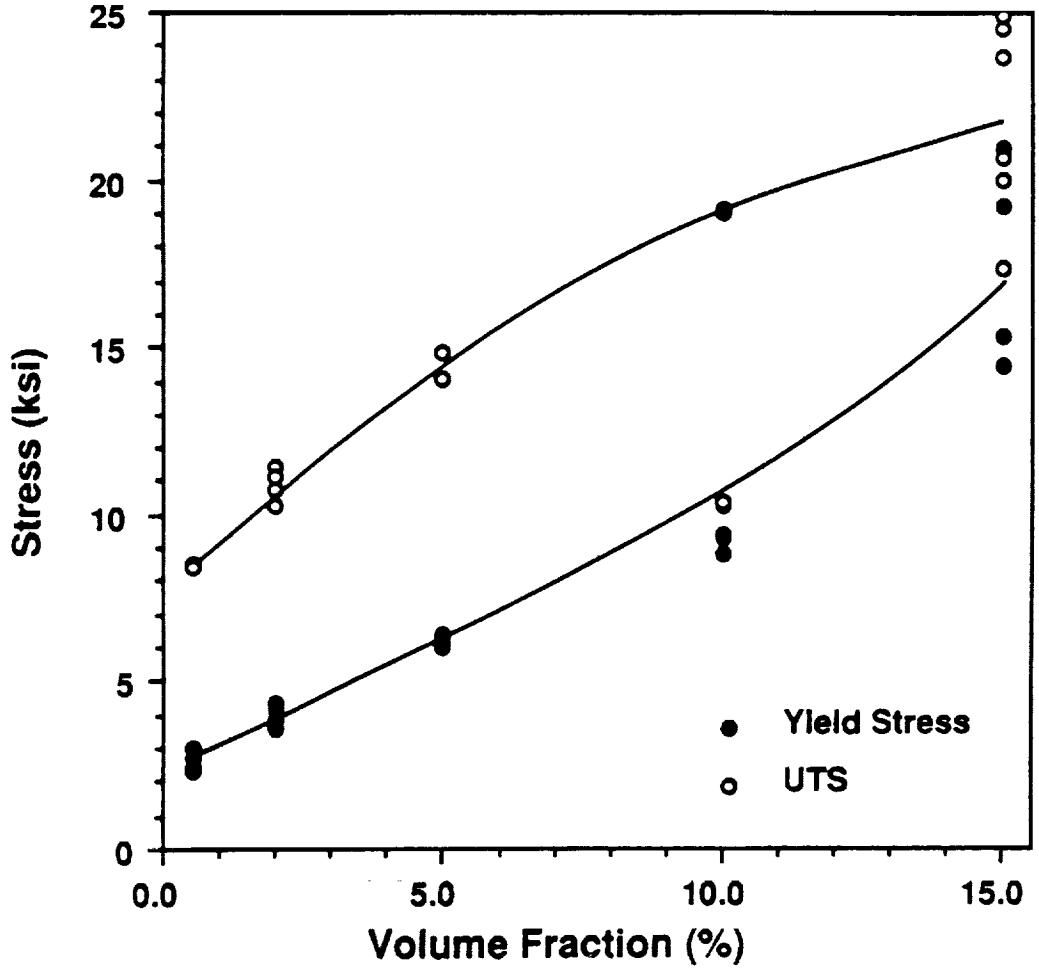

Figure 3.4 Dependence of yield stress and ultimate tensile strength on volume fraction of 0.3 μm TiB_2 for forged and annealed pure aluminum.

stress has not been determined, it is clear from the strong dependence of grain size on particle loading (shown in Fig. 3.2) that a substantial portion of the increase in strength observed with increasing loading is due to Hall-Petch strengthening.

The elongation to fracture in a 1 in. gauge section is plotted in Fig. 3.5 as a function of volume fraction for individual tensile tests. Elongation decreased monotonically with increasing volume fraction, a typical trend in composites. Ductility, as determined from the reduction in cross-sectional area, is plotted in Fig. 3.6. Ductility also decreased with increasing TiB_2 volume fraction. Although both the elongation to fracture and the ductility of these alloys decreased significantly with increasing particle loadings, the fracture mode remains ductile rupture. As shown in Fig. 3.7, these alloys exhibit a cup-and-ball fracture surface, in which dimple size is strongly dependent on particle loading. Roughly 50% of these dimples are occupied by a TiB_2 particle. It is thus quite likely that voids initiated at the particle/matrix interface.

3.3 Elevated-Temperature Tensile Properties

Elevated-temperature tensile tests were performed at a strain rate of 1.3×10^{-3} sec^{-1}. The 0.2% offset yield stress from these results (plotted in Fig. 3.8 as a function of temperature) decreased with increasing temperature. The decrease in yield stress was less pronounced among the weaker, lower loading alloys than in the stronger, higher loading

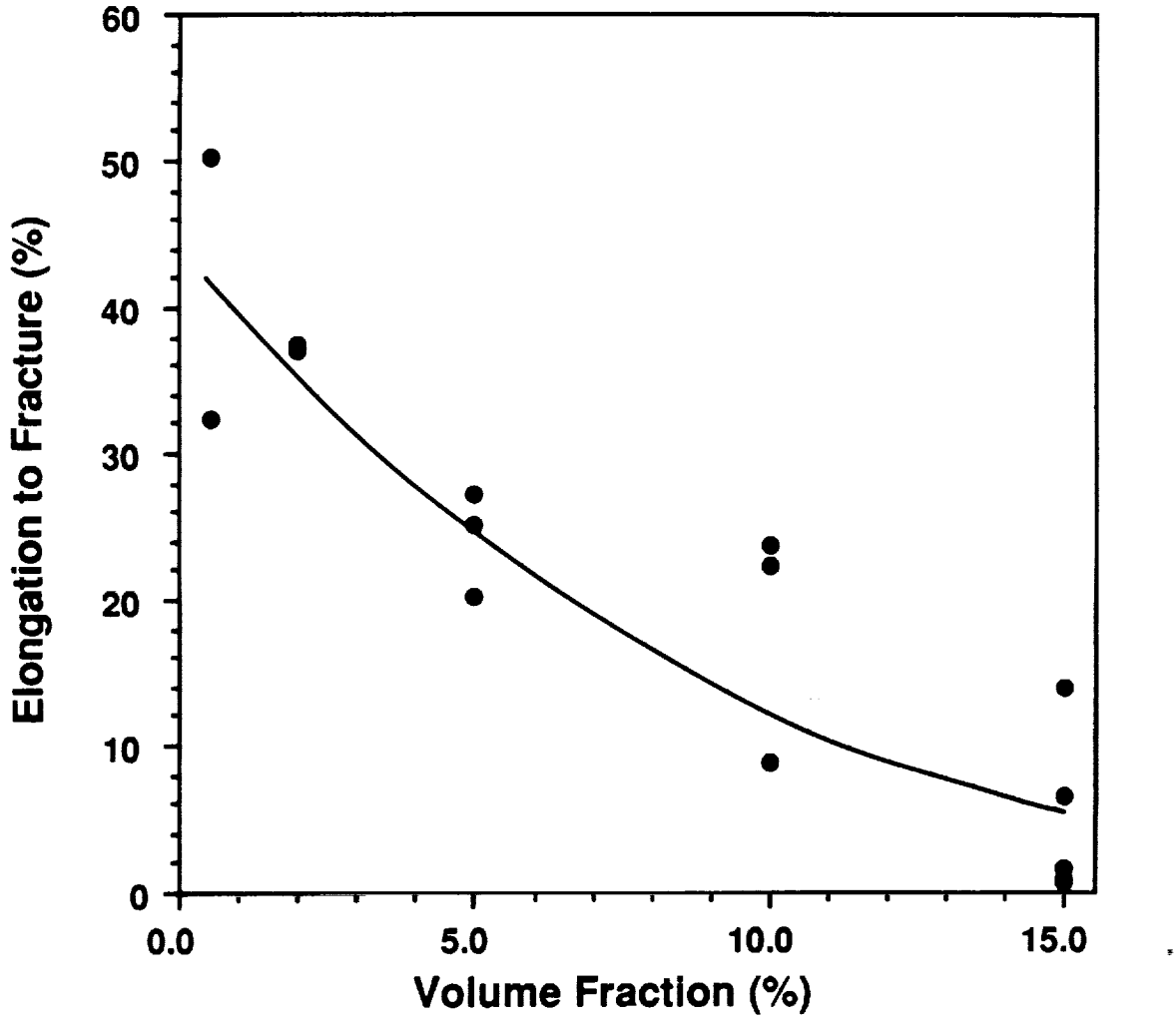

Figure 3.5 Dependence of elongation to fracture in a 1 in. gauge length on volume fraction of 0.3 μm TiB_2 for forged and annealed pure aluminum.

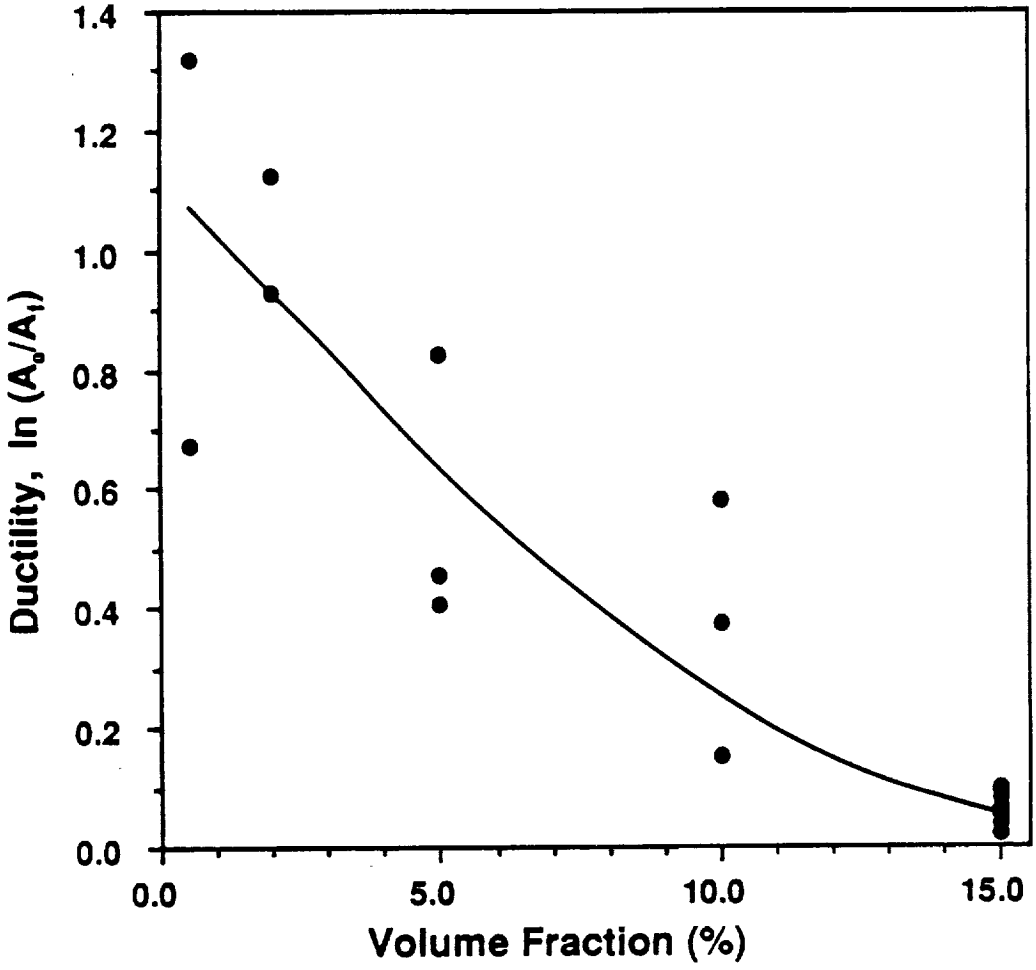

Figure 3.6 Dependence of ductility on volume fraction of 0.3 μm TiB_2 for forged and annealed pure aluminum.

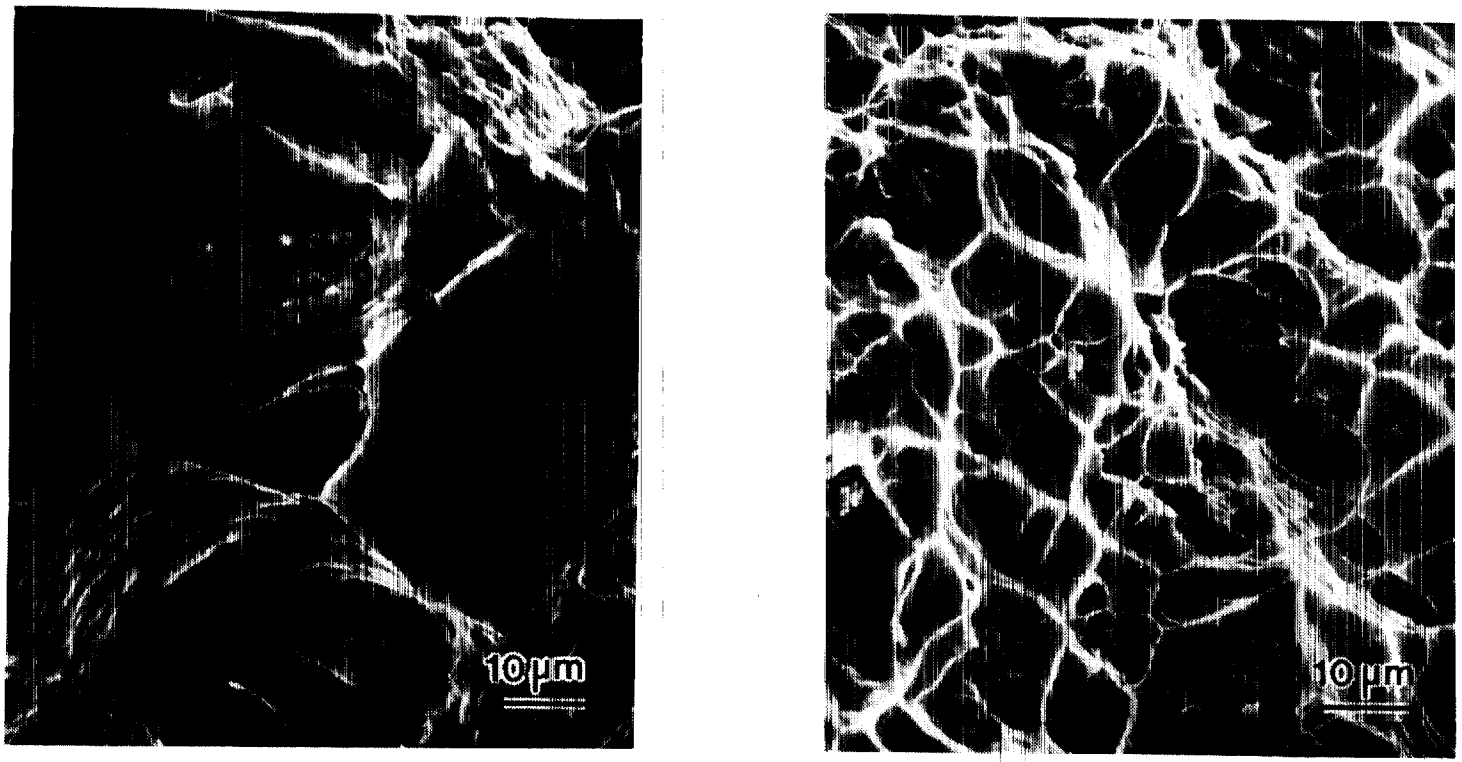

(a) (b)

Figure 3.7 Secondary electron micrographs of the fracture surfaces of samples of pure aluminum reinforced with (a) 0.5vol%, 0.3 μm TiB_2 and (b) 2vol%, 0.3 μm TiB_2, pulled in tension at room temperature.

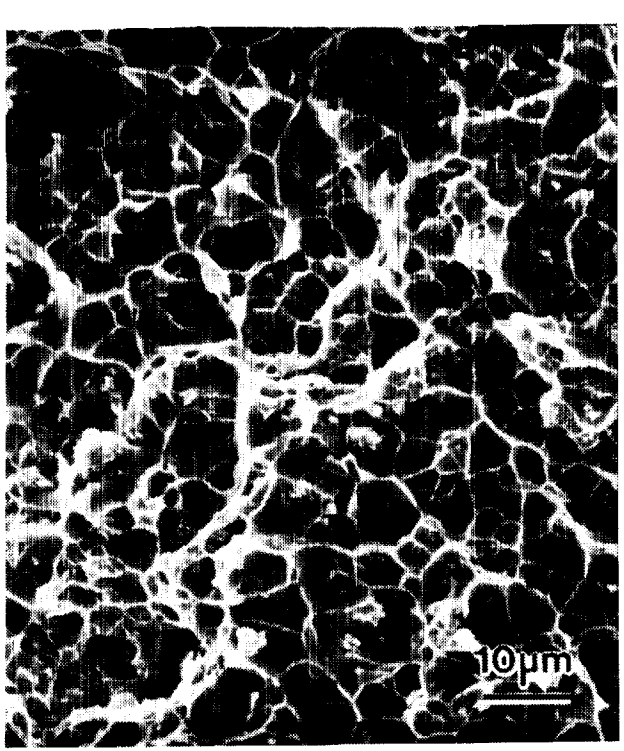

(c)

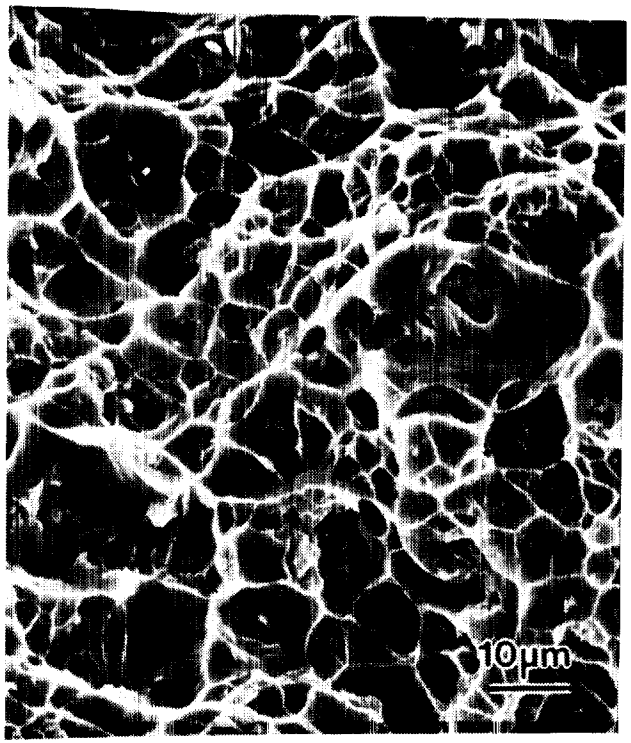

(d)

Figure 3.7 Secondary electron micrographs of the fracture surfaces of samples of aluminum reinforced with (c) 5vol%, 0.3 μm TiB_2 and (d) 10vol%, 0.3 μm TiB_2, pulled in tension at room temperature.

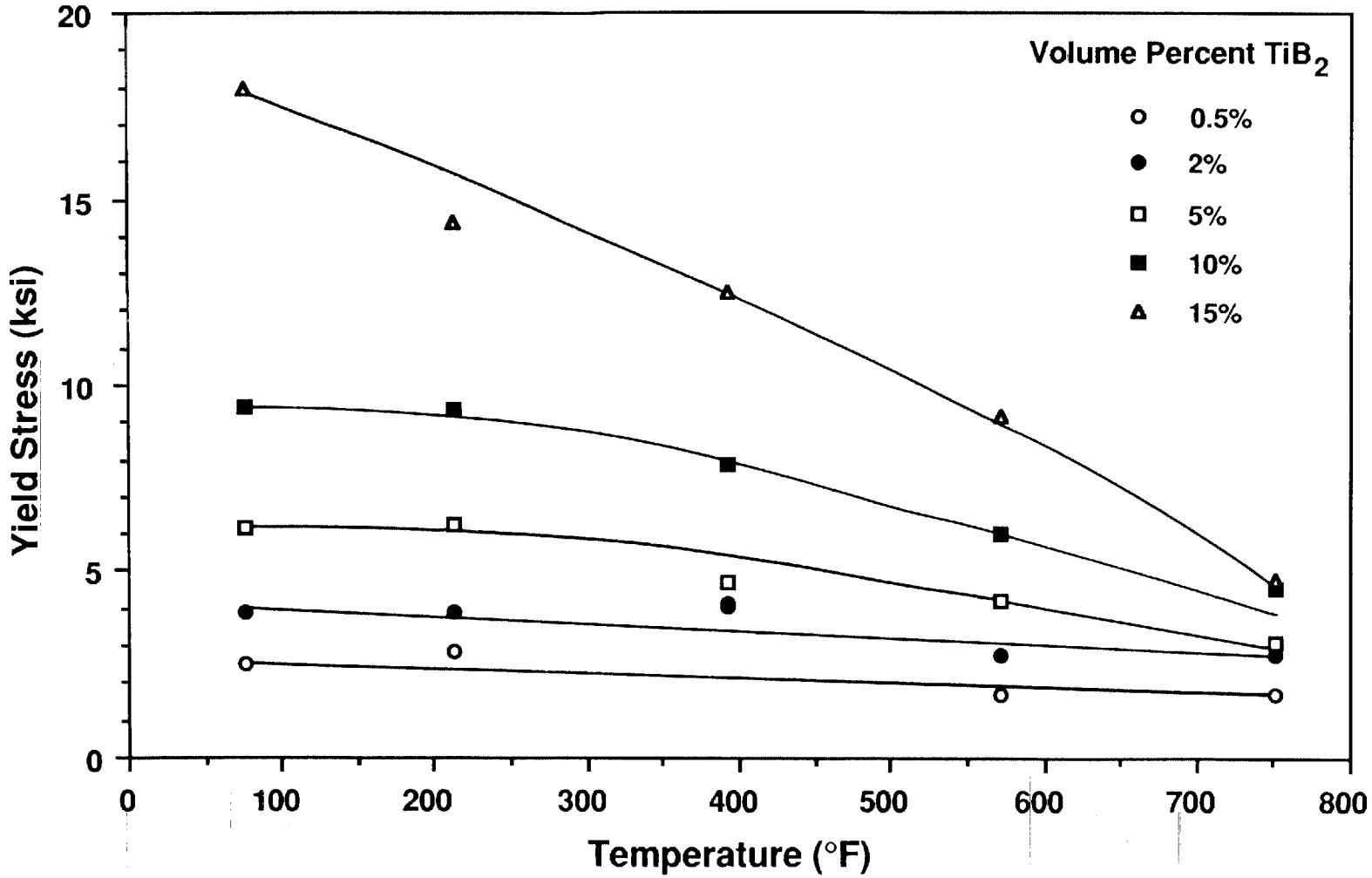

Figure 3.8 Yield stress as a function of test temperature for forged and annealed pure aluminum with various loadings of 0.3 μm TiB_2.

alloys. Figure 3.8 also shows that yield stress increased with increased particle loadings, although at the highest temperature there is a smaller proportional increase in strength between alloys. A corresponding plot, Fig. 3.9, shows the elongation to fracture as a function of temperature. In general the elongation of these materials increased gradually with increasing temperature.

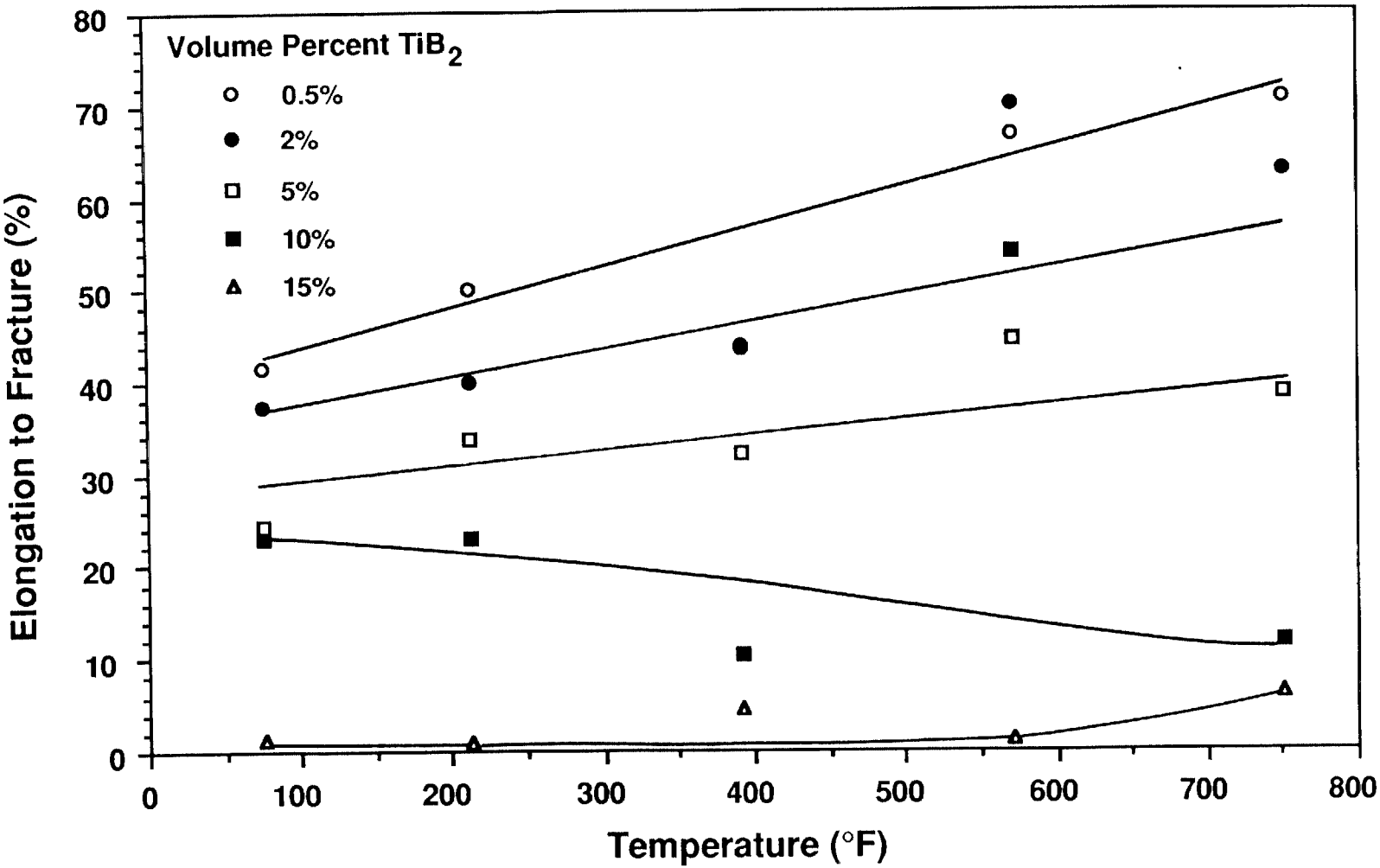

Figure 3.9 Elongation to fracture as a function of test temperature for forged and annealed pure aluminum with various loadings of 0.3 μm TiB_2.

4. TiB_2 IN Al-4%Cu-1.5%Mg

4.1 Materials

Aluminum-copper-magnesium alloys with a Cu:Mg ratio of approximately 2.2:1 form the pseudo-binary system aluminum-Al_2CuMg. The precipitation sequence in these alloys following solutionizing and quenching is:

supersaturated α → G.P. zones → S′ → S (Al_2CuMg).

The G.P. zones consist of copper and magnesium segregated to the {210} planes. The orthorhombic intermediate S′ phase nucleates heterogeneously on dislocations and grows as cylinders on $\{210\}_\alpha$ in the <001> direction. Corrugated S′ sheets are formed and intersect during the later stages of growth. Eventually, the S′ phase grows to the point that it loses coherency with the matrix, and the equilibrium S phase replaces it [3].

4.1.1 Processing

Alloys with 0, 2, 5, 10, and 15 vol% TiB_2 were fabricated in a Al-4wt%Cu-1.5wt%Mg matrix using both master alloys described in Sec. 2. The alloys were produced by induction melting 99.99% pure aluminum, master alloys of Cu and Mg, and the XD^{TM} master alloy. Sixty pound melts were cast into a 6 in. diameter mold and allowed to solidify. The ingots were then extruded into 2.75 in. by 0.63 in. bar at an aluminum extrusion house. The resulting extrusion ratio was 16:1. The chemical compositions of these alloys are listed in Table 4.1. Although the actual composition is slightly low in copper

Table 4.1

Chemical Composition of Unreinforced and TiB_2 Reinforced Al-Cu-Mg Alloys

Alloy Desigation	Nominal Loading (vol%)	Mean Size (μm)	Chemical Analysis (wt%) Cu	Mg	Si	Fe
0401	Unreinforced		3.47	1.47	0.03	0.05
0202	2	0.3	3.67	1.54	0.03	0.06
0205	5	0.3	3.68	1.50	0.04	0.14
0210	10	0.3	3.83	1.38	0.06	0.17
0302	2	1.3	3.55	1.57	0.03	0.06
0305	5	1.3	3.84	1.56	0.03	0.08
0310	10	1.3	3.84	1.55	0.04	0.10
0315	15	1.3	3.92	1.57	0.04	0.12

(Cu≈3.7%), it is quite close to the intended composition of Al-4%Cu-1.5%Mg.

4.1.2 Microstructure

There are two distinct distributions of TiB_2 in the as-cast ingots. In the alloys with 1.3 μm TiB_2, the particle distribution was uniform, whereas the alloys with 0.3 μm TiB_2 showed a pronounced cellular solidification structure. Figure 4.1(a-b) shows the difference in the as-cast microstructures in the two 10vol% ingots. The circular lightly shaded areas of Fig. 4.1(a) are regions of very low TiB_2 content.

As discussed by Stefanescu, Dhindaw, Kacar, and Moitra [1] there is a critical solidification-front velocity, V_{cr} above which the particles are engulfed at the liquid/solid interface. Below the critical velocity the particles are pushed. Omenyi and Neumann [2] showed that the critical velocity is related to the particle radius by:

$$V_{cr} = K\, r^{-n} \qquad (1)$$

where K is a constant and the exponent, n, ranges from 0.28 to 0.90. This equation shows that small particles are more likely to be rejected from the solidification front than large particles.

All of the Al-4%Cu-1.5%Mg alloys were cast under the same conditions, with the same amount of super-heat, and thus the same solidification rate; only the particle size of the TiB_2 reinforcement was different. Therefore, the difference in the as-cast structures of the alloys must be attributable to the difference in the critical velocities at these two particle

(b)

(a)

Figure 4.1 Optical micrographs of the as-cast microstructure of Al-4%Cu-1.5%Mg alloys with 10vol% TiB_2 of two particle sizes, (a) 0.3 μm and (b) 1.3 μm.

sizes. In the 0.3 μm TiB_2 ingots, the solidification rate was less than the critical velocity and the particles were rejected, whereas the solidification rate was greater than the critical velocity in the 1.3 μm ingots and the particles were engulfed.

The solidification cell structure of the 0.3 μm TiB_2 ingots was not eliminated by subsequent processing. Figure 4.2(a-b) shows orthogonal views of the extruded microstructure for the two 10% alloys. The 0.3 μm TiB_2 alloy [Fig. 4.2(a)] has particle-deficient regions that are elongated in the direction of extrusion, whereas the 1.3 μm TiB_2 alloy [Fig. 4.2(b)] has a uniform distribution of particles. The contrast between the extrusions and the various loadings is shown in greater detail in Figs. 4.3(a-c) and 4.4(a-d) where long transverse sections of the 0.3 μm and 1.3 μm alloys are shown.

The as-cast microstructure of the base and reinforced alloys contained coarse intermetallics typically observed in 2000-series alloys. These intermetallics are associated with the last eutectic liquid to solidify. In the as-extruded 0.3 μm TiB_2 alloys (shown in Fig. 4.3), the intermetallics are clearly associated with TiB_2 particle clusters. These clusters represent the TiB_2 particles and eutectic liquid that were rejected during solidification and were the last liquid to freeze. In the extruded 1.3 μm TiB_2 alloys the intermetallics are associated with TiB_2 particle clumps in the 2% loading alloy, Fig. 4.4(a), whereas in the alloys with higher loadings the intermetallics are randomly distributed and the TiB_2 clumps are not observed. This indicates that,

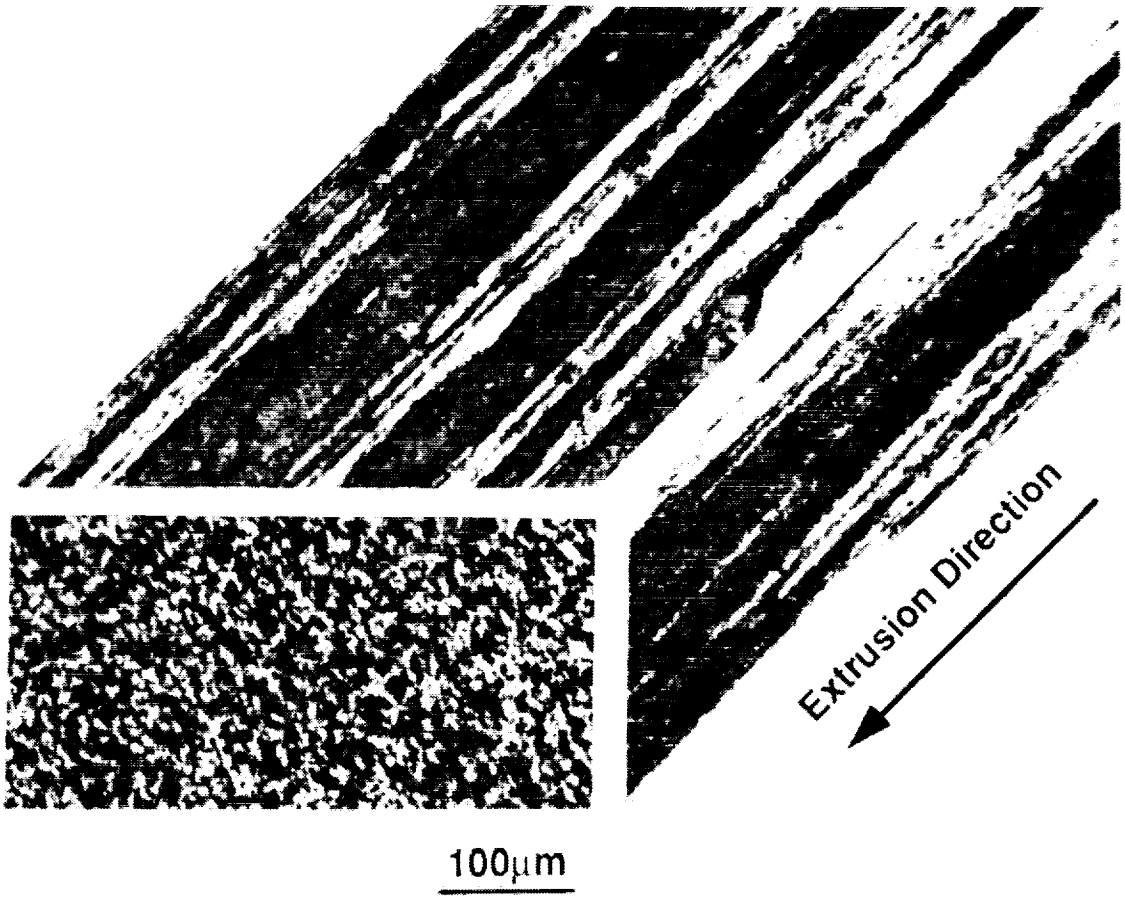

Figure 4.2(a) Orthogonal views of the extruded microstructure of alloys containing 10vol% TiB_2 particles with an average diameter of 0.3 μm.

ORIGINAL PAGE
BLACK AND WHITE PHOTOGRAPH

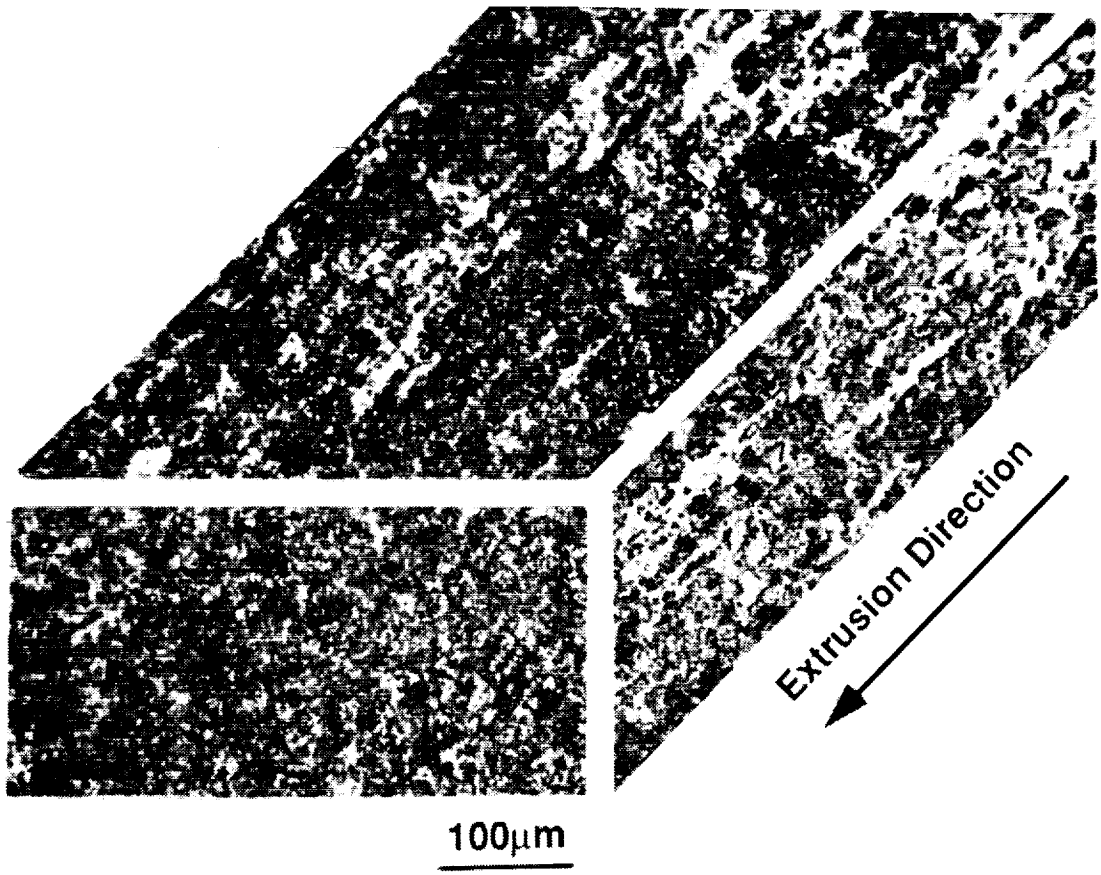

Figure 4.2(b) Orthogonal views of the extruded microstructure of alloys containing 10vol% TiB_2 particles with an average diameter of 1.3 μm.

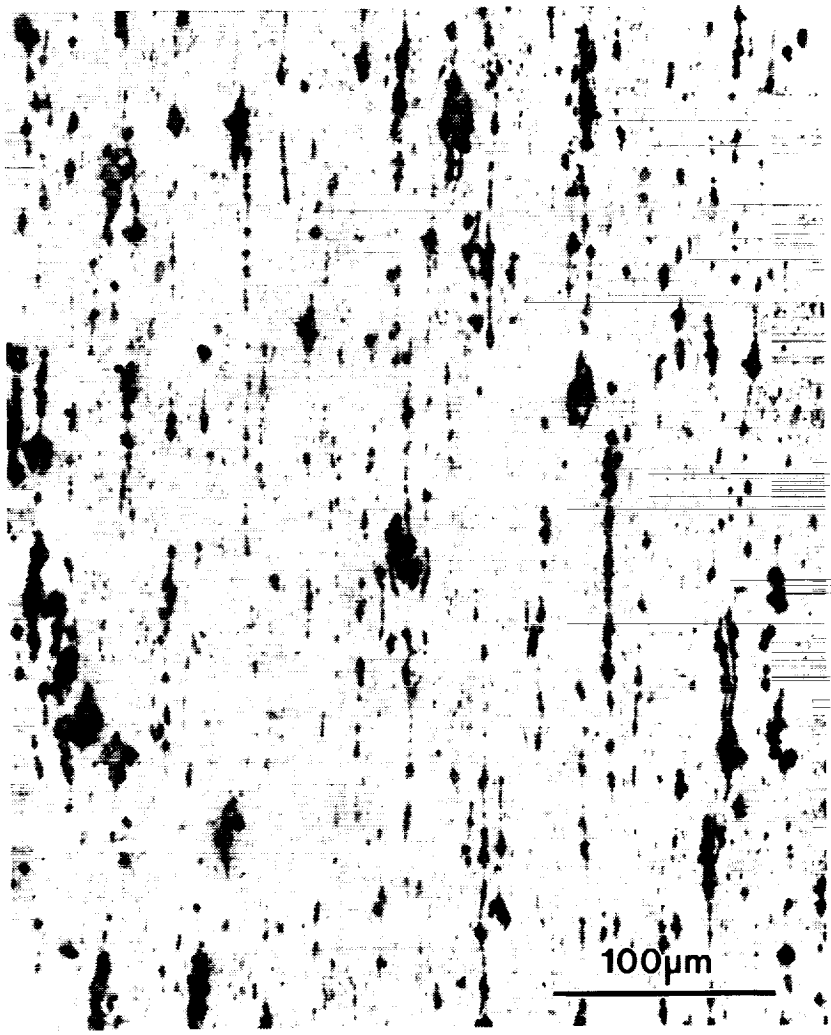

Figure 4.3(a) Optical micrographs of the long transverse direction of the extruded alloys with 0.3 μm particles of 2vol% TiB_2.

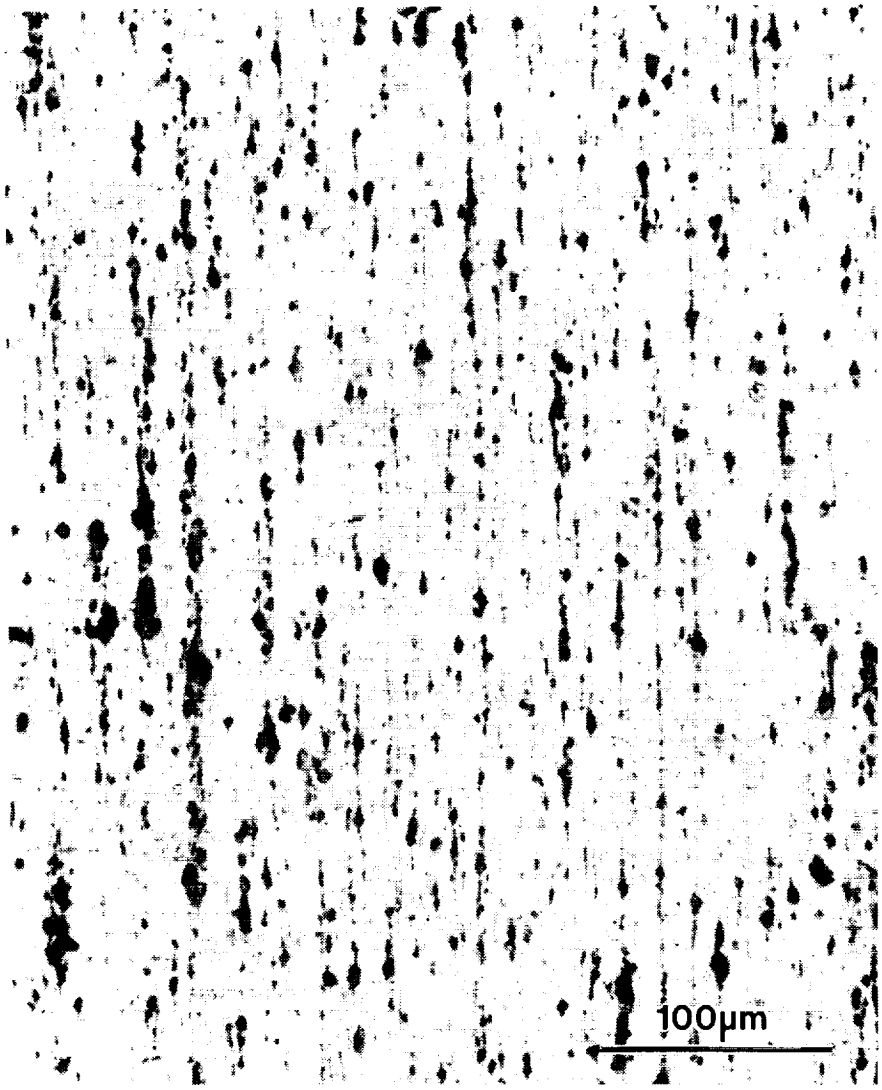

Figure 4.3(b) Optical micrographs of the long transverse direction of the extruded alloys with 0.3 μm particles of 5vol% TiB_2.

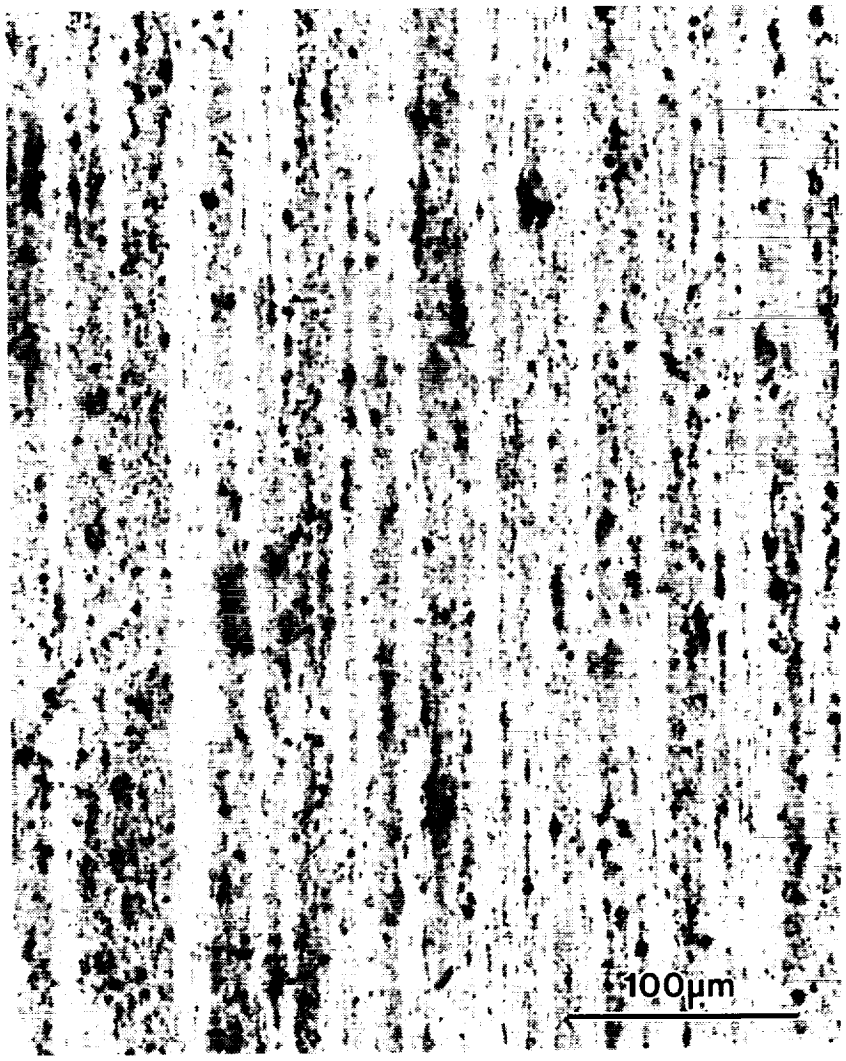

Figure 4.3(c) Optical micrographs of the long transverse direction of the extruded alloys with 0.3 μm particles of 10vol% TiB_2.

ORIGINAL PAGE
BLACK AND WHITE PHOTOGRAPH

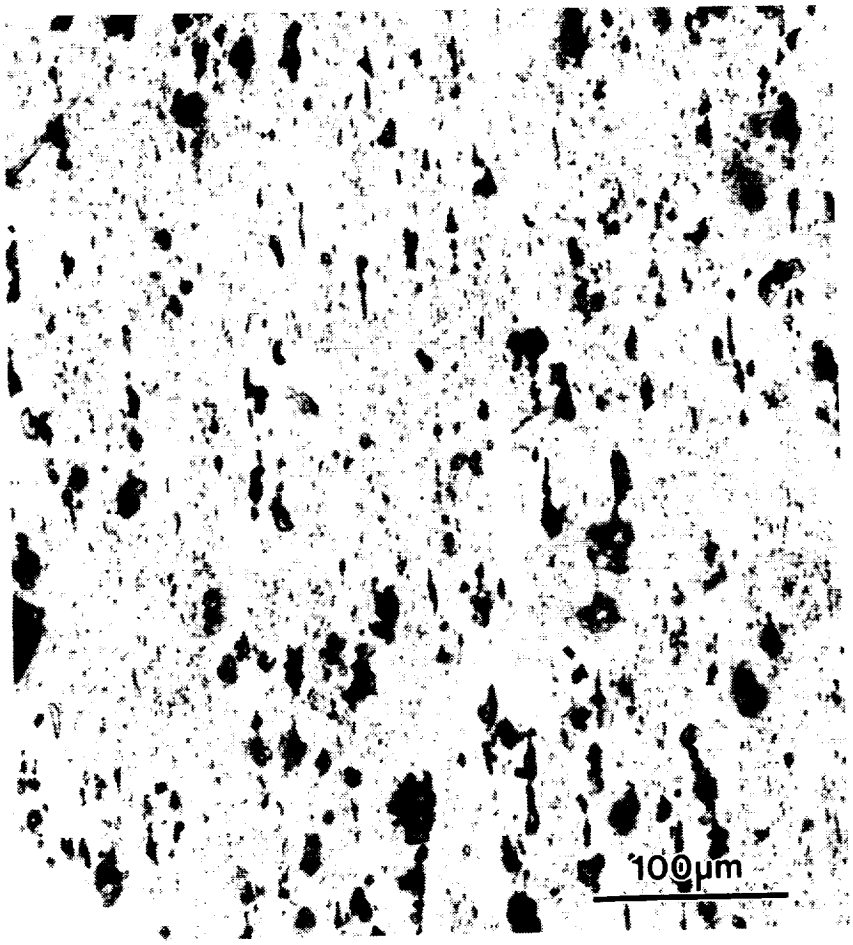

Figure 4.4(a) Optical micrographs of the long transverse direction of the extruded alloys with 1.3 μm particles of 2vol% TiB_2.

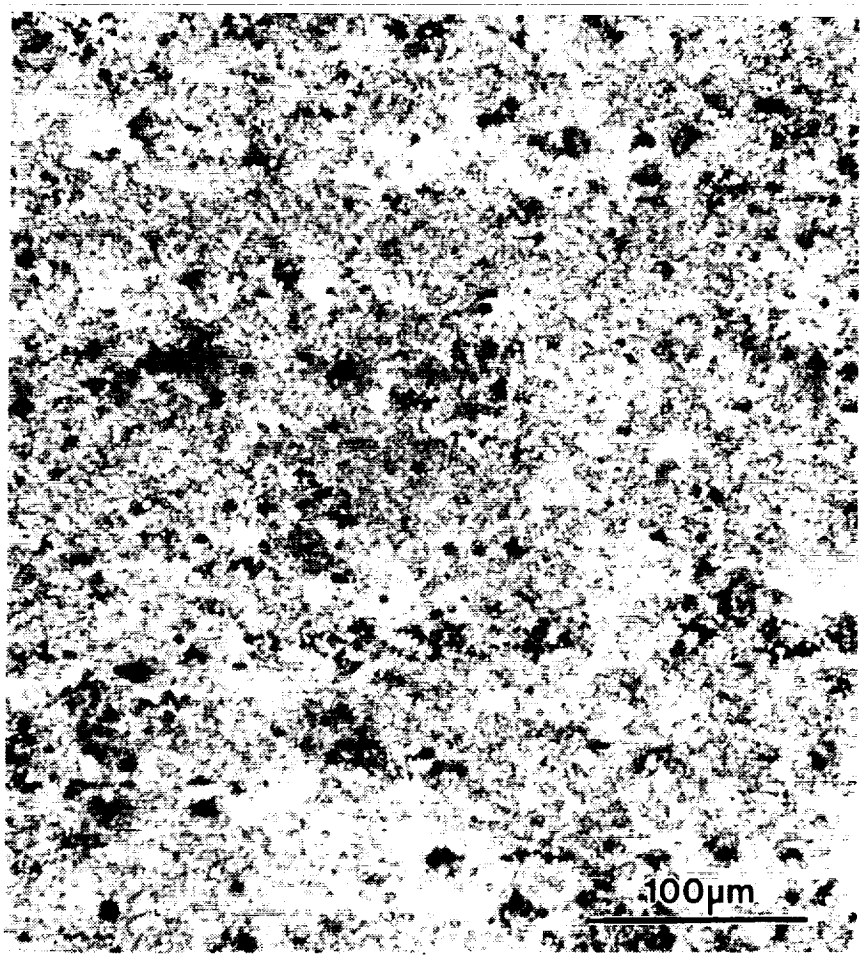

Figure 4.4(b) Optical micrographs of the long transverse direction of the extruded alloys with 1.3 μm particles of 5vol% TiB_2.

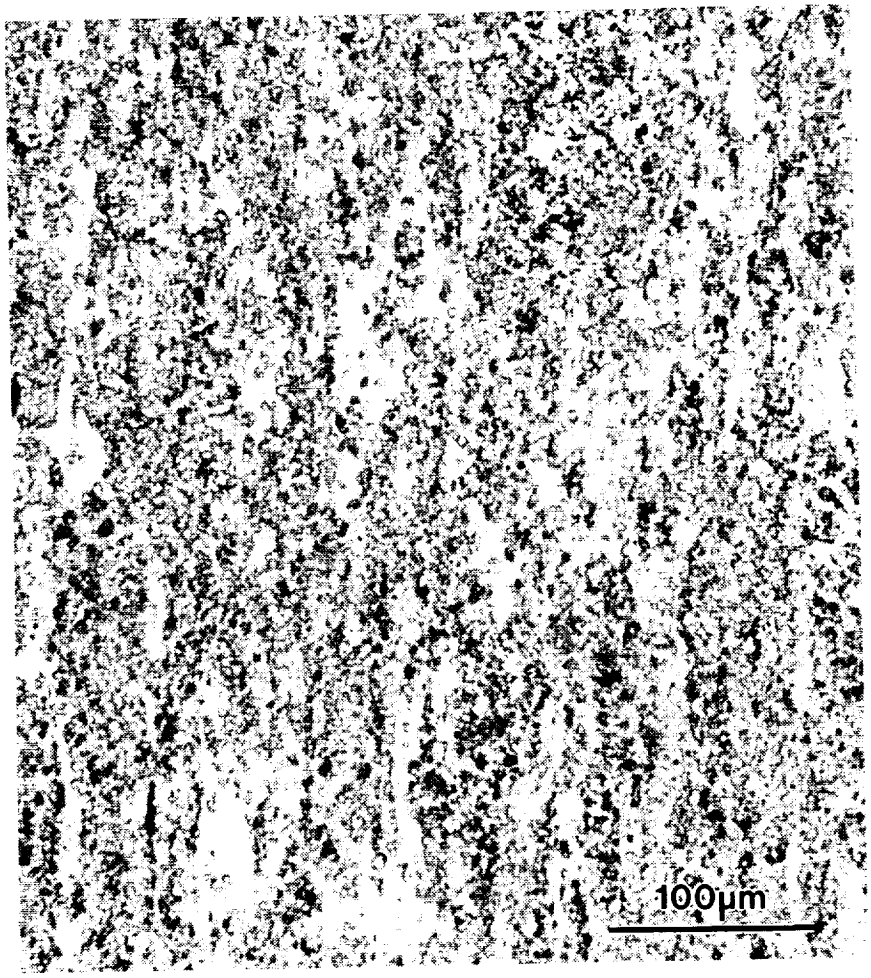

Figure 4.4(c) Optical micrographs of the long transverse direction of the extruded alloys with 1.3 μm particles of 10vol% TiB_2.

Figure 4.4(d) Optical micrographs of the long transverse direction of the extruded alloys with 1.3 μm particles of 15vol% TiB_2.

except in the 2% loading, the 1.3 μm TiB_2 were not pushed by the advancing solidification front.

4.2 Elastic Modulus

An important advantage of the MMC's is that they have a much higher modulus than that of the unreinforced matrix. In Fig. 4.5, Young's modulus (determined by ultrasonic measurements) is plotted as a function of volume fraction and particle size. These measurements were taken from extruded samples that were solutionized and naturally aged, although typically the modulus of aluminum alloys is independent of heat treatment. As the figure shows, the modulus of the alloy increased with increasing TiB_2 additions. For example, the modulus increased 30% with the addition of 15% reinforcement. Within the accuracy of this technique, particle size had no apparent effect on modulus.

Because of the anisotropic distribution of particles observed in the extruded microstructure, the variation of modulus with orientation was examined for the unreinforced and the two 10% TiB_2 alloys. As Table 4.2 shows, there was a very slight increase in elastic modulus in the longitudinal direction of all three alloys, but the size of this difference was not dependent on the particle size, distribution, or loading. Hence, the anisotropic distribution of particles in the 0.3 μm TiB_2 alloys is not manifest in the modulus. It is likely that the 0.1 msi increase observed in the longitudinal direction was due to the alloys having a slight crystallographic texture as a result of extrusion.

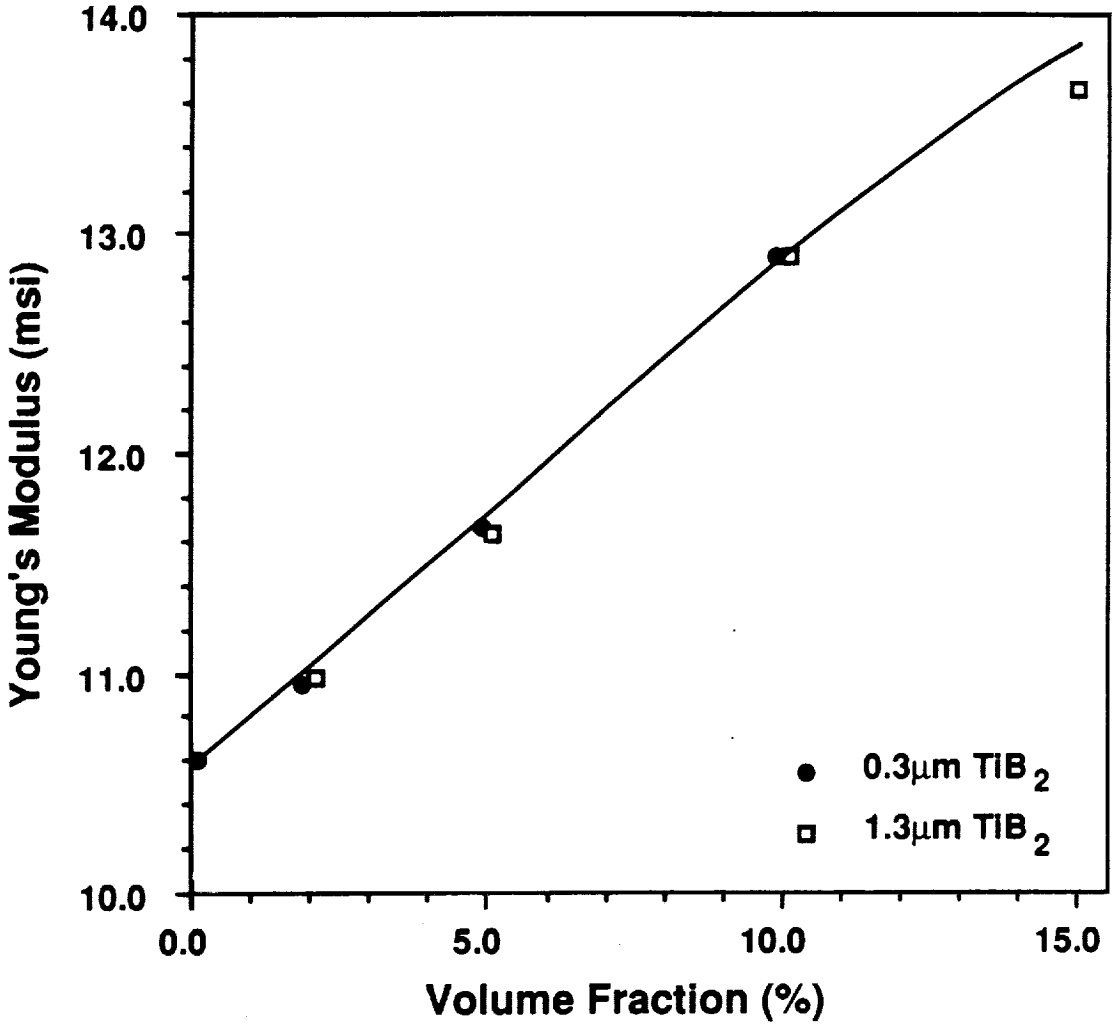

Figure 4.5 Dependence of Young's modulus on volume fraction of TiB_2 for the Al-4%Cu-1.5%Mg alloys.

Table 4.2

Young's Modulus of Al-4%Cu-1.4%Mg Extrusion vs Direction in Extruded Bar.

	Short Transverse (msi)	Long Transverse (msi)	Longitudinal (msi)	Density (g/cm^3)
Unreinforced	10.6	10.6	10.7	2.73
10vol% 0.3 μm TiB_2	12.9	12.8	13.0	2.93
10vol% 1.3 μm TiB_2	12.9	12.8	12.9	2.92

4.3 Tensile Properties

4.3.1 Isothermal-aging response

To determine the proper solutionizing temperature for these materials, differential thermal analysis (DTA) was performed on several of the TiB_2 reinforced alloys and the unreinforced alloy. In all of the alloys tested the onset of melting was found to occur at 940°F (504°C). There was no notable variation in this temperature with either loading or particle size. This temperature is consistent with the ternary phase diagram and is quite near the reported Al-Al_2Cu-Al_2CuMg eutectic temperature of 937°F [3]. For Al-4%Cu-1.5%Mg the ternary phase diagram indicates that the solvus and solidus are separated by approximately 40°F. Based on these results a solutionizing temperature of 920°F (493°C) was chosen.

After solutionizing for 2 hours, the alloys were quenched into cold water and allowed to naturally age for a minimum of 7 days. The hardness following solutionizing became constant after about 3 days; thus 7 days represents a substantially stable condition. Tensile blanks of the alloys were then artificially aged for various lengths of time at 350°F (177°C), 375°F (190°C), and 400°F (204°C) and allowed to air cool. These tensile samples were then tested in a screw-driven mechanical test frame using either an extensometer or a strain gauge. The strain gauges were used to obtain an accurate measurement of the proportional limit and initial work-hardening rate, whereas the extensometer was used to simplify the tests for which an accurate 0.2% offset yield was

sufficient.

Typically, the aging behavior of an aluminum alloy can be examined through hardness measurements taken as a function of aging time. However, hardness measurements obtained on the alloys showed a great deal of scatter and were not deemed to be reliable. For example, Fig. 4.6 shows the aging response of Al-4%Cu-1.5%Mg with 10% of 0.3 μm TiB_2 at 375°F, as determined by Vicker's and Rockwell B hardness and tensile tests. Clearly, the hardness measurements did not follow the trend in the tensile results for this material. In contrast, the tensile aging response of Al-4%Cu-1.5Mg with 10% 1.3 μm TiB_2 at 375°F, shown in Fig. 4.7, correlated quite well with the hardness results. The disparity between the tensile and hardness results for the 0.3 μm TiB_2 alloys is believed to be related to the poor distribution of TiB_2 in these alloys. Because the aging behavior could not be determined accurately using hardness measurements for the small-particle TiB_2 alloys, it was decided to use tensile tests to determine the aging response throughout this study.

Figure 4.8(a) shows the variation of yield stress with aging time at 375°F for the 0.3 μm TiB_2 containing alloys. In samples aged from the T4 condition, strength initially dropped (regression) and then increased until it reached a maximum (the peak aged, i.e., T6 condition), and then declined. Materials aged beyond the peak aged condition are referred to as overaged. The isothermal-aging response is plotted on a logarithmic scale in Fig. 4.8(b).

In Fig. 4.8(c), the elongations to fracture in a 1 in.

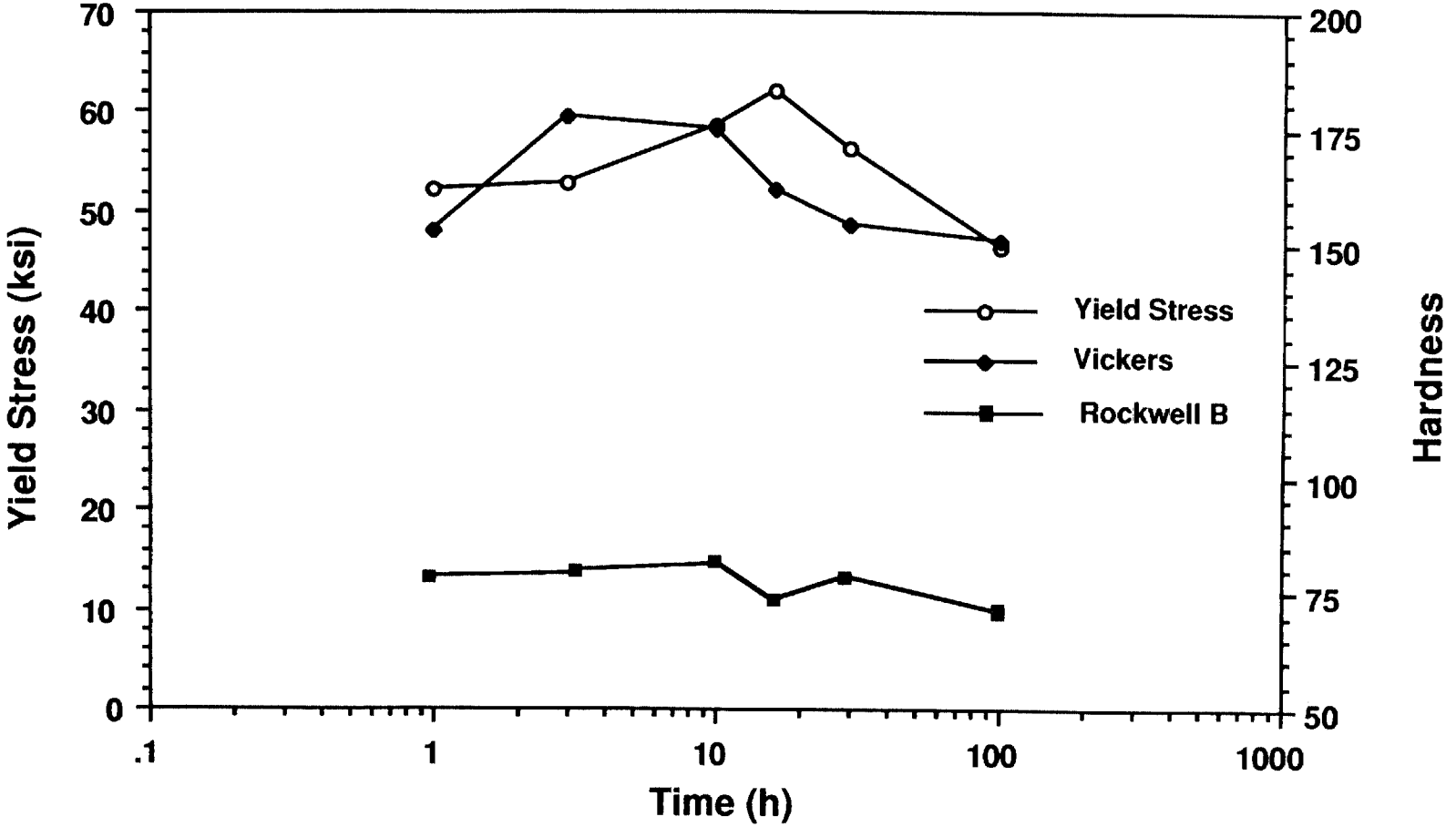

Figure 4.6 Aging response of the Al-4%Cu-1.5%Mg with 10vol% 0.3 μm TiB_2 particles, as measured by a tensile test, Vicker's microhardness, and Rockwell hardness.

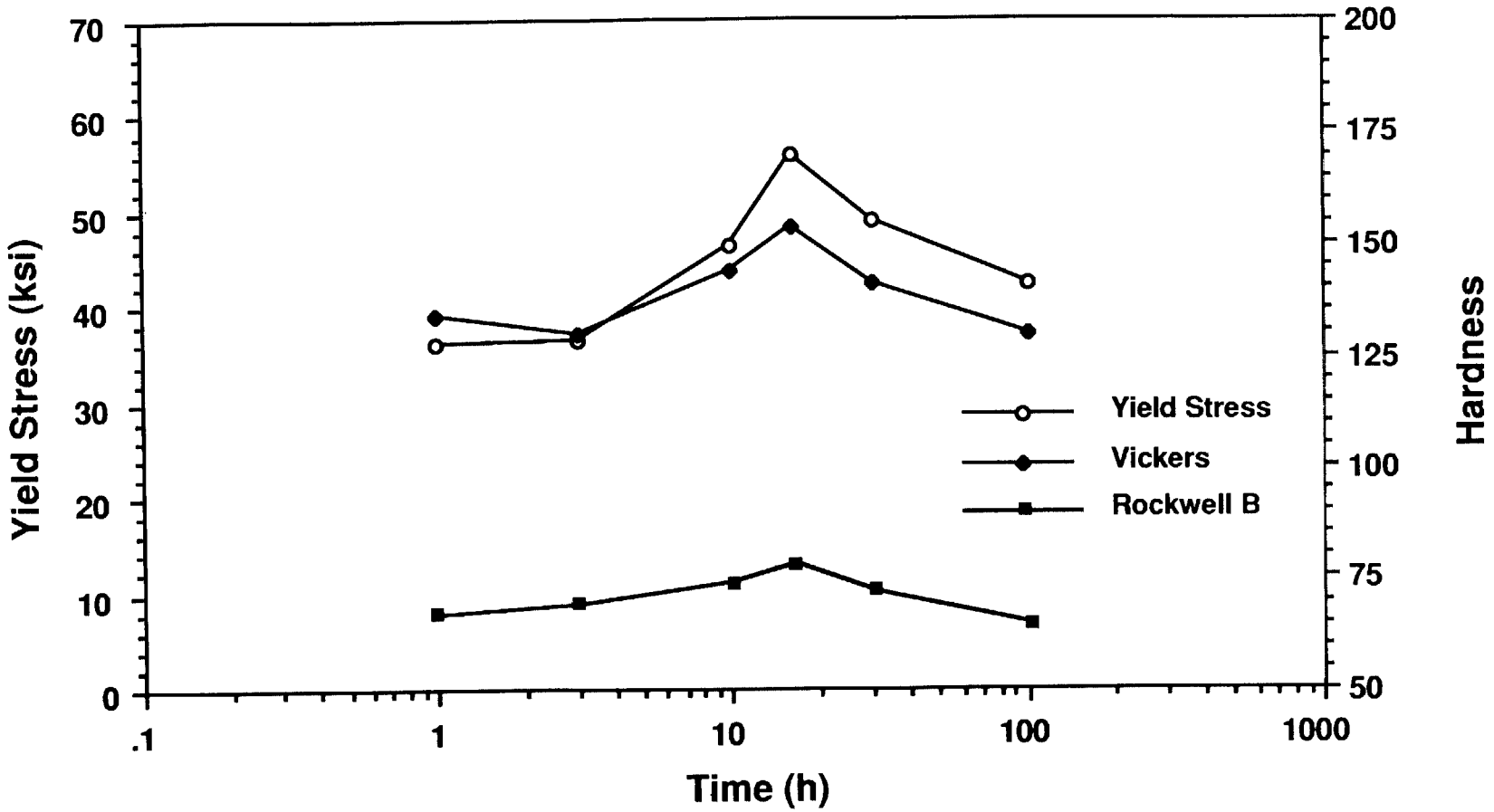

Figure 4.7 Aging response of the Al-4%Cu-1.5%Mg with 10vol% 1.3 μm TiB_2 particles, as measured by a tensile test, Vicker's microhardness, and Rockwell hardness.

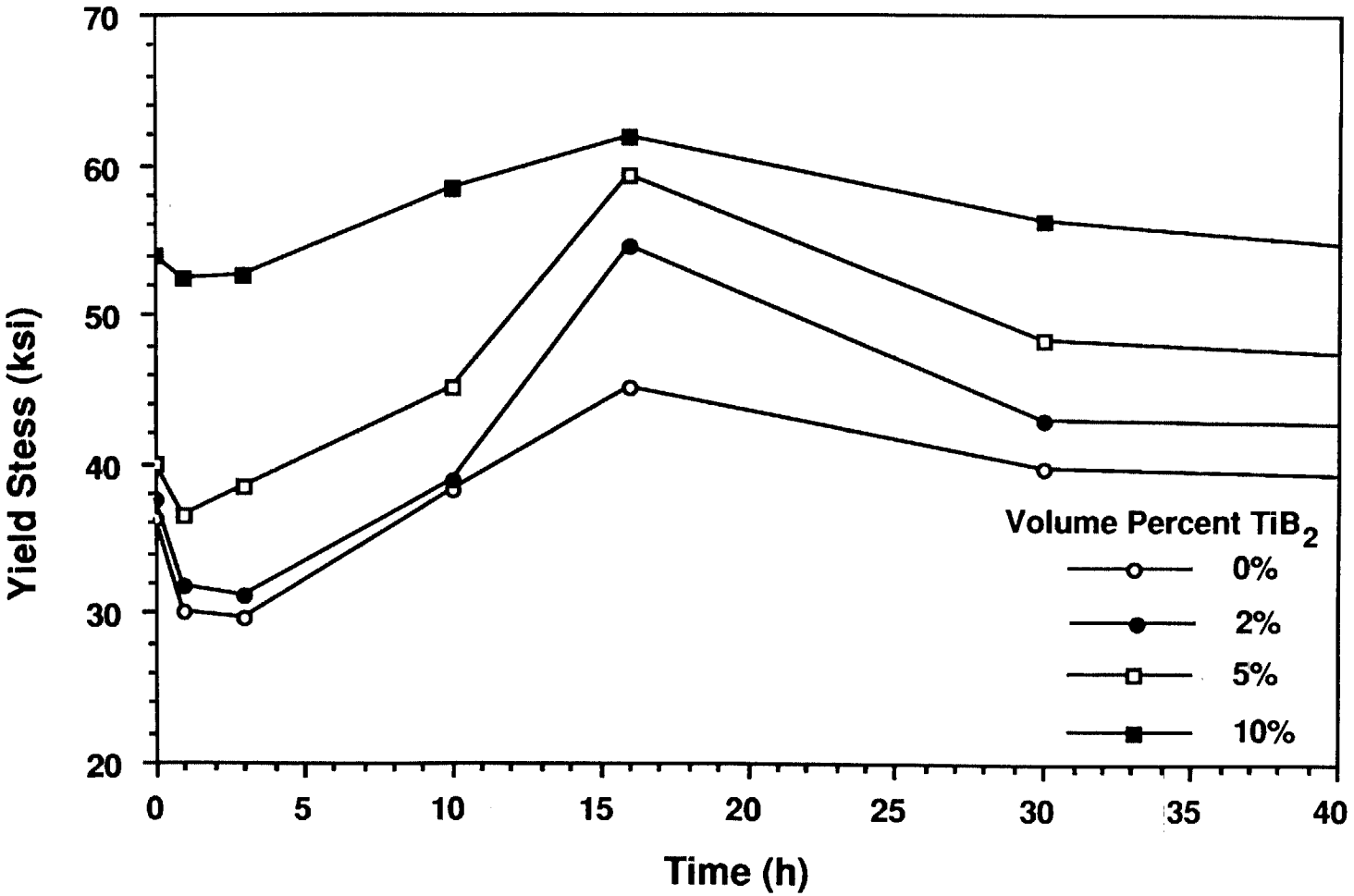

Figure 4.8(a) Variation of yield stress with time of aging at 375°F for the Al-4%Cu-1.5%Mg alloys containing 0.3 μm TiB_2 particles.

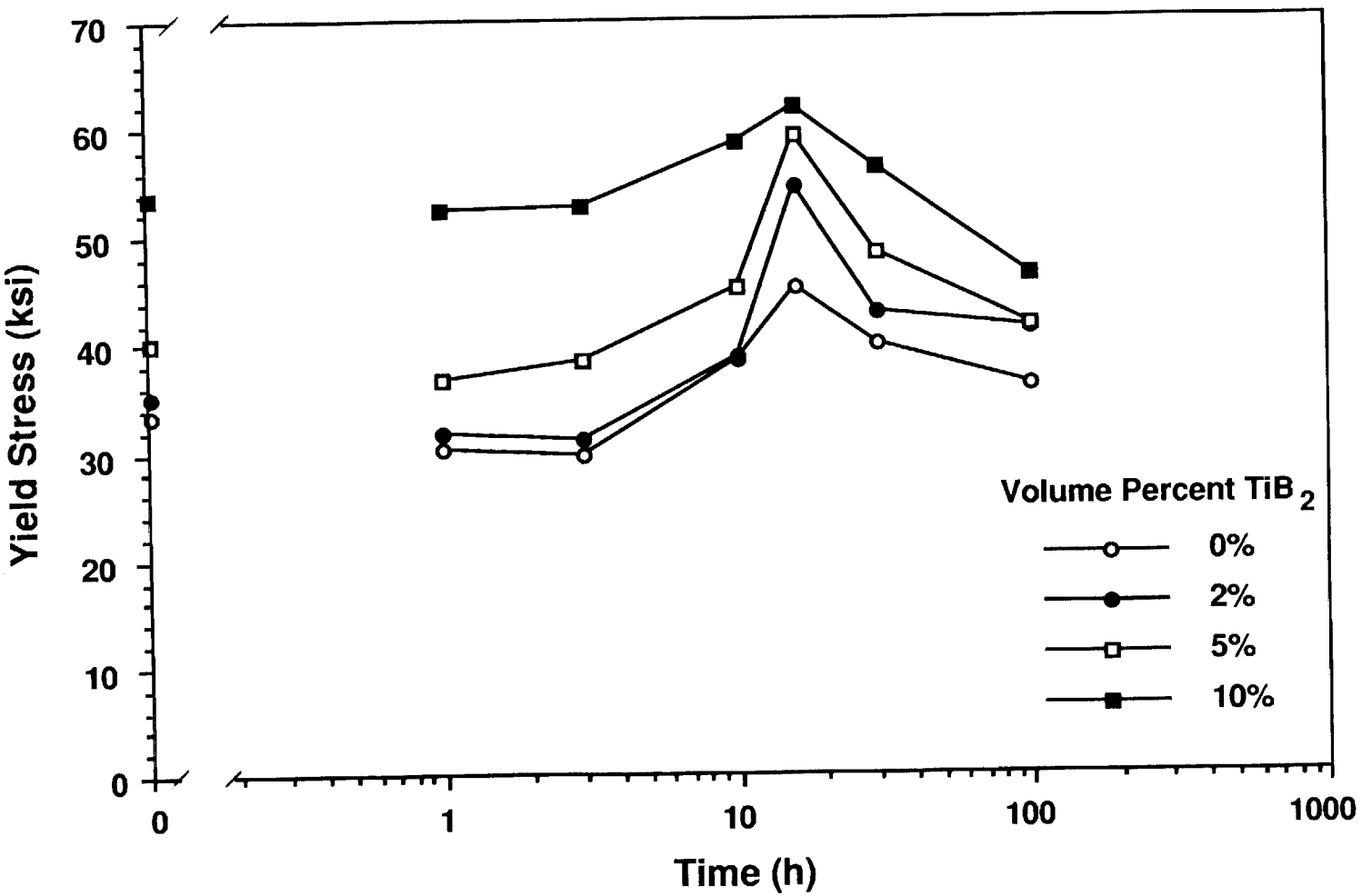

Figure 4.8(b) Variation of yield stress with time of aging at 375°F for the Al-4%Cu-1.5%Mg alloys containing 0.3 μm TiB_2 particles.

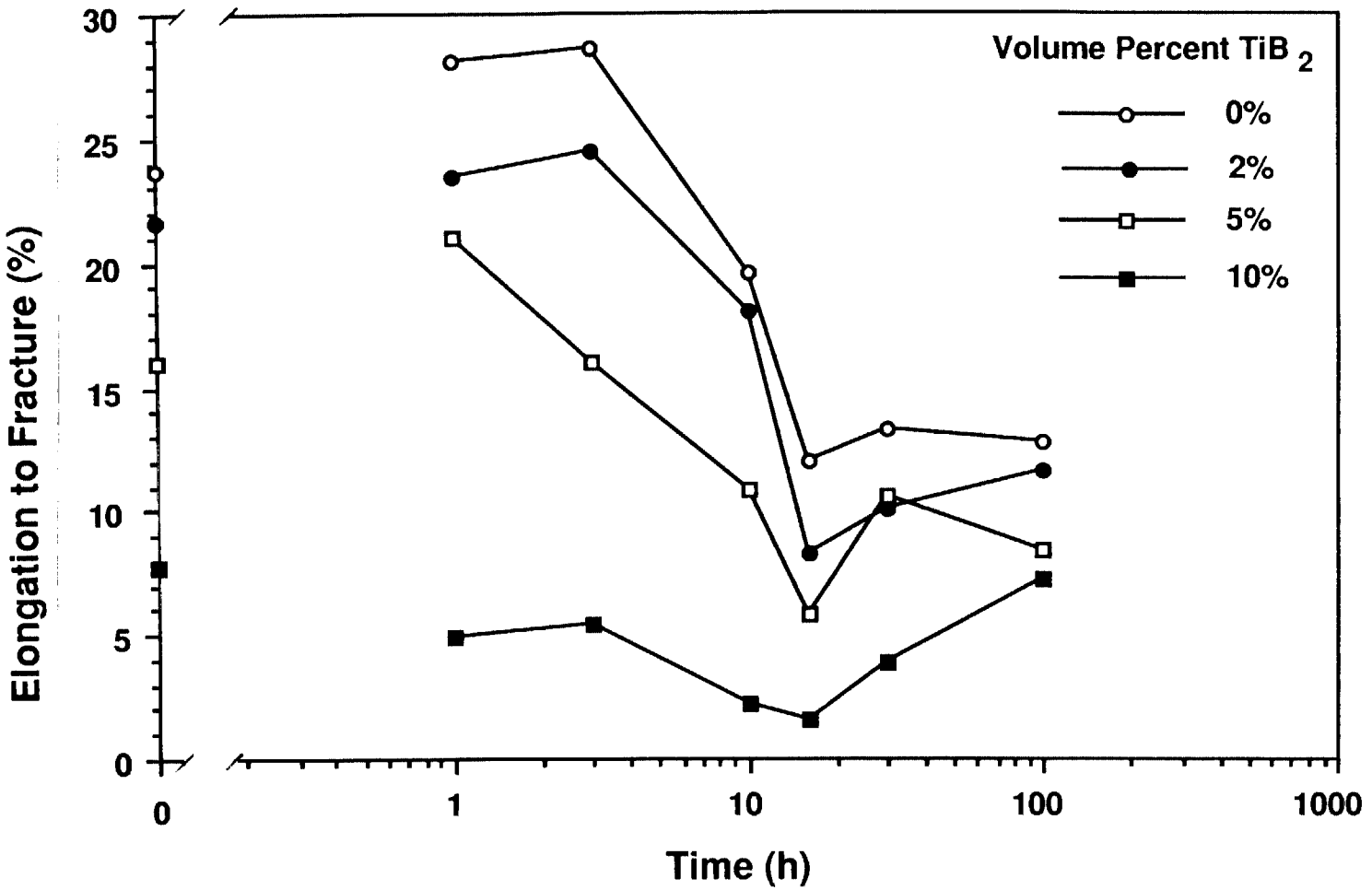

Figure 4.8(c) Variation of elongation to fracture with time of aging at 375°F for the Al-4%Cu-1.5%Mg alloys containing 0.3 μm TiB_2 particles.

gauge length are plotted for the 0.3 μm alloys at the same aging times shown in Fig. 4.8(b). For all volume fractions of TiB_2, elongation decreased with aging reaching a minimum at the peak-aged condition. Beyond this point, elongation increased, but not dramatically.

Figure 4.9(a-c) shows the isothermal-aging behavior at 375°F for the 1.3 μm TiB_2 containing alloys. The behavior was nearly identical to that observed in the alloys containing 0.3 μm TiB_2, although the smaller particles showed greater strength at the same loading.

Figures 4.10 and 4.11 show the variation of yield stress with time of aging at 350°F for the 0.3 μm and 1.3 μm TiB_2 containing alloys, and Figs. 4.12 and 4.13 show the variation at 400°F.

The data at all three aging temperatures show that the overall isothermal-aging behavior, as well as the time to peak strength, was not affected by the TiB_2 loading or particle size. This implies that the precipitation and coarsening sequence (i.e., solid solution → G.P. zones → S' → S) and rate were not altered by the presence of TiB_2. In other ceramic reinforced aluminum alloys, the presence of SiC substantially accelerates the aging time and also affects the distribution of precipitates within the 2024 matrix [4]. Similar results have also been reported for B_4C reinforced 6061 [5]. The practical implication of this is that the information and aging schedules typically used for the matrix can be directly applied to the TiB_2 reinforced alloy.

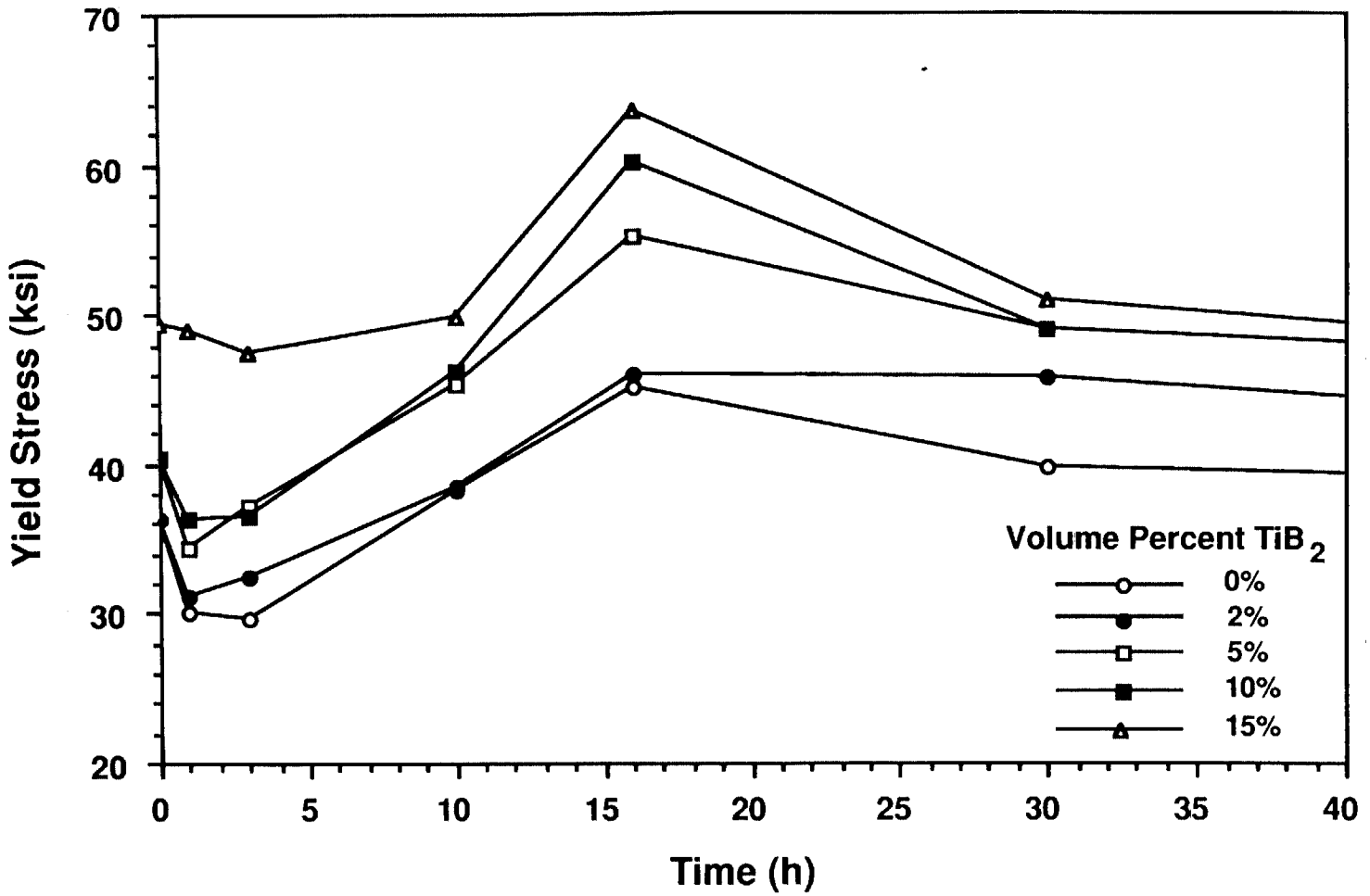

Figure 4.9(a) Variation of yield stress with time of aging at 375°F for the Al-4%Cu-1.5%Mg alloys containing 1.3 μm TiB_2 particles.

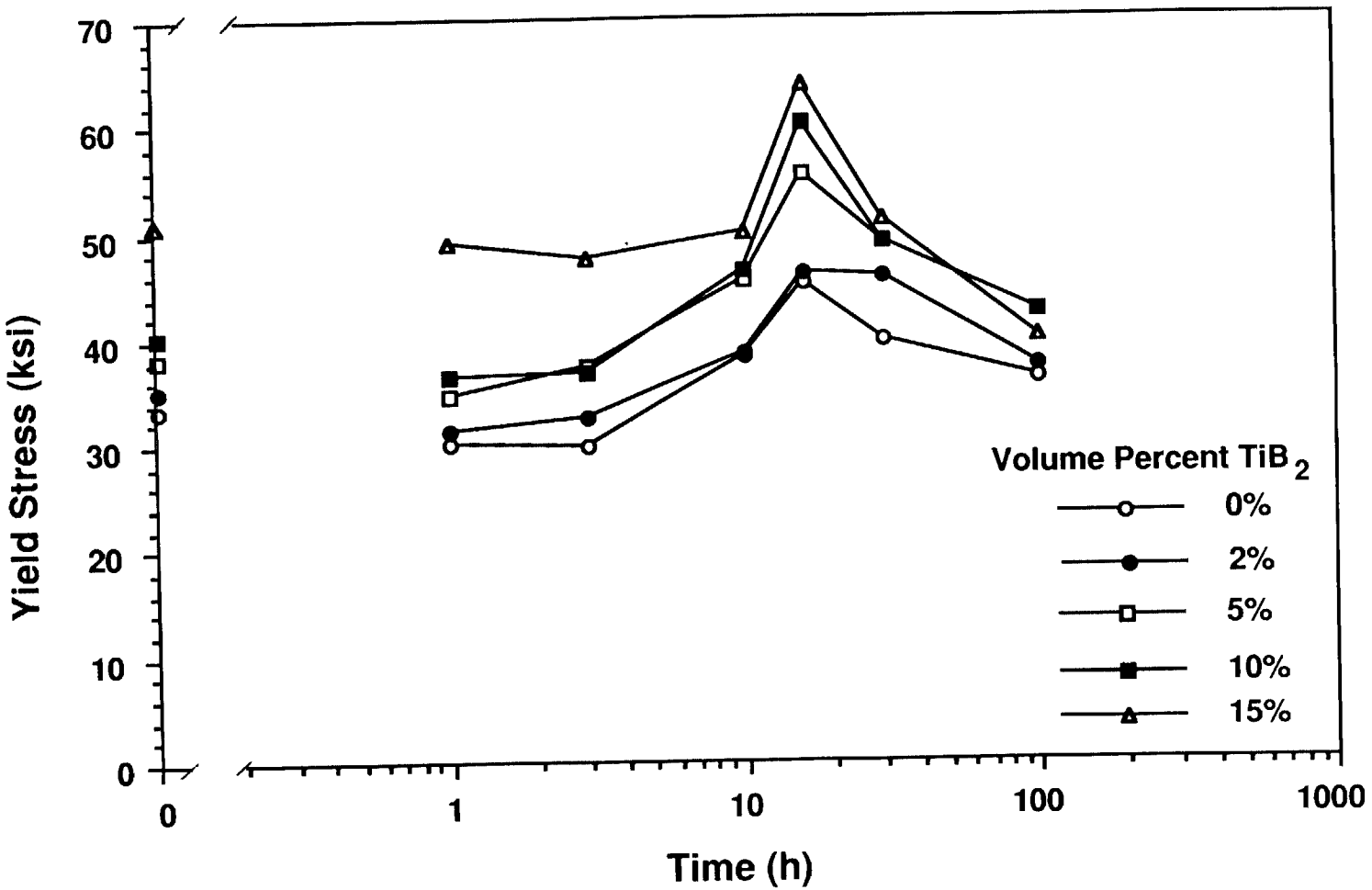

Figure 4.9(b) Variation of yield stress with time of aging at 375°F for the Al-4%Cu-1.5%Mg alloys containing 1.3 μm TiB_2 particles.

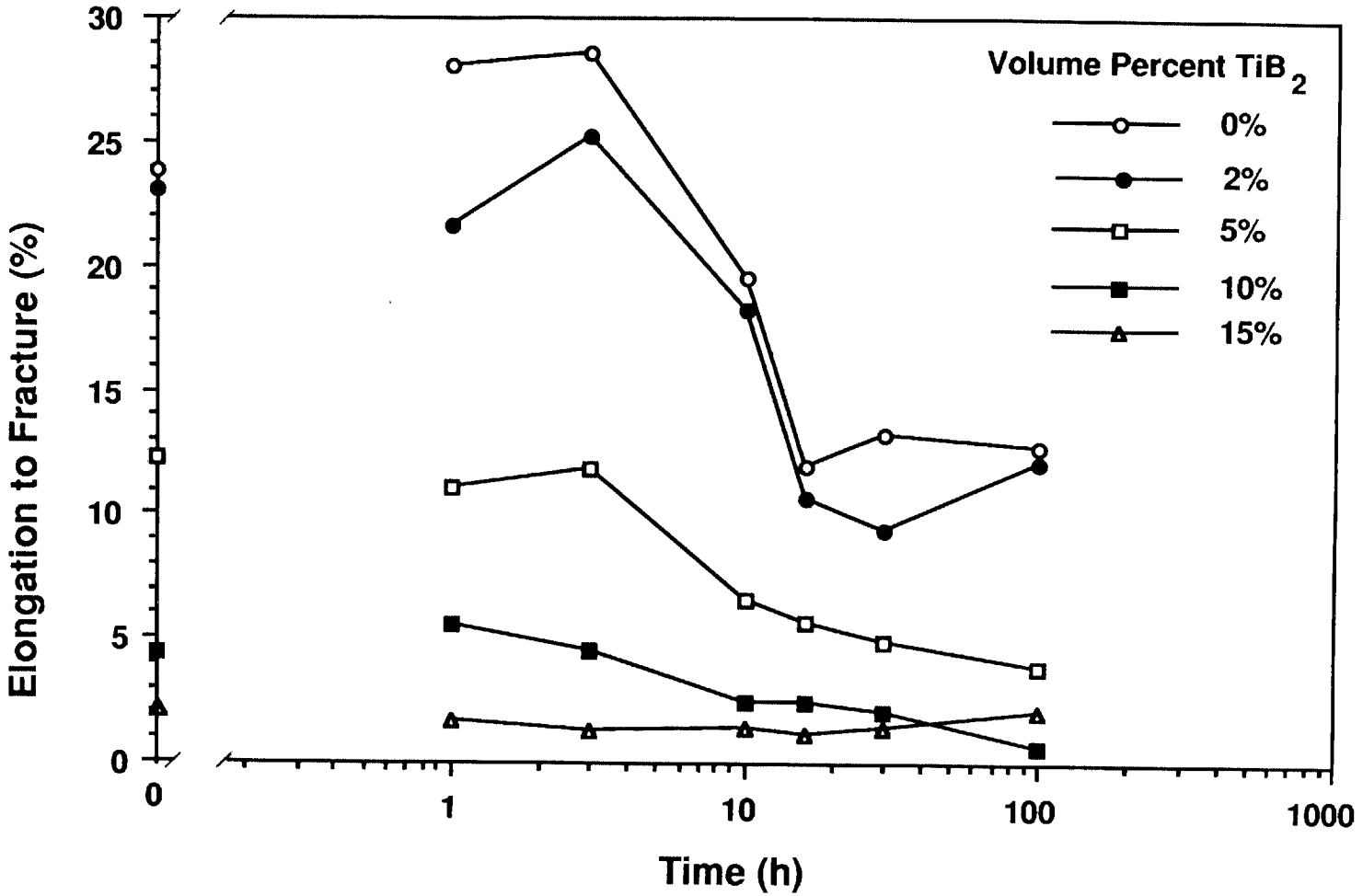

Figure 4.9(c) Variation of elongation to fracture with time of aging at 375°F for the Al-4%Cu-1.5%Mg alloys containing 1.3 μm TiB_2 particles.

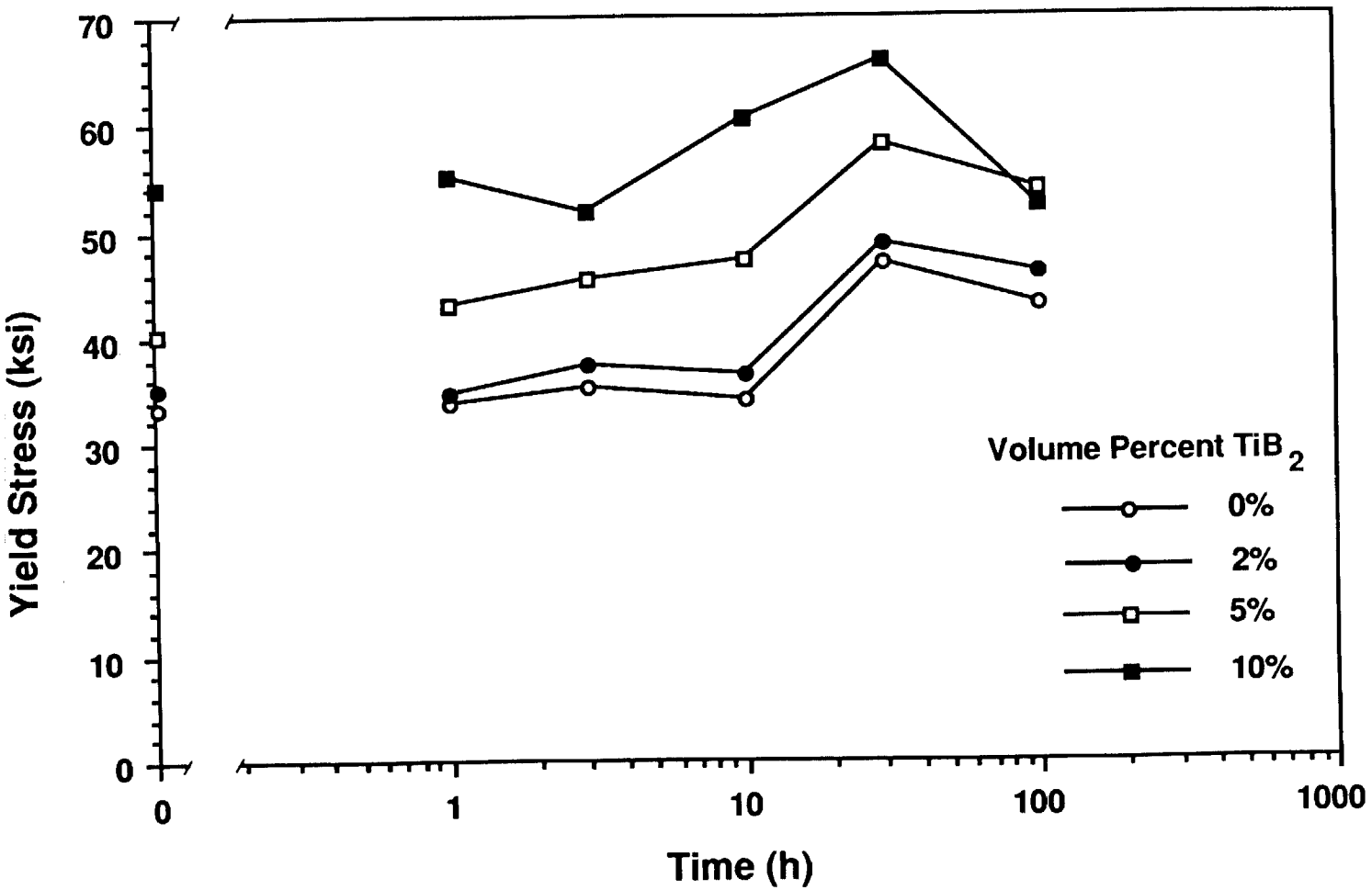

Figure 4.10 Variation of yield stress with time of aging at 350°F for the Al-4%Cu-1.5%Mg alloys containing 0.3 μm TiB_2 particles.

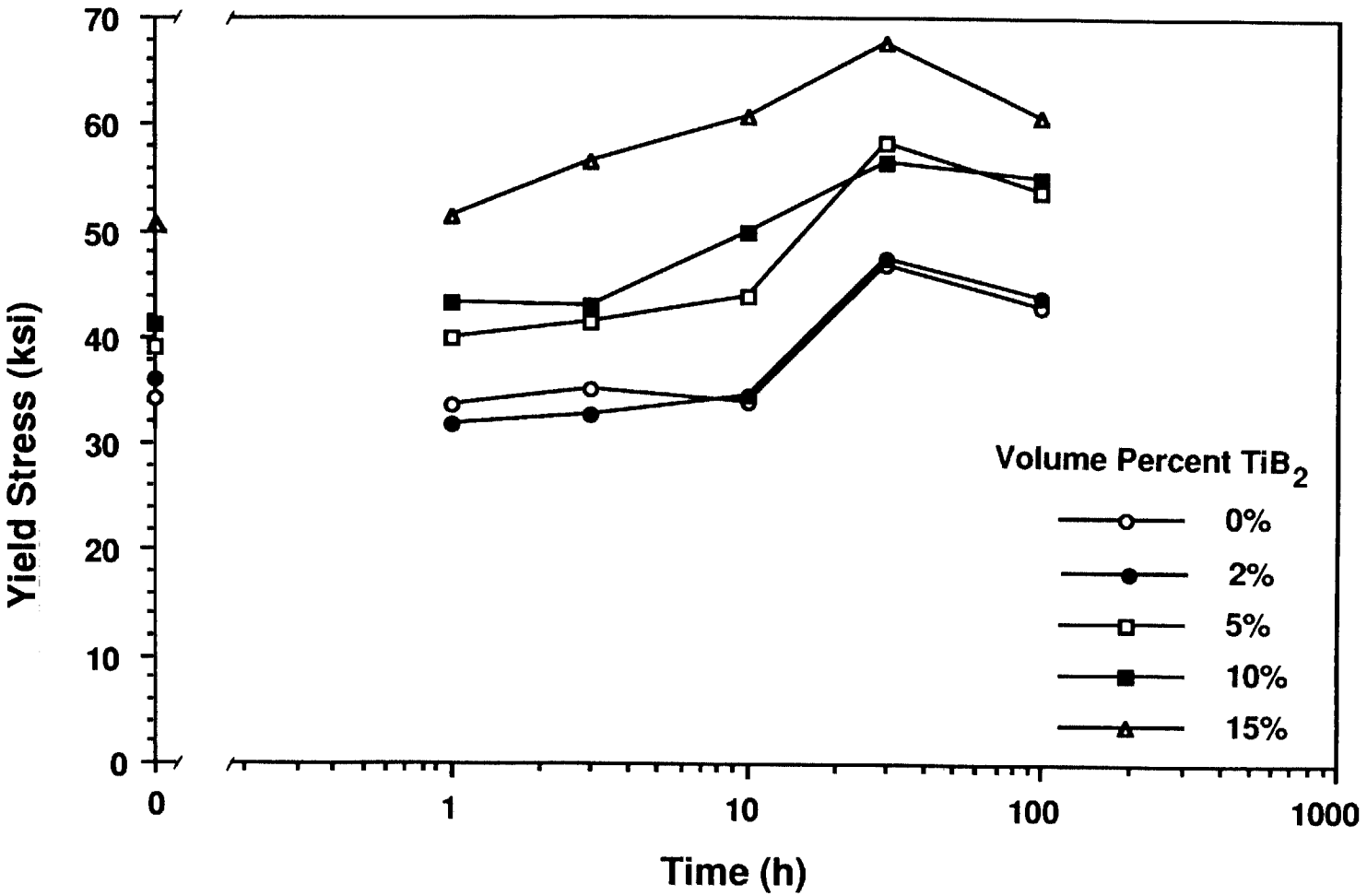

Figure 4.11 Variation of yield stress with time of aging at 350°F for the Al-4%Cu-1.5%Mg alloys containing 1.3 μm TiB_2 particles.

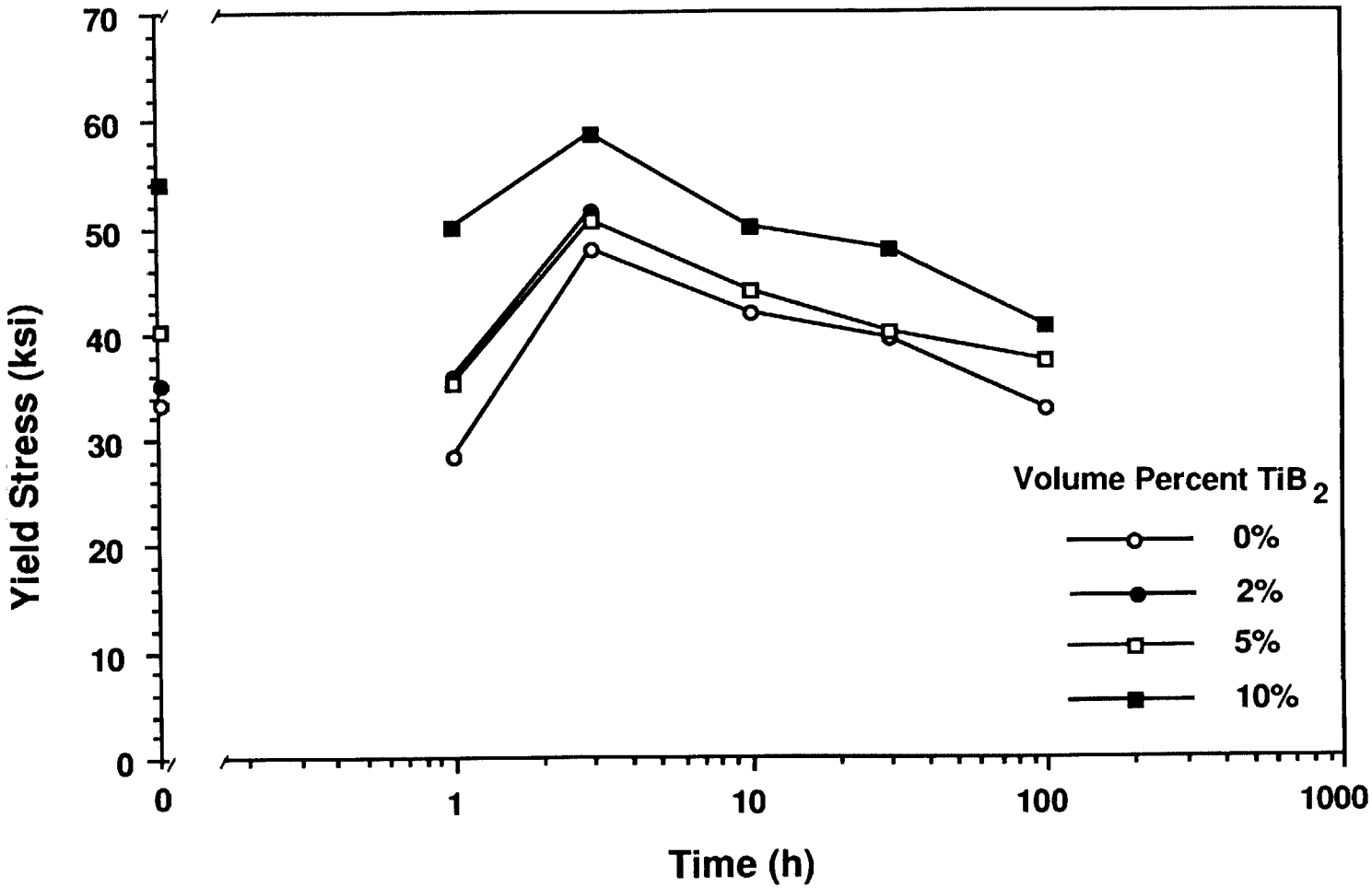

Figure 4.12 Variation of yield stress with time of aging at 400°F for the Al-4%Cu-1.5%Mg alloys containing 0.3 μm TiB_2 particles.

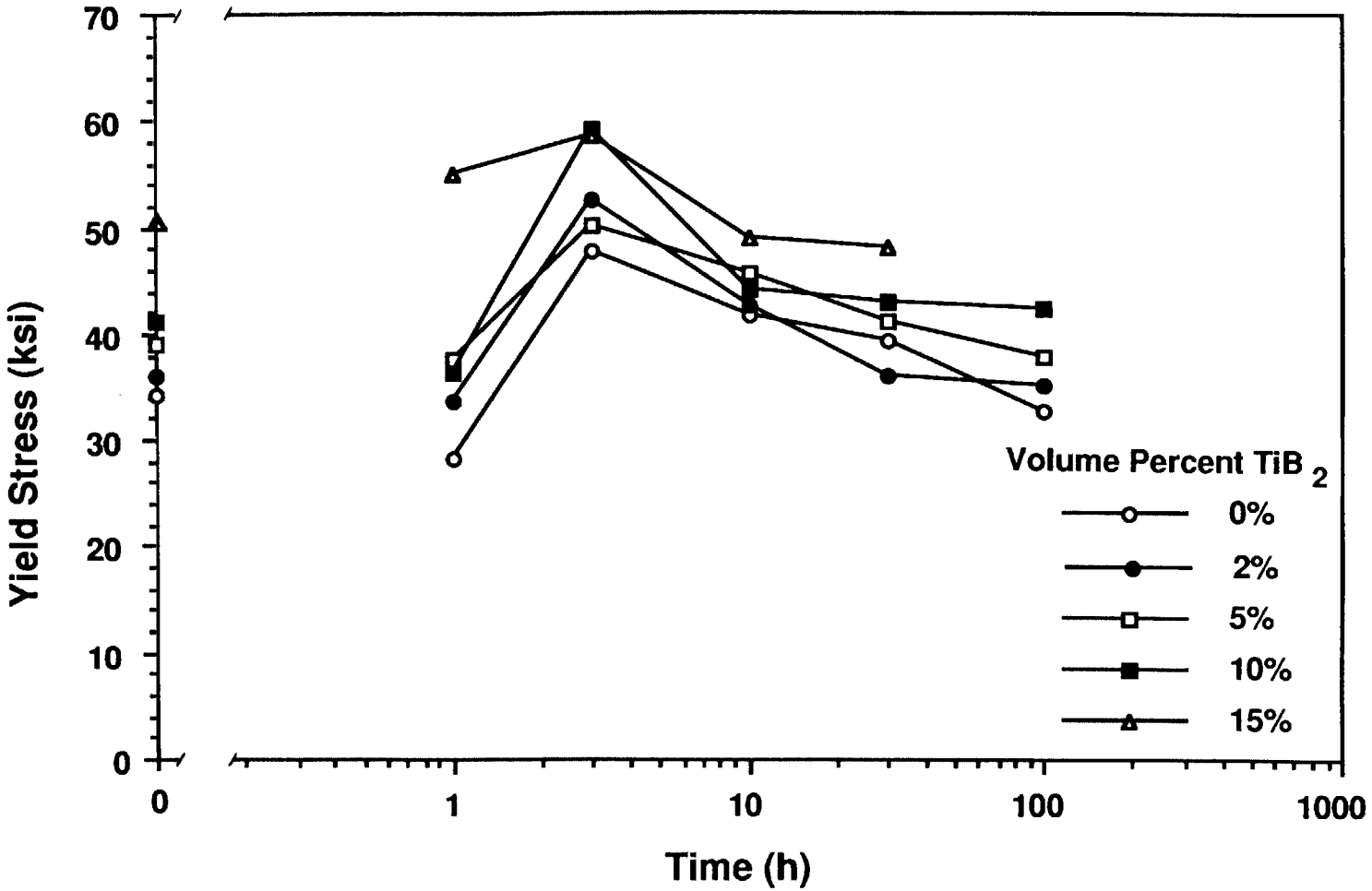

Figure 4.13 Variation of yield stress with time of aging at 400°F for the Al-4%Cu-1.5%Mg alloys containing 1.3 μm TiB_2 particles.

4.3.2 Effect of loading and particle size

To better understand the role of the TiB_2 particles on the tensile properties of these alloys, consider the tensile properties for a few specific aging conditions. In Fig. 4.14, the 0.2% offset yield stress and elongation to fracture are plotted as a function of particle loading and size for the naturally aged (T4) condition. In Fig. 4.15, the yield stress and elongation are plotted for alloys aged at 375°F for 16 hours from the T4 condition, which corresponds to the peak aged (T6) condition. With both heat treatments, the yield stress increased with increasing particle loading. At any given loading, the alloys with the small particles showed a greater increase in strength than the large particles. Additionally, for both heat treatments the elongation decreased as particle loading increased, regardles of particle size.

To determine whether the increase in 0.2% offset yield stress is due to plastic yielding at a high stress or is simply a result of differences in the work-hardening rate of the various alloys, consider the variation of the proportional limit (the first deviation of the stress-strain curve from perfect linear elasticity) with particle loading. The proportional limit and the 0.2% offset yield stress are shown in Fig. 4.16 for the alloys containing the 0.3 μm TiB_2 particles in the T6 condition. Figure 4.17 shows a similar plot for the alloys containing the 1.3 μm TiB_2 also, in the T6 condition. In both figures, the proportional limit changed at nearly the same rate as the yield stress, steadily increasing

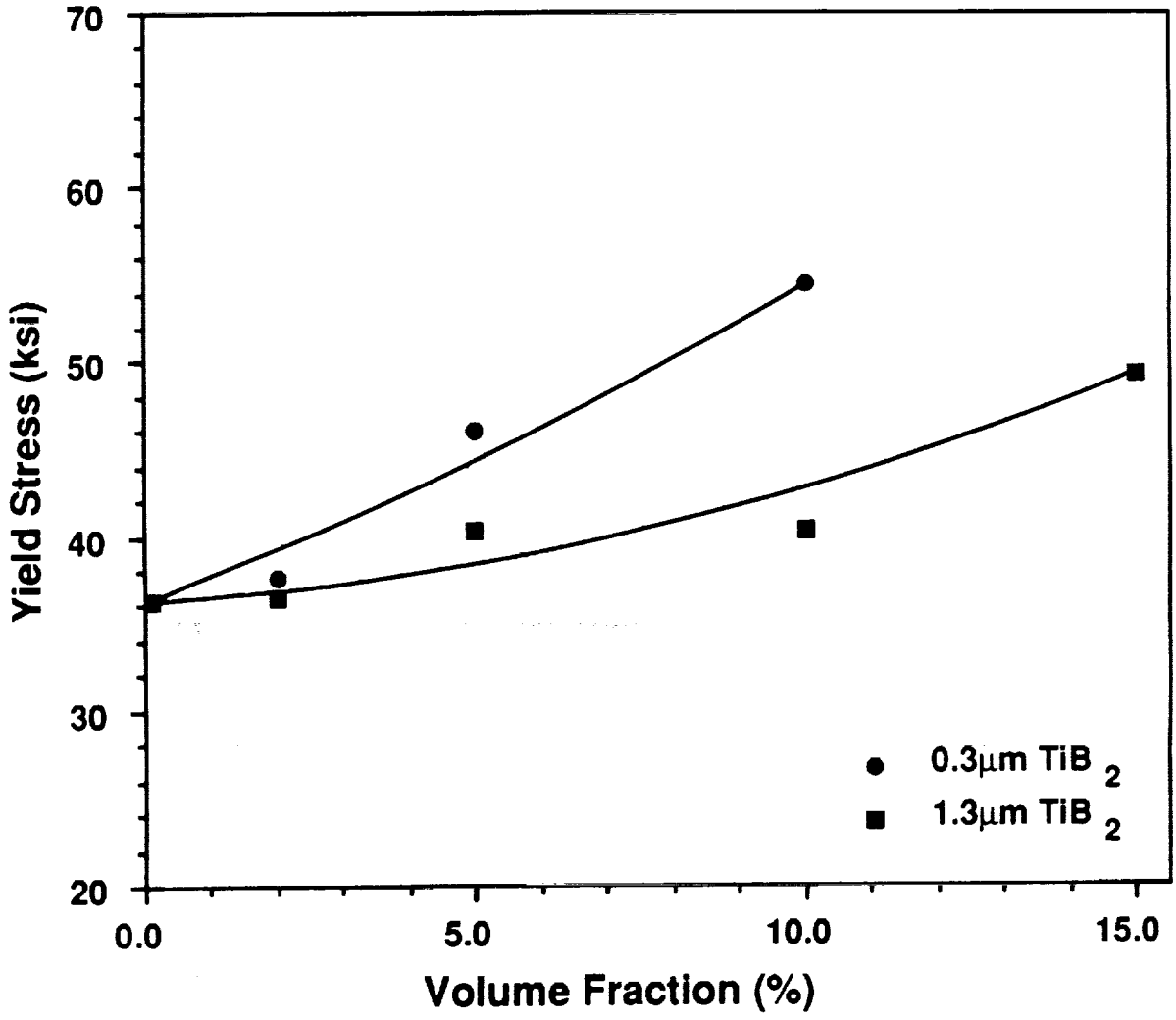

Figure 4.14(a) Variation of yield stress with volume fraction of TiB_2 for Al-4%Cu-1.5%Mg alloys in naturally aged (T4) condition.

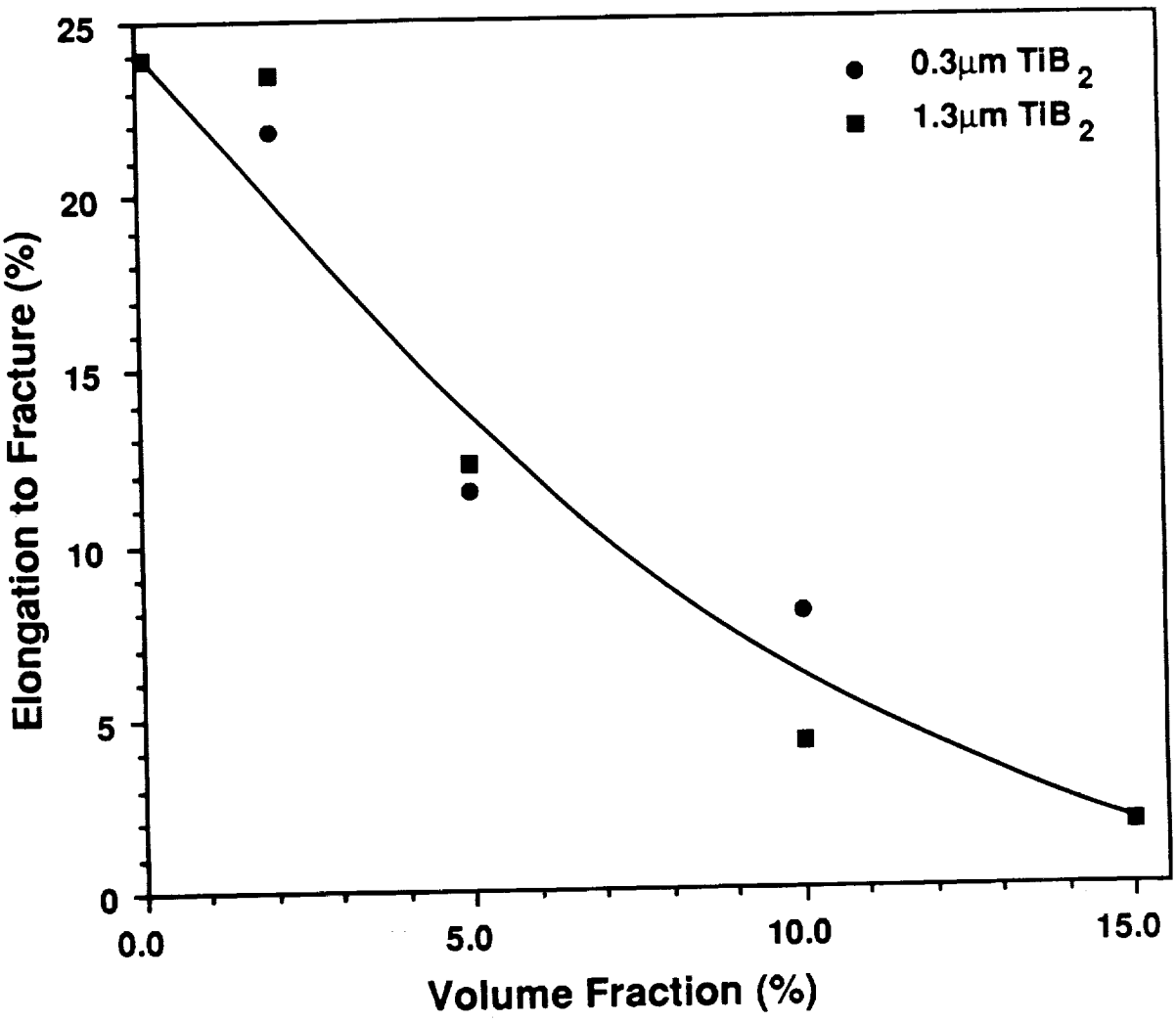

Figure 4.14(b) Variation of elongation with volume fraction of TiB_2 for Al-4%Cu-1.5%Mg alloys in naturally aged (T4) condition.

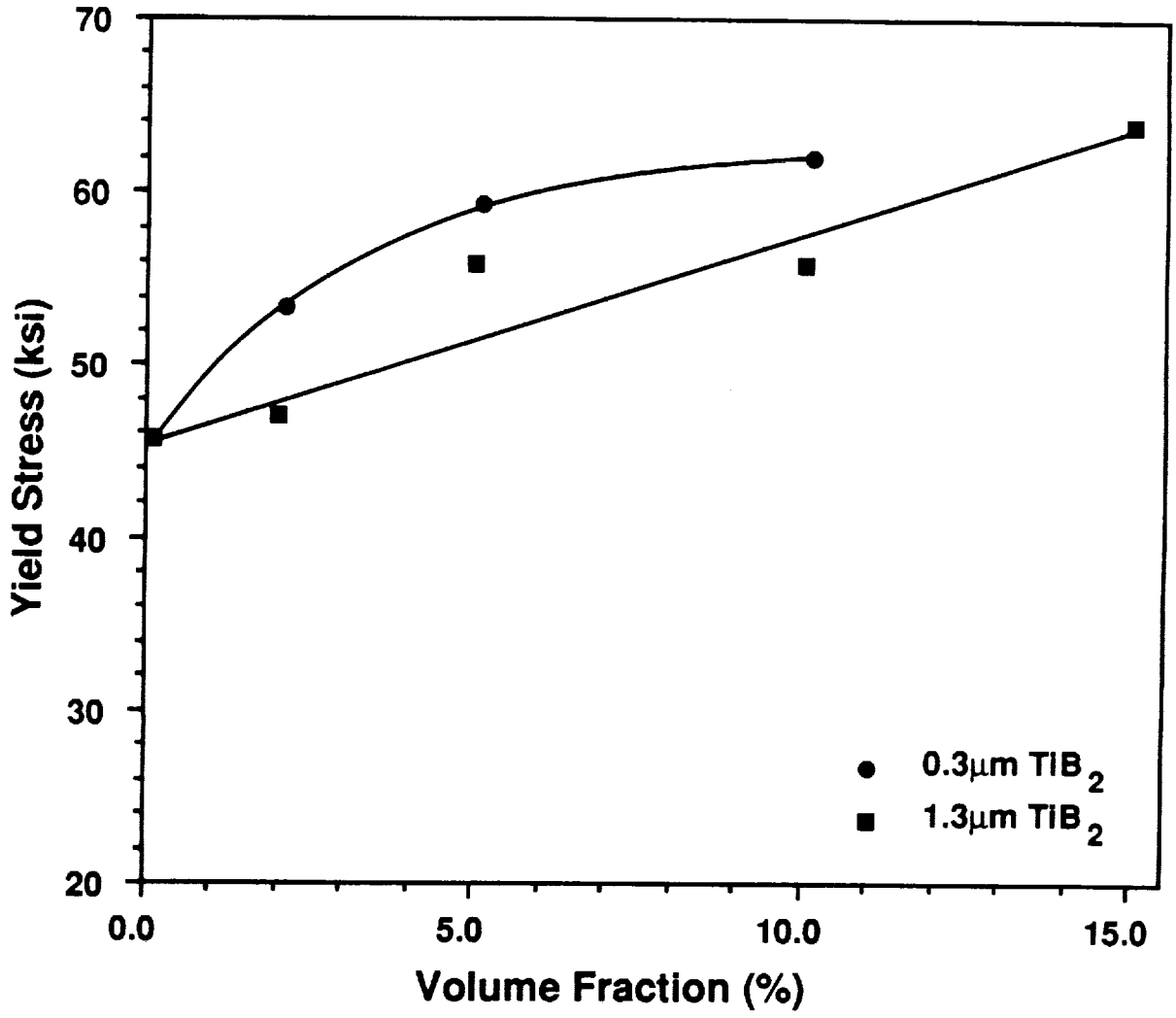

Figure 4.15(a) Variation of yield stress with volume fraction of TiB_2 for Al-4%Cu-1.5%Mg alloys in the peak aged (T6) condition.

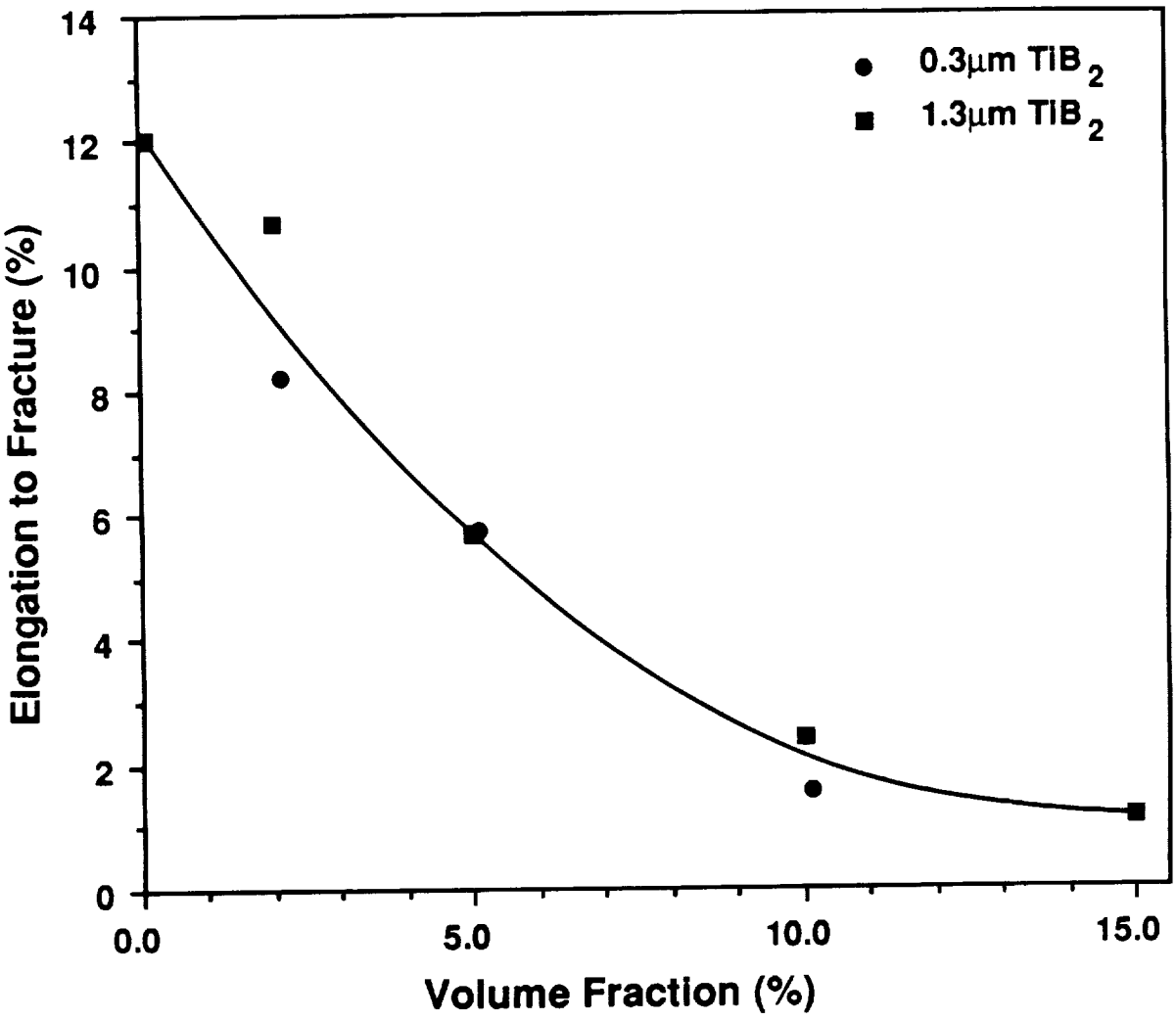

Figure 4.15(b) Variation of elongation with volume fraction of TiB_2 for Al-4%Cu-1.5%Mg alloys in the peak aged (T6) condition.

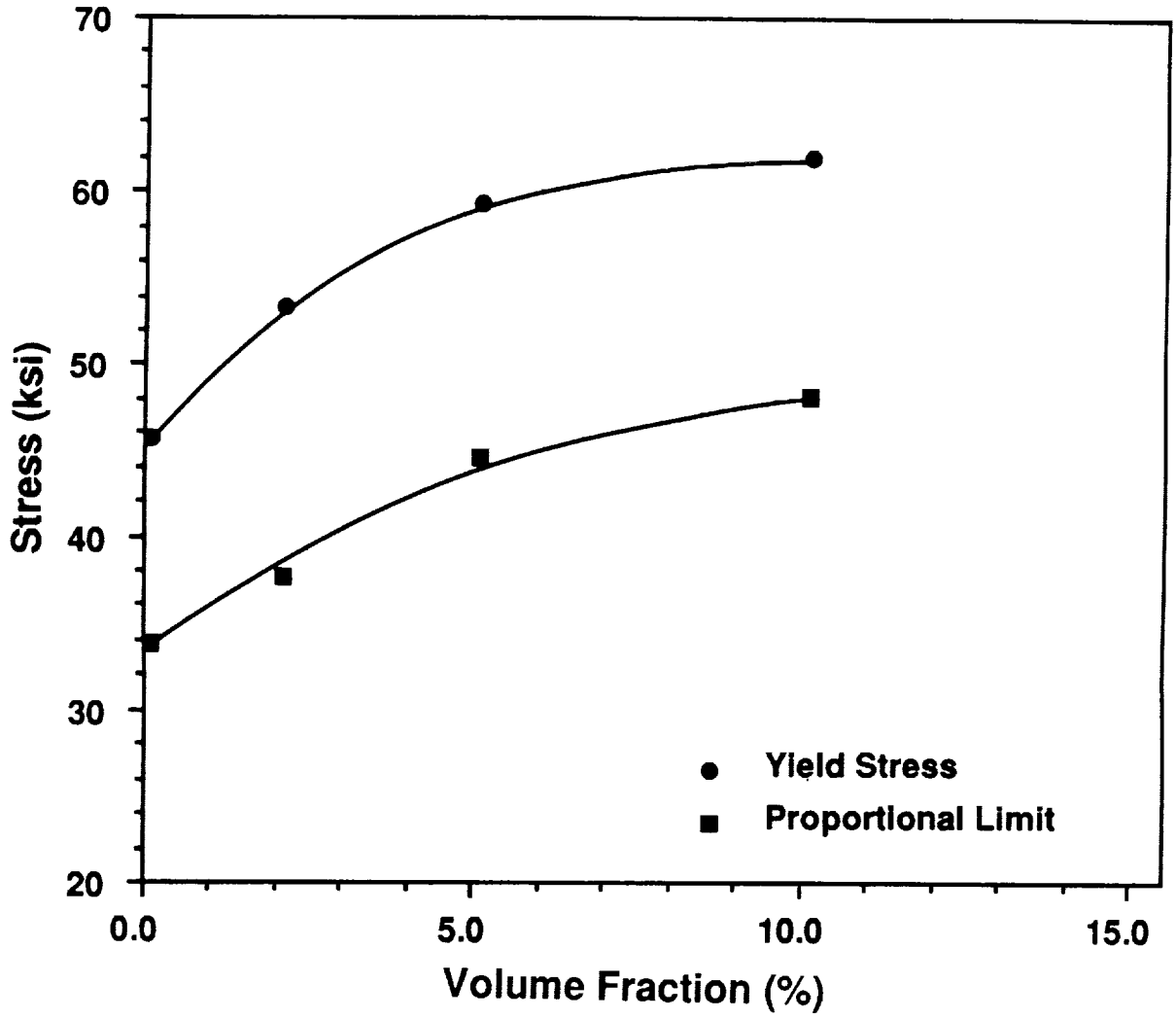

Figure 4.16 Variation of yield stress and proportional limit with volume fraction of 0.3 μm TiB_2 particles for Al-4%Cu-1.5%Mg alloys in the peak aged (T6) condition.

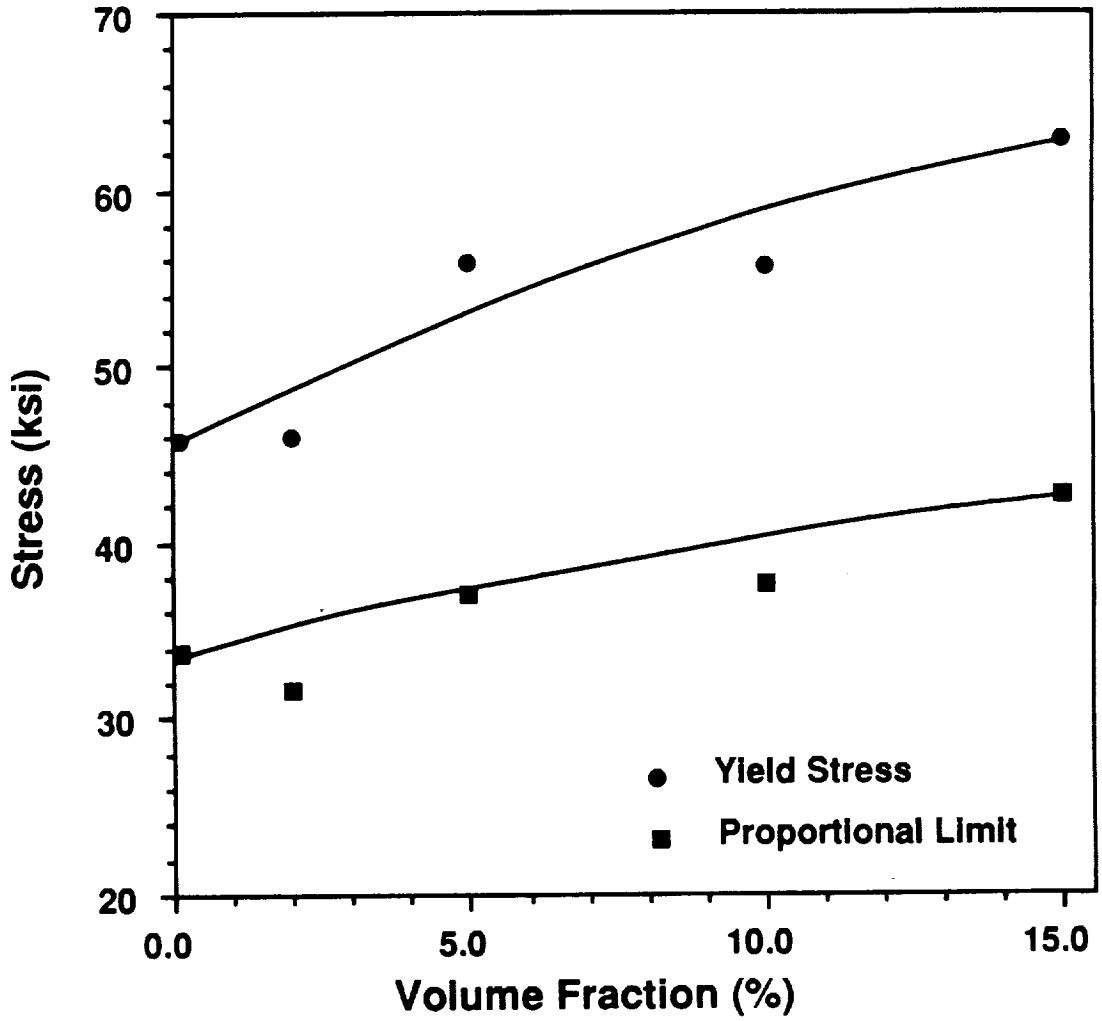

Figure 4.17 Variation of yield stress and proportional limit with volume fraction of 1.3 μm TiB_2 particles for Al-4%Cu-1.5%Mg alloys in the peak aged (T6) condition.

with increasing loading. This indicates that the onset of plastic yielding is affected by particle loading.

4.4 Fracture Toughness

In this section the fracture toughness of the XD^{TM} reinforced Al-4%Cu-1.5%Mg alloys is examined as a function of particle size, loading, and artificial aging of the matrix. These measurements were made using fatigue precracked compact tension samples according to ASTM standard E-399. Of the 56 samples tested, none failed during tensile precracking. However, most of the fracture toughness measurements were not valid to the ASTM E-399 standard because the samples were of insufficient thickness. The 0.625 in. (1.58 cm) thick extrusions were not thick enough to achieve plane strain conditions because of the combination of yield strength and toughness exhibited by most of these alloys. Valid plane-strain fracture toughness (K_{IC}) measurements were obtained only for the higher loading materials in the near peak aged condition. The valid K_{IC} measurements are listed in Table 4.3 as a function of aging time and TiB_2 loading. The near peak aged 10 and 15vol% TiB_2 containing alloys exhibit a K_{IC} of approximatly 20 ksi$\sqrt{in}$.

To avoid the size constraints imposed by the plane-strain criteria of E-399, we used the equivalent energy method to determine the value K_{ee}. This method is also a standardized ASTM procedure (ASTM E-992) and has been used successfully on steel samples. As Fig. 4.18 shows, the total energy under the curve to P_{max} was calculated and then a perfectly elastic

Table 4.3

Plane Strain Fracture Toughness (K_{IC})
of Al-4%Cu-1.4%Mg Alloys
Aged at 375°F from the T4 Condition

TiB_2 Loading and Size	Aging Time (h)		
	10	16	30
10% 0.3 μm	19.7 ksi$\sqrt{in}$	-	22.4
10% 1.3 μm	20.0	-	-
15% 1.3 μm	18.8	17.8	17.4

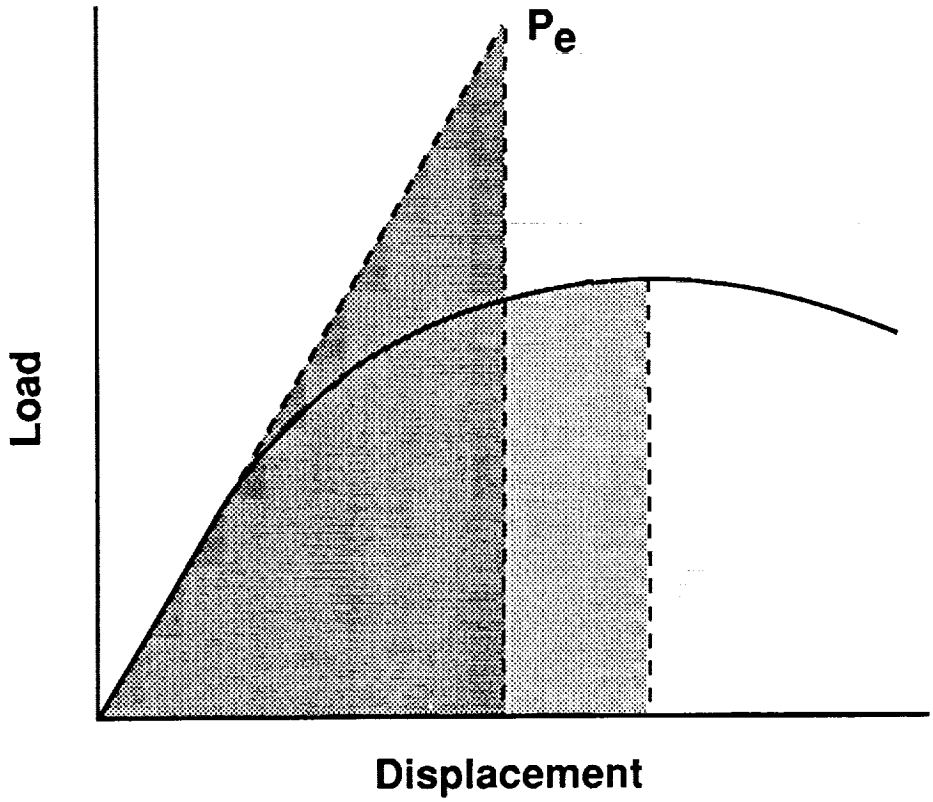

Figure 4.18 Schematic of load-displacement curve and construction of a ideally elastic material with an equivalent energy used to determine P_e.

load-displacement triangle with equal energy was created. The peak of the triangle (P_e in Fig. 4.18) corresponds to the load used to calculate the critical stress intensity. This is a standardized procedure that will work with even the most ductile materials.

Although the values of K_{ee} compare well with the valid K_{IC} measurements generated, they do not provide an absolute measure of the plane-strain fracture toughness, K_{IC}. Instead, $K_{ee}$is an estimate of fracture toughness, which can be used as an aid in determining trends.

4.4.1 Isothermal-aging response

Figures 4.19 and 4.20 show the equivalent energy fracture toughness (K_{ee}) as a function of aging time at 375°F from the T4 condition. The measurements for the alloys containing 0.3 μm diameter TiB_2 particles are shown in Fig. 4.19, and the measurements for the alloys with 1.3 μm TiB_2 particles are shown in Fig. 4.20. The fracture toughness decreased with aging, reaching a minimum slightly before the peak in strength. With overaging, fracture toughness increased slightly. This behavior is similar to conventional 2000-series alloys.

4.4.2 Effect of loading and particle size

The K_{ee} values for the T4 and T6 aged materials are plotted as a function of loading in Fig. 4.21. Although there is some noise, these data clearly show that the fracture toughness initially dropped off quickly with the addition of

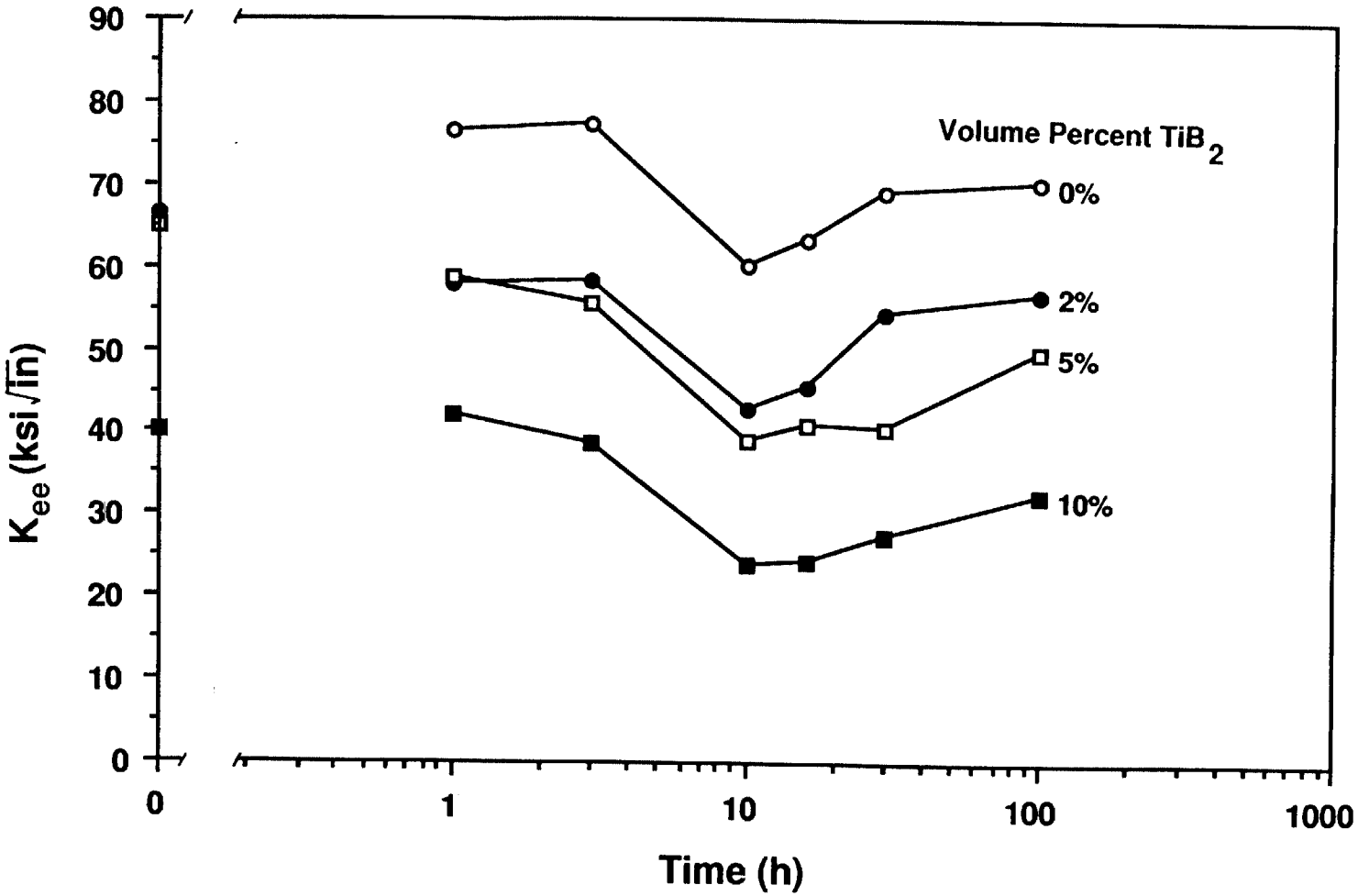

Figure 4.19 Equivalent energy fracture toughness vs aging time at 375°F for the Al-4%Cu-1.5%Mg alloys containing 0.3 μm TiB_2 particles.

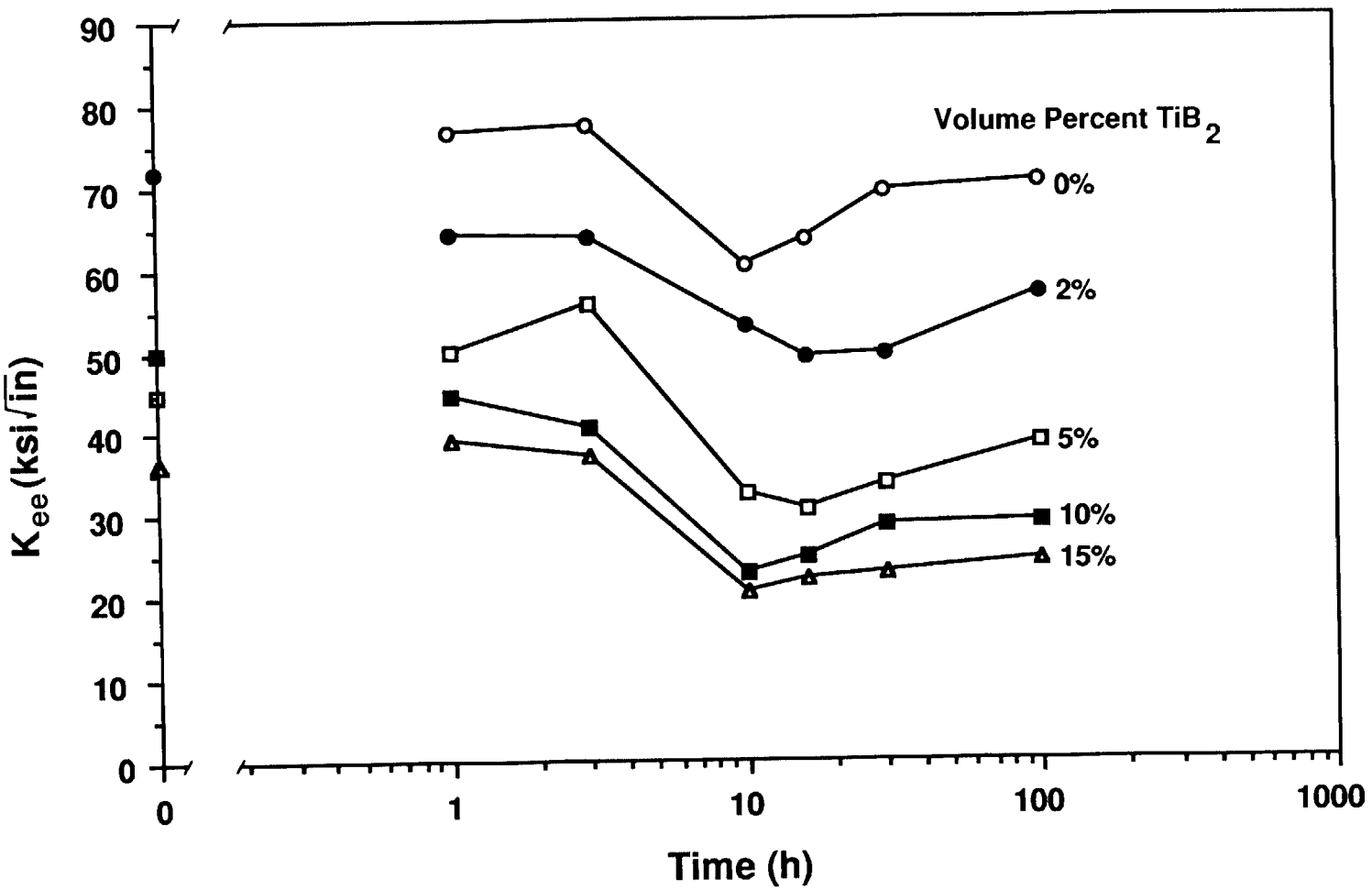

Figure 4.20 Equivalent energy fracture toughness vs aging time at 375°F for the Al-4%Cu-1.5%Mg alloys containing 1.3 μm TiB_2 particles.

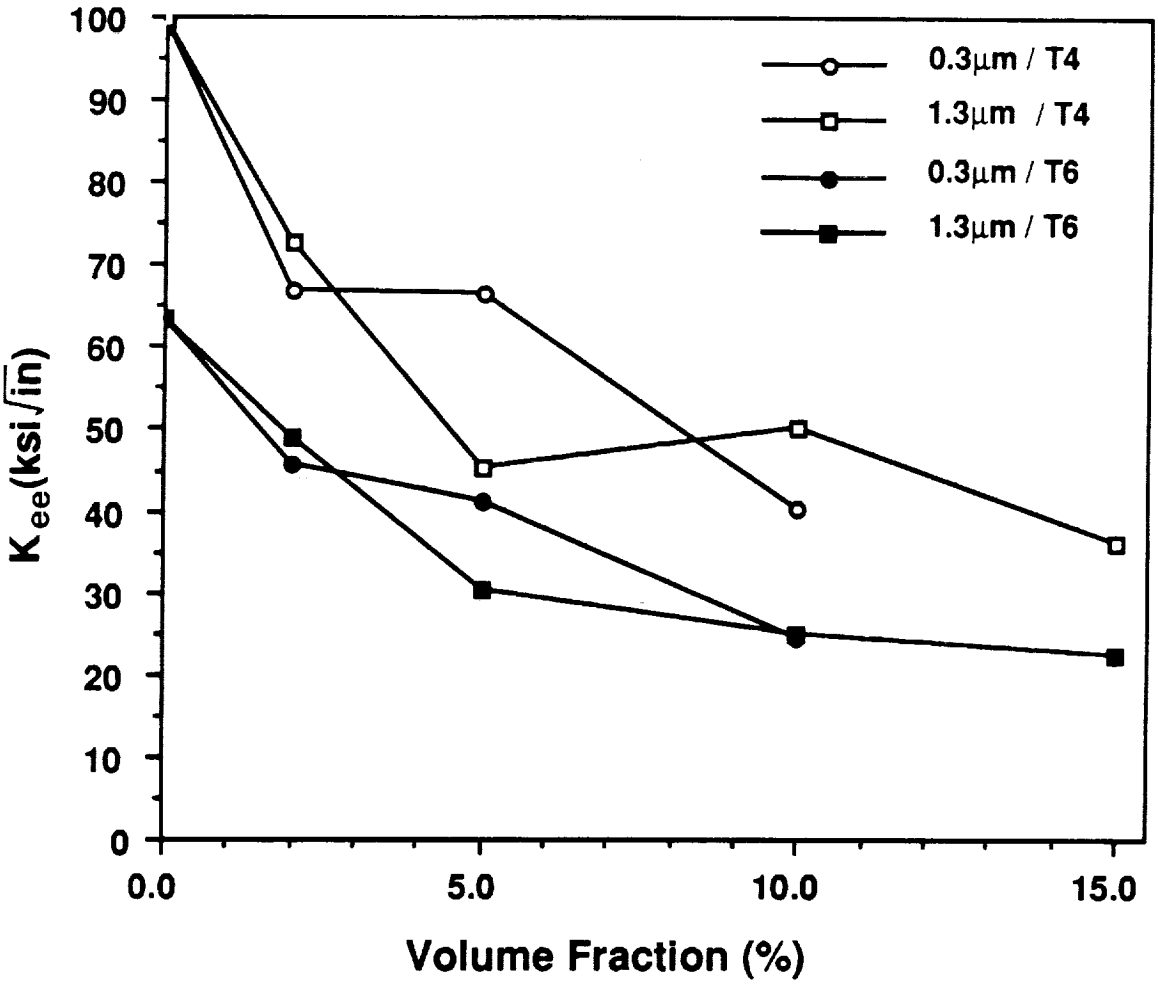

Figure 4.21 Equivalent energy fracture toughness vs TiB_2 particle loading for the naturally aged (T4) and peak aged (T6) materials.

TiB_2 volume fractions up to about 5%, and then remained nearly constant up to 15%. Thus, beyond the initial penalty, increased particle loadings did not severely affect fracture toughness. It also appears that the fracture toughness was insensitive to particle size in the range tested.

4.5 Elevated-Temperature Tensile Properties

The elevated-temperature tensile properties of the XD^{TM} reinforced Al-4%Cu-1.5%Mg alloys were examined as a function of particle size and loading. Alloys in the peak aged (T6) condition were exposed to an elevated temperature for 0.5 h and then tested at a strain rate of 1.3×10^{-3} sec^{-1}. For the alloys containing 0.3 μm TiB_2 particles, the 0.2% offset yield stress is shown as a function of temperature and TiB_2 loading in Fig. 4.22; the ultimate tensile strength is shown in Fig. 4.23, and the elongation to fracture in a 1.0 in. gauge length is shown in Fig. 4.24. Figures 4.25, 4.26, and 4.27 are the corresponding plots of yield stress, ultimate tensile strength, and elongation to fracture, respectively as a function of test temperature, for the alloys containing 1.3 μm TiB_2 particles.

The general features of the yield stress vs temperature curves, shown in Figs. 4.22 and 4.25, are the same regardless of particle size and loading. With increasing temperature, the yield stress fell off gradually at first and then rapidly at temperatures above 400°F. The yield stress curves are displaced to higher stresses with increasing particle loading, although at very high temperatures (650°F) the yield stress of

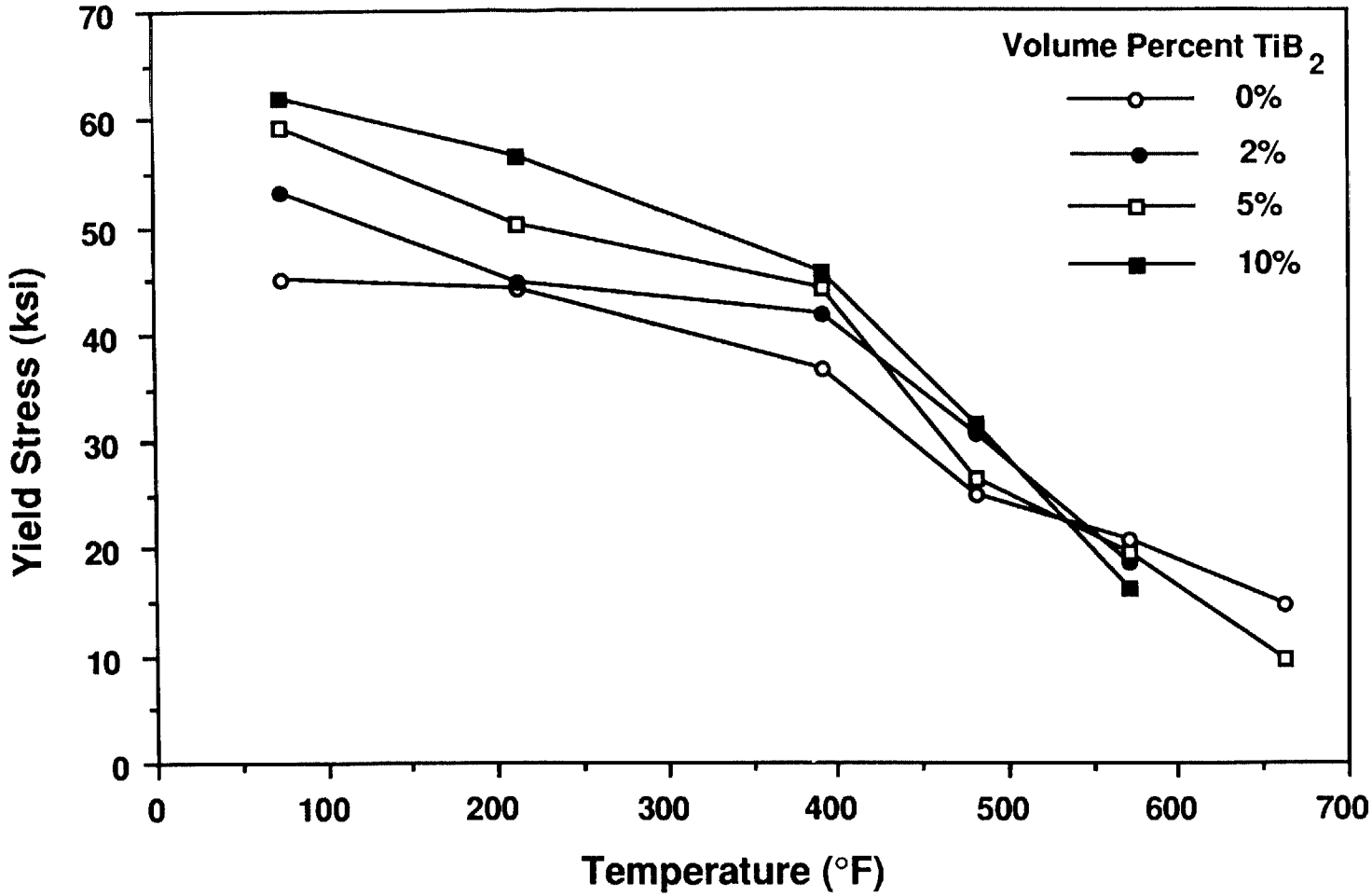

Figure 4.22 Yield stress as a function of test temperature for Al-4%Cu-1.5%Mg with 0.3 μm TiB_2 particles. Materials tested from the peak aged (T6) condition with 0.5 h exposure at temperature.

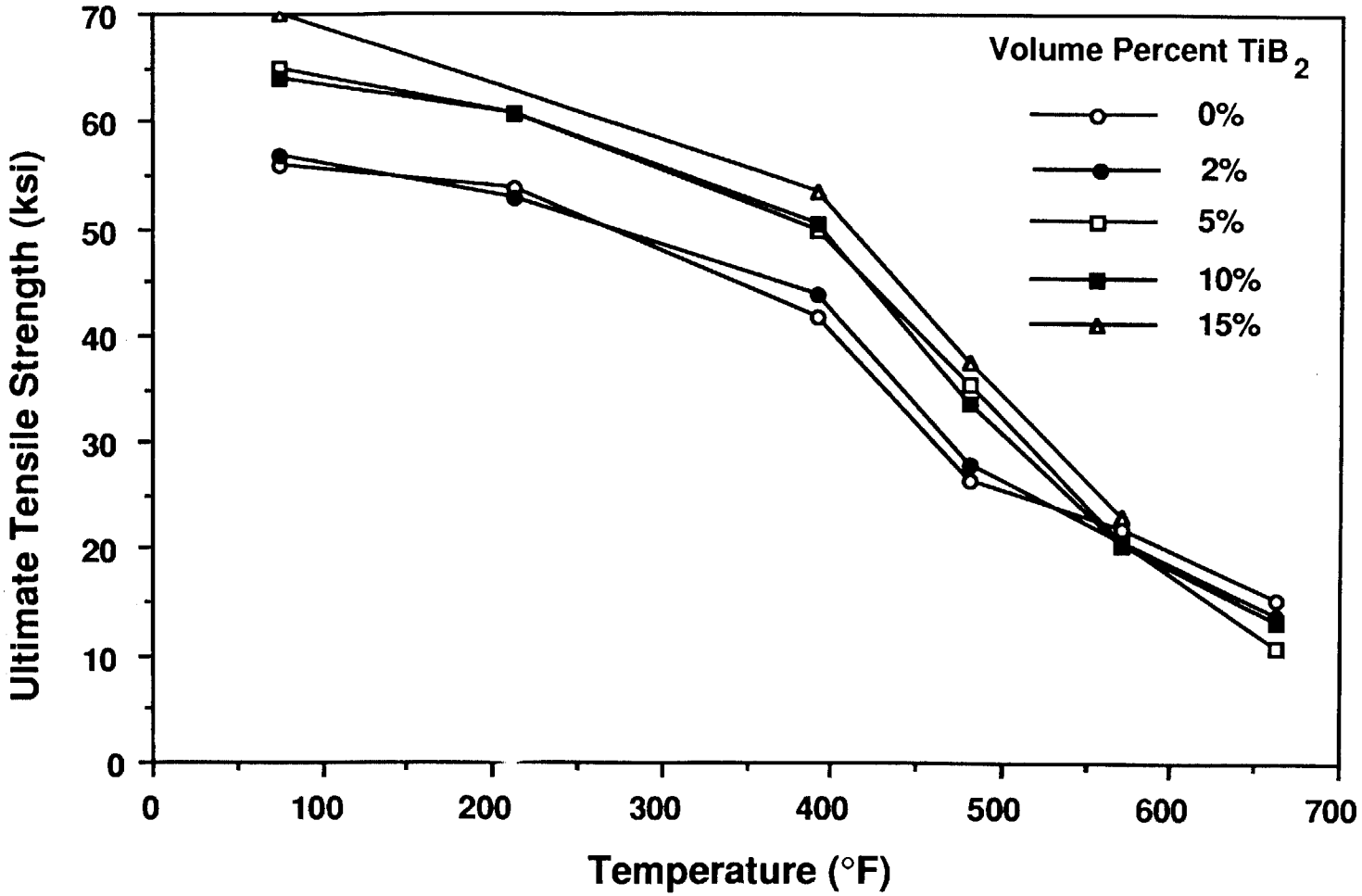

Figure 4.23 Ultimate tensile strength as a function of test temperature for Al-4%Cu-1.5%Mg with 0.3 μm TiB_2 particles. Materials tested from the peak aged (T6) condition with 0.5 h exposure at temperature.

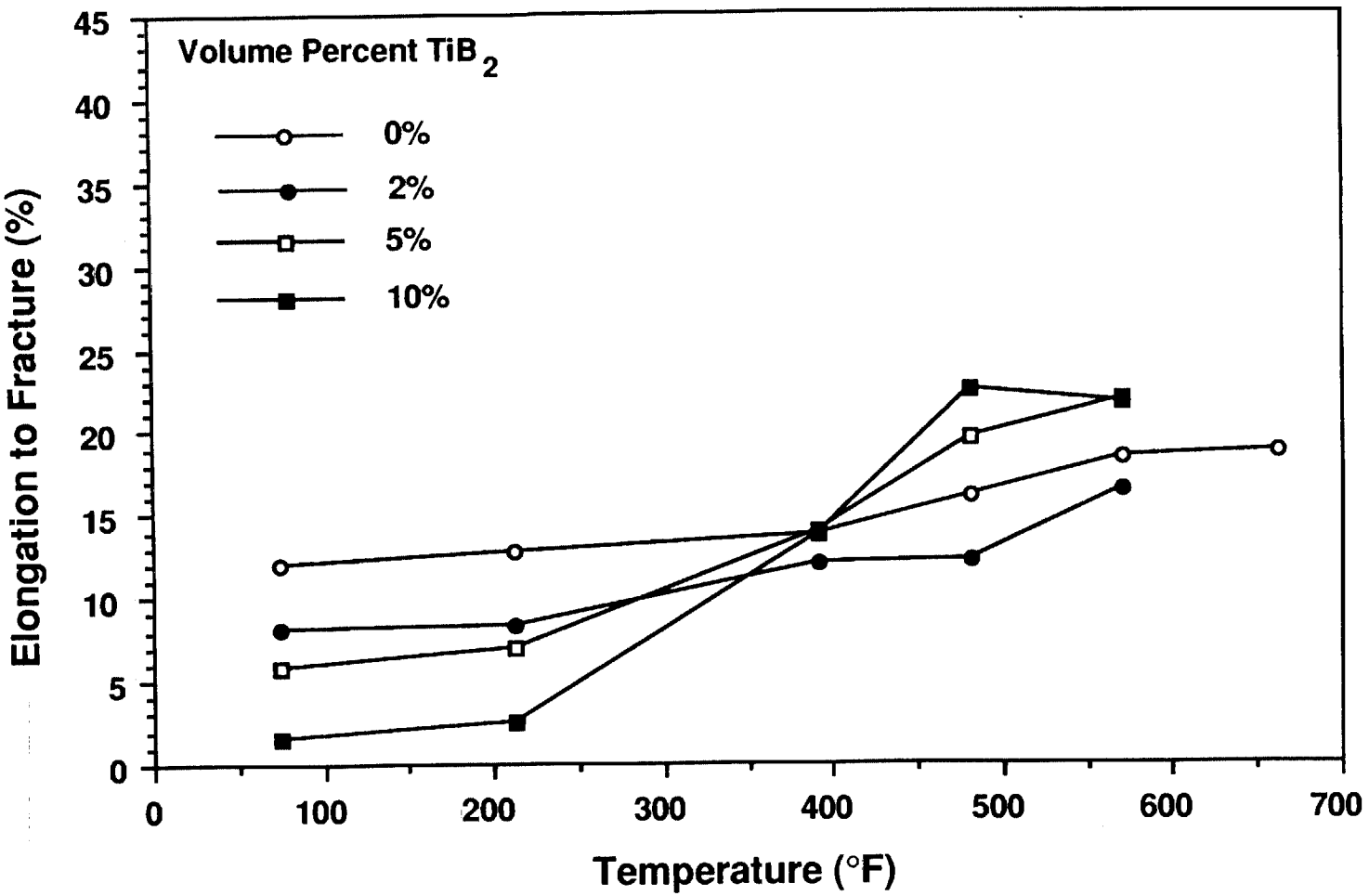

Figure 4.24 Elongation to fracture as a function of test temperature for Al-4%Cu-1.5%Mg with 0.3 μm TiB_2. Materials tested from the peak aged (T6) condition with 0.5 h exposure at temperature.

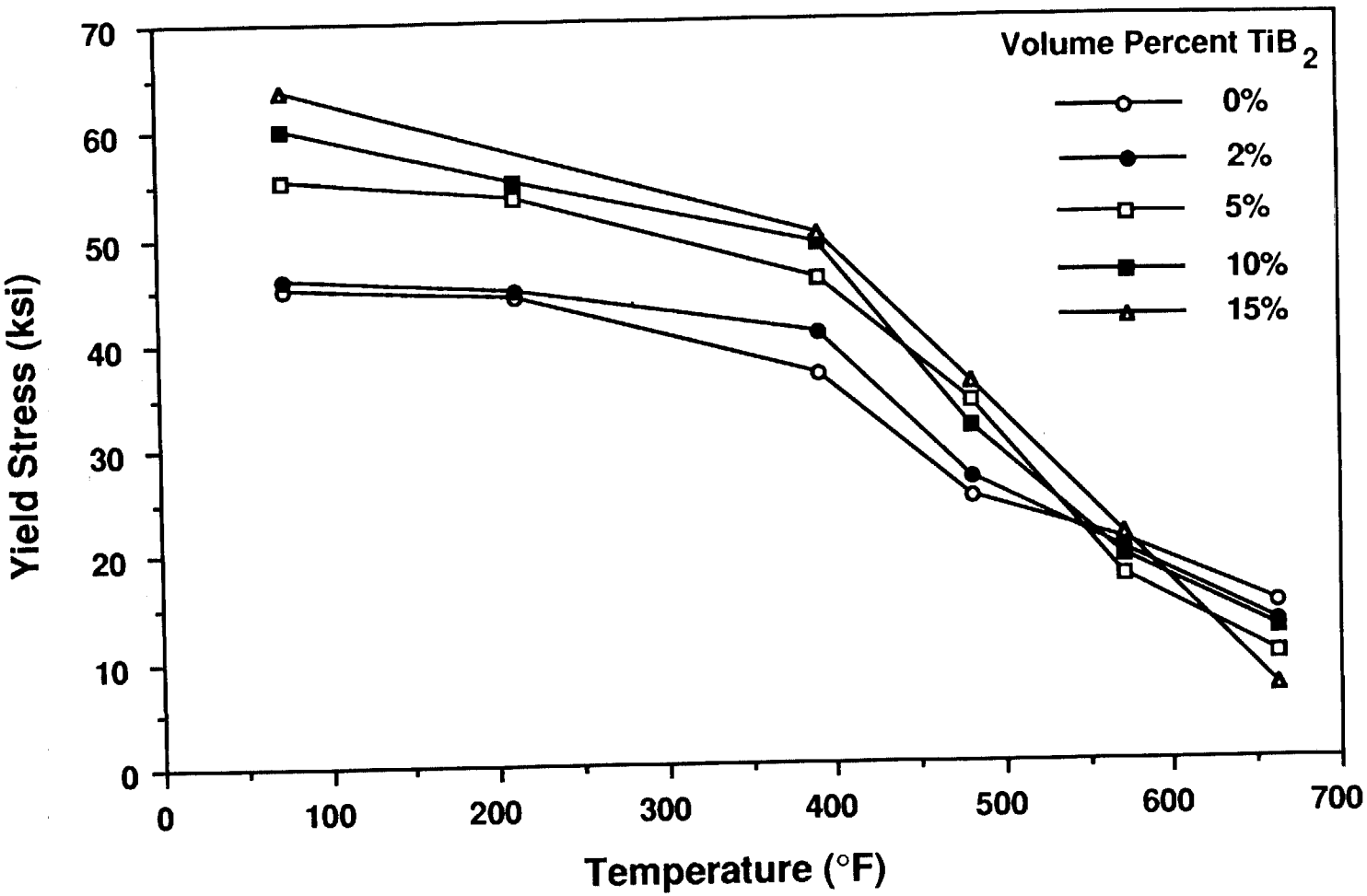

Figure 4.25 Yield stress as a function of test temperature for Al-4%Cu-1.5%Mg with 1.3 μm TiB_2 particles. Materials tested from the peak aged (T6) condition with 0.5 h exposure at temperature.

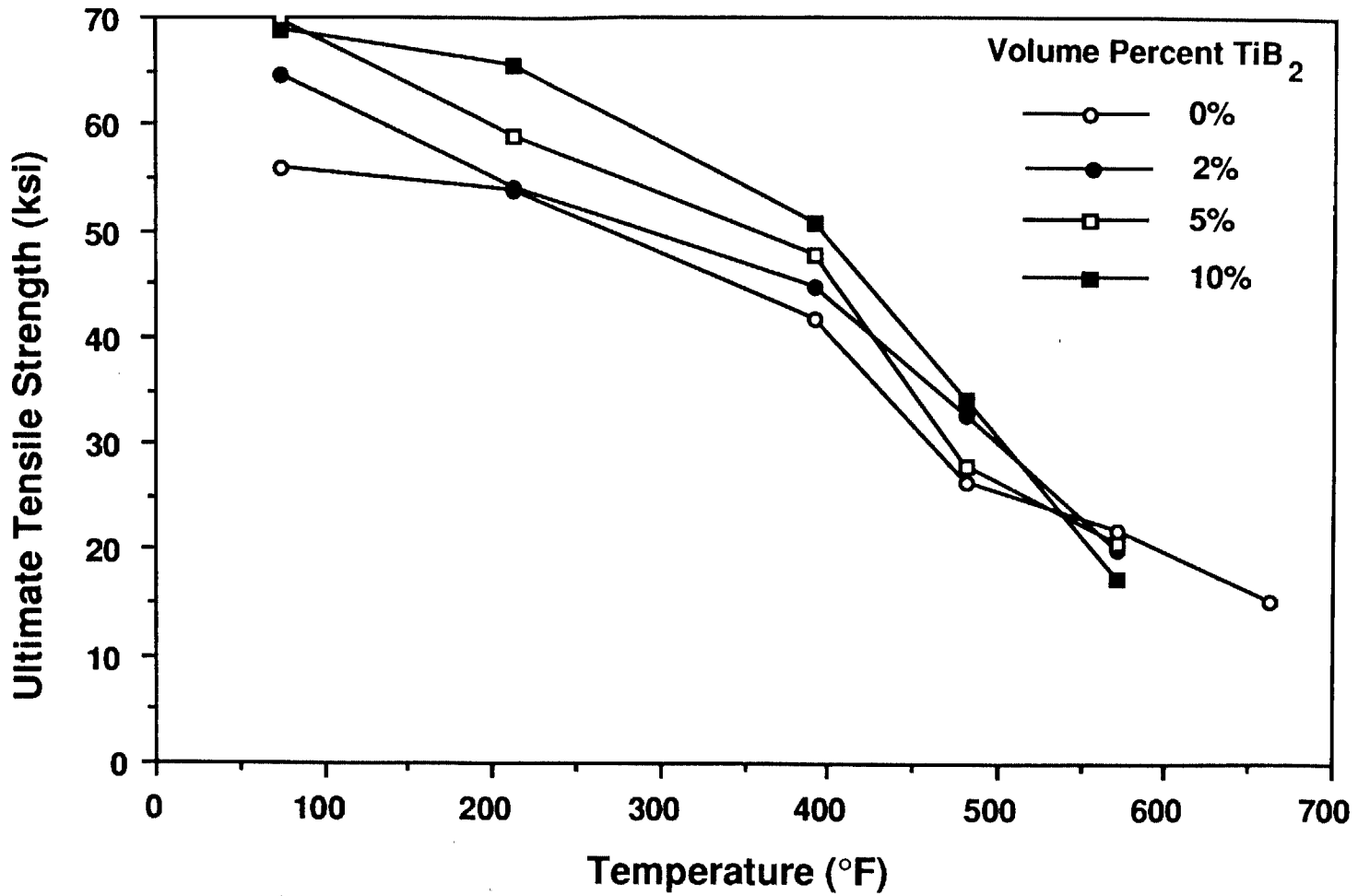

Figure 4.26 Ultimate tensile strength as a function of test temperature for Al-4%Cu-1.5%Mg with 1.3 μm TiB_2 particles. Materials tested from the peak aged (T6) condition with 0.5 h exposure at temperature.

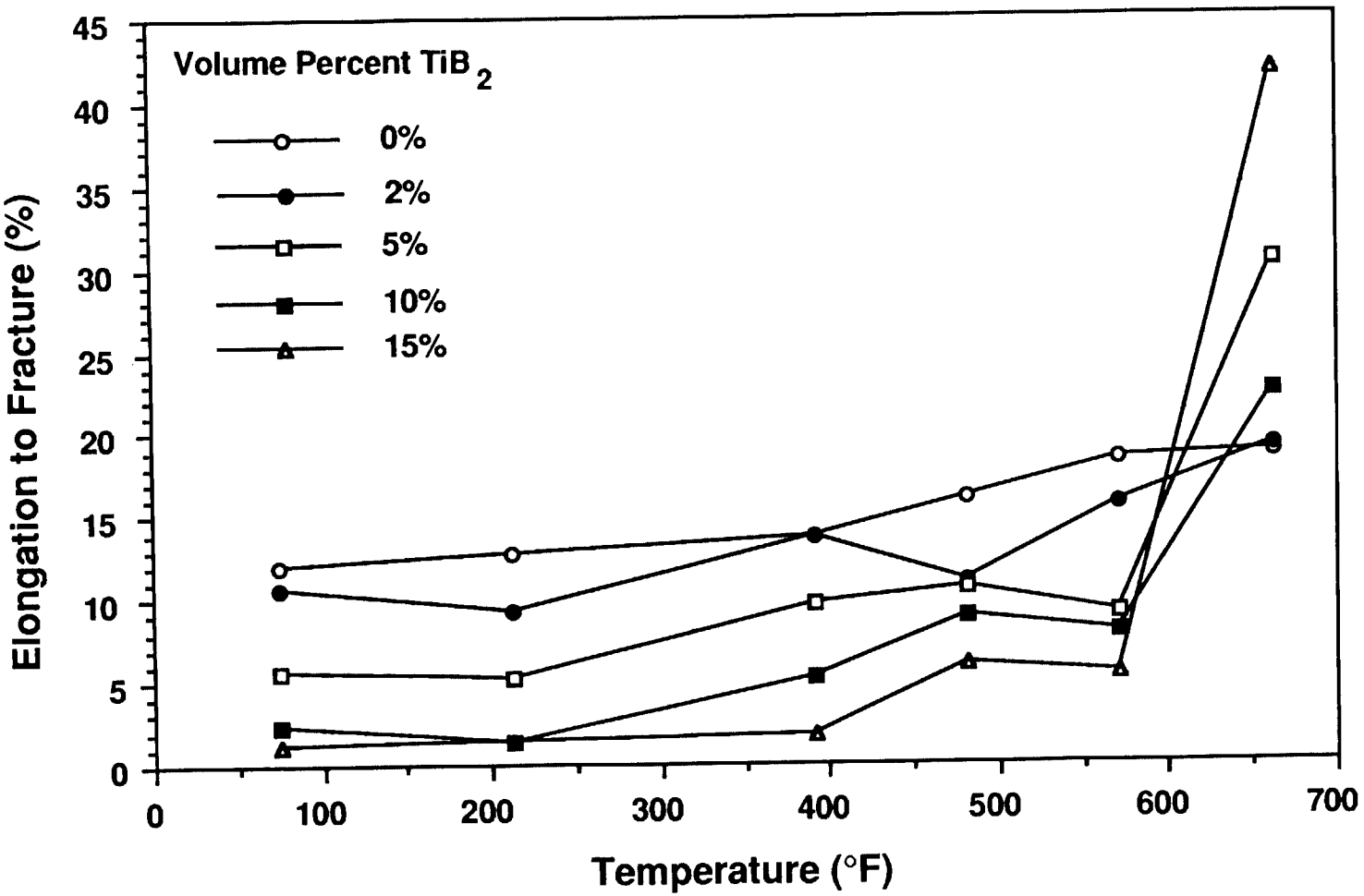

Figure 4.27 Elongation to fracture as a function of test temperature for Al-4%Cu-1.5%Mg with 1.3 μm TiB_2 particles. Materials tested the from peak aged (T6) condition with 0.5 h exposure at temperature.

all the materials fell to a similar value. The rapid drop in yield stress regardless of particle loading at about 400°F indicates that the mechanisms of strengthening in the reinforced alloys can be defeated by thermally activated processes. The results of the ultimate tensile stress data, shown in Figs. 4.23 and 4.26, are similar to the behavior revealed by the yield stress data.

As Figs. 4.24 and 4.27 show, the elongation to fracture was quite constant with increasing temperature, with a rapid increase in elongation at higher temperatures. The increase in elongation at high temperatures was more pronounced as the volume fraction of TiB_2 increases. Thus, elongation decreased with increasing particle loading at low temperatures, and increased with increasing particle loading at high temperatures.

5. SUMMARY

The influence of reinforcement size, volume fraction, and matrix deformation behavior on the strength, fracture toughness, and high-temperature strength of a precipitation strengthened aluminum metal matrix composite (MMC) was examined. The MMC's were produced by the XD^{TM} process using pure aluminum and Al-4%Cu-1.5%Mg matrices reinforced with 0 to 15vol% TiB_2 particles either 0.3 μm or 1.3 μm in diameter. The alloys were cast by conventional aluminum foundry practice and then forged, or extruded and heat treated.

The effect of artificial isothermal-aging upon of the tensile and fracture properties of these alloys was examined. The TiB_2 reinforced alloys' responses to heat treatment were identical to that of the unreinforced alloy. Even though a significant increase in the tensile yield strength was observed with the addition of TiB_2, there was no shift in the aging time to peak strength. Similarly, fracture toughness decreased with the addition of TiB_2, though the aging time to minimum fracture toughness did not shift.

The tensile properties and fracture toughness were also examined as a function of the particle size and loading. The strength of the alloys increased with TiB_2 loading, and at equivalent loadings, the alloy with the smaller TiB_2 particles showed greater strength. The elongation to fracture decreased with increased TiB_2 loading and appeared to be independent of particle size. Fracture toughness decreased with TiB_2 additions up 5% and then leveled off from 5% to 15%. Fracture toughness also seemed to be independent of TiB_2 particle size.

Finally, the tensile properties of these MMC's were examined as a function of temperature. With increasing temperature the yield stress fell off gradually at first, and then dropped rapidly at temperatures above 400°F. Increased loadings of TiB_2 displaced the yield stress curves to higher stresses; although, at very high temperatures (650°F) the yield stresses of all the materials fell to a similar value. The rapid drop in yield stress that occurred at 400°F, regardless of particle loading, indicates that the predominant strengthening mechanism in the Al-4%Cu-1.5%Mg+TiB_2 alloys can be defeated by thermally activated processes.

6. REFERENCES

[1] D.M. Stefanescu, B.K. Dhindaw, S.A. Kacar, and A. Moitra, "Behavior of Ceramic Paritcles at Solid-Liquid Metal Interface in Metal Matrix Composites," Met. Trans., 19A; 2847 (1988).

[2] S.N. Omenyi and A.W. Neumann, "Thermodynamic Aspects of Particle Engulfment by Solidifying Melts," J. Appl. Phys., 47(9), 3956 (1976).

[3] L.F. Mondolfo, Aluminum Alloys: Structure and Properties, Butterworth Co., London (1976).

[4] T. Christman and S. Suresh, " Microstructural Developpment in an Aluminum Alloy-SiC Whisker Composite," Acta Met., 36; 1691 (1988).

[5] T.G. Nieh and R.F. Karlak, "Aging Characteristics of B_4C Reinforced 6061-Aluminum," Scripta Met., 18; 25 (1984).

NASA
National Aeronautics and Space Administration

Report Documentation Page

1. Report No.	2. Government Accession No.	3. Recipient's Catalog No.
NASA CR-4276		

4. Title and Subtitle	5. Report Date
The Mechanisms of Dispersion Strengthening and Fracture in Al-Based XD™ Alloys	February 1990
	6. Performing Organization Code

7. Author(s)	8. Performing Organization Report No.
R. M. Aikin, Jr.	MML TR 89-54c
	10. Work Unit No.
	505-63-01

9. Performing Organization Name and Address	11. Contract or Grant No.
Martin Marietta Laboratories 1450 South Rolling Road Baltimore, Maryland 21227	NAS1-18531
	13. Type of Report and Period Covered
12. Sponsoring Agency Name and Address	Contractor Report
National Aeronautics and Space Administration Langley Research Center Hampton, VA 23665-5225	14. Sponsoring Agency Code

15. Supplementary Notes

Langley Technical Monitor: William D. Brewer
Interim Report - 7/87-2/89

16. Abstract

The influence of reinforcement size, volume fraction, and matrix deformation behavior on room and elevated temperature strength, and the fracture toughness of metal matrix composites of both pure aluminum and Al-4%Cu-1.5%Mg with 0-15vol% TiB_2 have been examined. Higher TiB_2 volume fractions increased the tensile yield strength both at room and elevated temperatures, and reduced the elongation to fracture. Tensile tests also indicate that small particles provided a greater increase in strength for a given volume fraction than larger particles, whereas elongation to fracture appeared to be insensitive to reinforcement size. The fracture toughness of the Al-4%Cu-1.5%Mg alloys decreased rapidly with TiB_2 additions of 0 to 5vol% and more slowly with TiB_2 additions of 5 to 15vol%. Fracture toughness appears to be independent of TiB_2 particle size. The isothermal-aging response of the precipitation strengthened Al-4%Cu-1.5%Mg alloys was not altered by the presence of TiB_2.

17. Key Words (Suggested by Author(s))	18. Distribution Statement
Metal Matrix Composites	Unclassified - Unlimited Subject Category 24

19. Security Classif. (of this report)	20. Security Classif. (of this page)	21. No. of pages	22. Price
Unclassified	Unclassified	88	A05

NASA FORM 1626 OCT 86

For sale by the National Technical Information Service, Springfield, Virginia 22161-2171

NASA-Langley, 1990